Homology Modeling of Toll-Like Receptor Ligand-Binding Domains: A Leucine-Rich Repeat Assembly Approach

Dissertation

Fakultät für Geowissenschaften

Ludwig-Maximilians-Universität München

vorgelegt von

Tiandi Wei

München, den 24. Februar 2010

Erstgutachter: Prof. Dr. Wolfgang M. Heckl

Zweitgutachter: Prof. Dr. Robert W. Stark

Prüfungstermin: 26.05.2010

Abstract

Toll-like receptors (TLRs) are in the front-line during the initiation of an innate immune response against invading pathogens. TLRs are type I transmembrane proteins that are expressed on the surface of immune system cells. They are evolutionarily conserved between insects and vertebrates. To date, 13 groups of mammalian TLRs have been identified, ten in humans and 13 in mice. They share a modular structure that consists of a leucine-rich repeat (LRR) ectodomain, a single transmembrane helix and a cytoplasmic Toll/interleukin-1 receptor (TIR) domain. Most TLRs have been shown to recognize pathogen-associated molecular patterns (PAMPs) from a wide range of invading agents and initiate intracellular signal transduction pathways to trigger expression of genes, the products of which can control innate immune responses. The TLR signaling pathways, however, must be under tight negative regulation to maintain immune balance because over-activation of immune responses in the body can cause autoimmune diseases.

The TLR ectodomains are highly variable and are directly involved in ligand recognition. So far, crystal structures are missing for most TLR ectodomains because structure determination by X-ray diffraction or nuclear magnetic resonance (NMR) spectroscopy experiments remains time-consuming, and sometimes the crystallization of a protein can be very difficult. Computational modeling enables initial predictions of three-dimensional structures for the investigation of receptor-ligand interaction mechanisms. Computational methods are also helpful to develop new TLR agonists and antagonists that have therapeutic significance for diseases.

In this dissertation, an LRR template assembly approach for homology modeling of TLR ligand-binding domains is discussed. To facilitate the modeling work, two databases, TollML and LRRML, have been established. With this LRR template assembly approach, the ligand-binding domains of human TLR5-10 and mouse TLR11-13 were modeled. Based on the models of human TLR7, 8 and 9, we predicted potential ligand-binding residues and possible configurations of the receptor-ligand complex using a combined procedure. In addition, we modeled the cytoplasmic TIR domains of TLR4 and 7, the TLR adaptor protein MyD88 (myeloid differentiation primary response protein 88) and the TLR inhibitor SIGIRR (Single immunoglobulin interleukin-1 receptor-related molecule) to investigate the structural mechanism of TLR negative regulation.

Abstract

Contents

Contents

1. Introduction

Toll-like receptors (TLRs) are a class of membrane-bound proteins that are widely expressed in insects, plants and animals. They recognize invading microbial pathogens and rapidly initiate intracellular signal transduction pathways to trigger expression of genes, whose products can control innate immune responses [1]. Therefore, TLRs have opened up a range of therapeutic possibilities, in particular for infectious diseases. Understanding the mechanisms of TLR-ligand interactions from a structural point of view will contribute to the development of new TLR agonists and antagonists that have therapeutic significance for diseases.

TLRs share a modular structure that consists of a leucine-rich repeat (LRR) ectodomain, a single transmembrane helix and a cytoplasmic Toll/interleukin-1 receptor (TIR) domain. The ectodomains are highly variable across different TLRs. They are directly involved in the recognition of a variety of pathogen-associated molecular patterns (PAMPs). By contrast, the intracellular TIR domain is conserved across all TLRs and shared by downstream signaling adaptor molecules. Until now, four crystal structures of TLR ectodomain-ligand complexes have been determined [2-5]. These structures demonstrate how the LRR-based platform is adapted to the ligand recognition. Compared with the very limited number of known structures of TLRs, the high-throughput genome sequencing projects, however, have led to the identification of more than 2,000 TLR sequences [6]. Thus, the structures of most TLRs are still unknown because structure determination by X-ray diffraction or nuclear magnetic resonance (NMR) spectroscopy experiments remains time-consuming, and crystallization of a protein complex can be very difficult. It is clear that the discrepancy between the rate at which novel protein sequences are discovered and the rate at which detailed structural information on proteins can be obtained from X-ray or NMR methods will persist for the foreseeable future. In this regard, protein structure prediction methods are powerful tools to bridge the gap between sequence determination and structure determination. Protein structure prediction refers to the effort of generating three-dimensional models from amino acid sequences using computer algorithms. Homology modeling is currently the most accurate protein structure prediction method. It can carry out rapid and large-scale structure predictions for TLRs based on those known TLR structures. The resulting models will be useful to infer structure-function relationships and to provide targets for mutagenesis experiments. A large amount of previous research showed the feasibility and reliability of homology modeling applied to structural studies of proteins [7-11].

In this thesis, we focus on model construction and analysis of TLR ligand-binding domains with computational methods. Due to different repeat numbers and distinct arrangements of LRRs contained in TLR ligand-binding domains, a standard homology modeling method failed to predict a proper model. We developed an LRR template assembly method for homology modeling of the ligand-binding domains of

human TLR5-10 and mouse TLR11-13, the crystal structures of which have not been determined. This approach is supported by two databases, TollML and LRRML. Then, we analyzed the models of human TLR7, 8 and 9, which respond to microbial nucleic acids, with a number of protein structure analysis programs to suggest potential ligand-binding residues and possible receptor dimer-ligand complex forms. These results provide determinate targets for further mutagenesis experiments.

Over-activation of the nucleic acid recognition TLRs can lead to autoimmune diseases such as systemic lupus erythematosus [12-15]. Understanding the mechanisms of negative regulation of TLR signaling is highly important for the treatment of autoimmune diseases caused by TLRs. Previous studies showed that SIGIRR (Single immunoglobulin interleukin-1 receptor-related molecule) is an endogenous inhibitor of TLR signaling. Thus, we modeled the cytoplasmic TIR domains of TLR4 and 7, the TLR adaptor protein MyD88 (myeloid differentiation primary response protein 88) and SIGIRR. Through protein-protein docking studies, we suggested models of TIR complexes involved in the TLR inhibition. *In vivo* deletion experiments supported our hypothesis that SIGIRR may exert its inhibitory effect mainly via its BB-loop region.

This dissertation starts with a brief overview (Chapter 1) of the thesis. In Chapters 2-5, the biological background of TLRs, basic theories of protein structure prediction and the research motivation are described. Chapter 6 details the relevant computational methods that were used in this study. Chapter 7 comprises the extended abstracts of six published scientific papers on important aspects of *in silico* structural investigations of TLRs: an LRR template assembly approach for homology modeling of TLR ligand-binding domains, models of ligand-binding domains of human/mouse TLR5-13, structural analyses of human TLR7/8/9 and models of inhibition mechanisms of TLR signaling pathways. Finally, Chapter 8 summarizes our findings and attempts to suggest future studies.

2. Toll-Like Receptors

2.1 Immune System

The immune system can be understood as a network of biological structures and processes that work together to defend the body against attack by foreign "invaders". There are two major divisions of the human immune system, the innate immune system and the adaptive immune systems [16]. The innate immune system is the first-line host defense that provides an immediate but non-specific response against invading pathogens such as bacteria and viruses. The adaptive immune system is the second-line defense that mediates a delayed and specific response [17]. The innate immune recognition relies on a limited number of germline-encoded pattern recognition receptors (PRRs). These PRRs can recognize PAMPs which are unique to microbial pathogens [18]. Recognition of these PAMPs allows the immune system to distinguish infectious non-self from non-infectious self. The adaptive immune responses are essential for control of pathogens that escape elimination by the innate immune response and are important for the development of a long-term immunological memory [16, 19]. Because of its role in the immune memory, the adaptive immune system's contribution to pathogen elimination and vaccine development has been widely studied [20-22].

The PRRs of the innate immune system serve an essential role not only in recognition of pathogens but also in directing the course and type of innate immune responses generated following exposure to foreign antigens. The best understood group of PRRs is the Toll-like receptor (TLR) family [23]. "Toll" originally refers to a cell surface receptor that governs the dorsal-ventral orientation in the early *Drosophila melanogaster* larvae [24]. Together with other antimicrobial peptides it was later found to play a crucial role in antifungal defense in adult *Drosophila* [25]. Sequencing of the *Drosophila* genome revealed nine proteins belonging to the Toll family [26]. Although a function in host defense has so far only been attributed to some of them, it is assumed that each is involved in the host defense against pathogens. In 1997, the first mammalian proteins that are structurally related to *Drosophila* Toll were identified by Medzhitov and co-workers. These receptors were designated as human TLR4 [27]. In turn, Beutler and co-workers used positional cloning to show that TLR4-deficient mice could not respond to lipopolysaccharides [28]. This result identified TLR4 as one of the key components of the receptor for lipopolysaccharides. The progress of genome sequencing projects has led so far to the identification of 13 groups of TLRs in mammalian genomes, ten (TLR1-10) in humans and 13 (TLR1-13) in mice and more than 20 in non-mammalian genomes [29].

2.2 Structure of Toll-Like Receptors

TLRs are type I integral membrane glycoproteins consisting of a ligand-binding ectodomain (500-800 amino acids) and a cytoplasmic signaling domain (TIR domain, ca. 150 amino acids) [30] (Figure 1). The ectodomain contains 17-26 tandem LRR motifs and resembles a solenoid bent into a horseshoe shape. At both ends, there are terminal LRRs (N/C-terminal LRR) that shield the hydrophobic core of the solenoid. All TLR ectodomains are decorated with several N-linked glycans, which are likely to influence receptor surface representation, trafficking and pattern recognition. For example, TLR2 and 4 require glycosylations for function [31]. The ectodomains are highly variable across different TLRs. They are directly involved in the recognition of a variety of PAMPs. In contrast to the ectodomain, the intracellular TIR domain is conserved across all TLRs and shared by downstream signaling adaptor molecules. It contains a central five-stranded parallel β-sheet that is surrounded by a total of five helices on both sides [32] (basic protein structure conceptions introduced in section 3.2). The ectodomain and the TIR domain are joined by a single transmembrane helix stretch (ca. 20 amino acids), which determines the subcellular localization of TLRs [33]. Upon receptor ligation, a TIR signaling complex is formed between the receptor and the adaptor TIR domains [34].
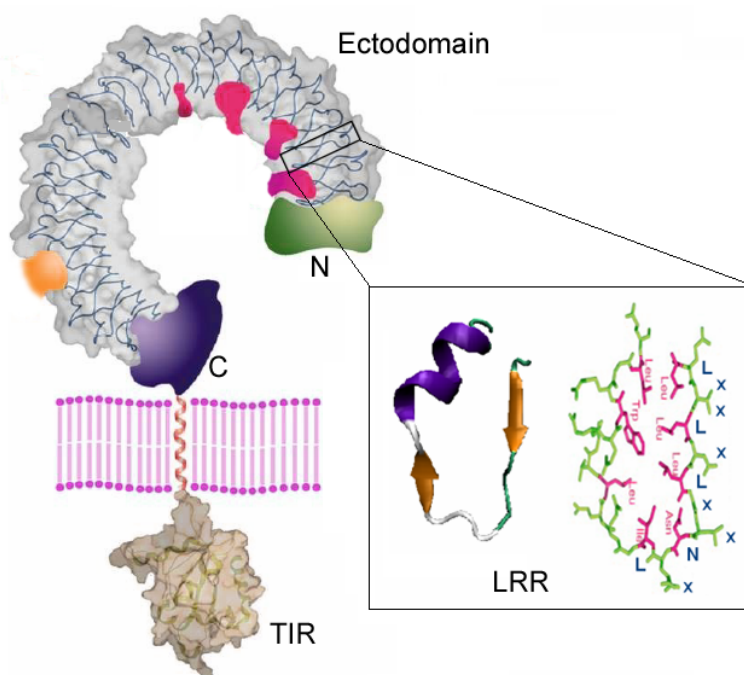

Figure 1: Structure of the TLR and LRR.

LRRs are arrays of 20 to 30 amino acid long protein segments that are unusually rich in the hydrophobic amino acid leucine. An LRR motif can be divided into a highly conserved segment (HCS) and a variable segment (VS) (Figure 1). The HCS consists of an 11 or 12 residue long stretch with the consensus sequence LxxLxLxxN(Cx)xL. Here,

the letter L stands for Leu, Ile, Val or Phe; N stands for Asn, Thr, Ser or Cys; and x is any amino acid. The VS is quite diverse in length and consensus sequence. Accordingly, eight classes of LRRs have been proposed as follows [35, 36]: RI-like (RI), Cysteine-containing (CC), Bacterial (S), SDS22-like (SDS22), Plant-specific (PS), Typical (T), *Treponema pallidum* (Tp) and CD42b-like (CD42b). Of these, the T and S types have been observed in TLRs [37]. Protein domains with LRR architecture form curved or horseshoe-shaped solenoid structures where an LRR is a turn of the solenoid. The concave side of the LRR domain is defined by a parallel β-sheet with each LRR HCS contributing one strand. The strands are interwoven with a variety of structural elements on the convex side, which is constituted by the VSs of LRRs (Figure 1).
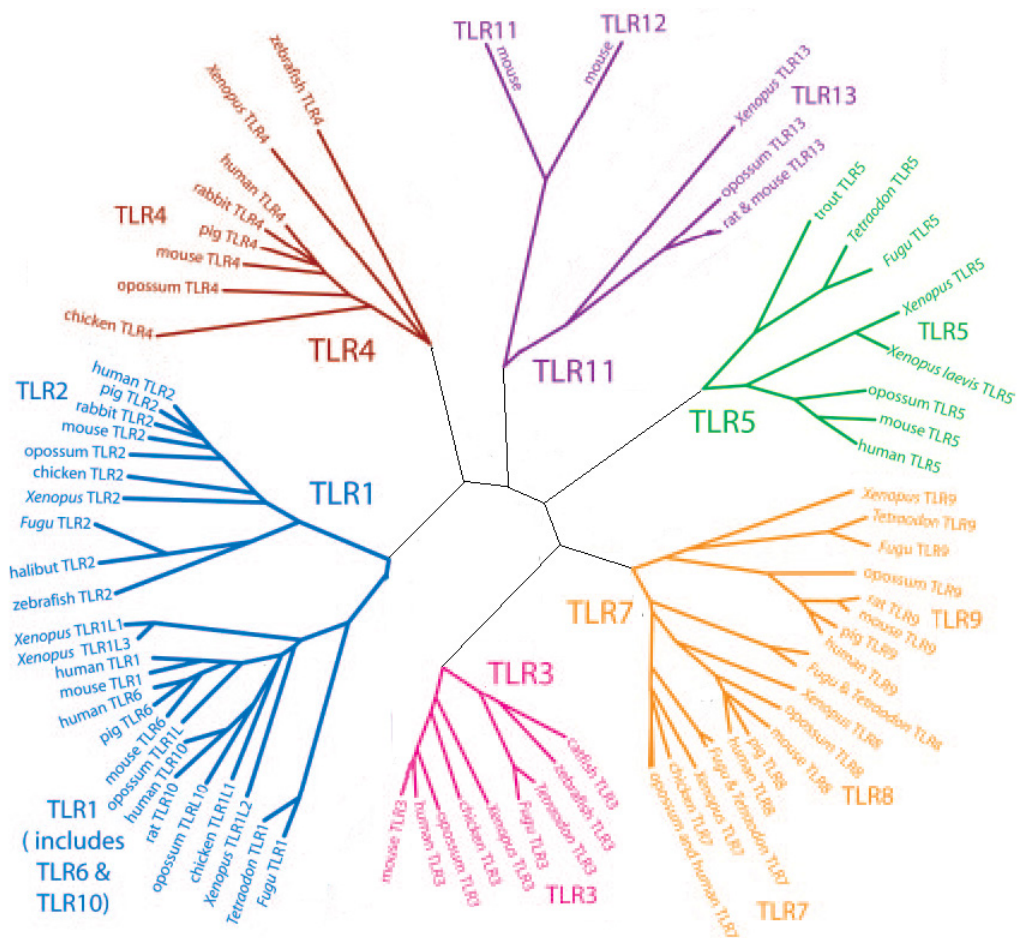
Figure 2: Molecular tree of the vertebrate TLR1-13. Adapted from [38] with permission from the National Academy of Sciences, USA.

TLR protein sequences are now available for a number of vertebrate species. Using these sequences, a complete molecular phylogenetic analysis of the known vertebrate TLRs against the complete sequences of *Takifugu rubripes* TLRs was performed, providing a comprehensive overview (Figure 2) [38]. Accordingly, mammalian TLRs can be divided into six major families. The *TLR1* family consists of TLR1, 2, 6 and 10. This family contains fewer (20-21) LRRs than the other families. TLR3 constitutes the *TLR3* family. It contains 25 LRRs. TLR4 constitutes the *TLR4* family with 23 LRRs.

TLR5 constitutes the *TLR5* family with 22 LRRs. The *TLR7* family consists of TLR7, 8 and 9 and contains 27 LRRs. A remarkable feature of the *TLR7* family is the presence of a less structured region between LRR14 and 15 of the ectodomain. TLR11, 12 and 13 are included into the *TLR11* family, which contains 24-27 LRRs.

2.3 Function of Toll-Like Receptors

TLRs recognize broad classes of PAMPs and are emerging as a central player in initiating and directing immune responses to pathogens [1, 39]. Their ligands are lipoproteins or lipopeptides as recognized by TLR2 complexed with TLR1 or 6, viral double-stranded RNAs (dsRNAs) by TLR3, lipopolysaccharides by TLR4, bacterial flagellins by TLR5, single-stranded RNAs (ssRNAs) and synthetic imidazoquinolines by TLR7 or 8, microbial CpG DNAs by TLR9, and *Toxoplasma gondii* profilin by TLR11 [40]. So far, no ligands have been identified for TLR10, 12 and 13. Table 1 illustrates ligands and localizations of all known mammalian TLRs. TLR3, 7, 8 and 9, all of which recognize nucleic acids, are not expressed on the cell surface like other TLRs but are exclusively expressed in endosomal compartments. In the case of bacterial infection, immune cells engulf bacteria by phagocytosis. The CpG DNA is then exposed after degradation of bacteria in endosomes or endolysosomes. In the case of viral infection, viruses invade cells by endocytosis, and the viral contents (nucleic acids) are exposed to the cytoplasm by fusion of the viral membrane and the endosomal membrane. Thus, the bacterial or viral nucleic acids may be recognized by these endosomal TLRs [41]. Because pathogen and host nucleic acids have very similar structures, these endosomal TLRs may face an extra challenge to induce antipathogen immune responses while avoiding the induction of autoimmune diseases by inappropriate recognition of self nucleic acids. Recent studies have revealed an over-activation of TLR3, 7, 8 and 9 in systemic lupus erythematosus and several other autoimmune diseases [12-15, 42].

TLRs	Ligands	Ligand origins	Localization
TLR1-2	Triacyl-lipopeptides	Bacteria	Cell surface
TLR2	Lipoproteins, lipopeptides	Bacteria	Cell surface
TLR3	Double-stranded RNA, Poly(I-C)	Viruses	Endosome, lysosome
TLR4	Lipopolysaccharides	Gram-negative bacteria	Cell surface
TLR5	Flagellins	Bacteria	Cell surface
TLR6-2	Diacyl-lipopeptides	Mycoplasmas	Cell surface
TLR7, 8	Single-stranded RNA, imidazoquinolines	Viruses, synthetic compounds	Endosome, lysosome
TLR9	Unmethylated CpG DNA	Bacteria	Endosome, lysosome
TLR10	unknown	unknown	Cell surface
TLR11	Profilin	Apicomplexan parasites	Cell surface
TLR12, 13	unknown	unknown	unknown

Table 1: Ligands and localizations of mammalian TLRs.

After the recognition of PAMPs, the TLR intracellular TIR domain recruits adaptor molecules to activate the downstream signaling pathways. The signaling pathways culminate in the induction of antimicrobial factors such as interferons, tumor necrosis factors and interleukins through transcription factors NF-κB and IRFs (Figure 3). Except for TLR3, all TLRs utilize MyD88 as an adaptor protein to recruit downstream signaling molecules including the protein kinases IRAK4 (interleukin-1 receptor type I-associated protein kinases 4), IRAK1 and TRAF6 (tumor necrosis factor receptor-associated factor 6). TRAF6 functions together with a series of ubiquitins that lead to the activation of a protein kinase complex consisting of TAK1, TAB1 and TAB2. The activated TAK1 kinase results in the activation of the IκB kinase and subsequent nuclear translocation of NF-κB. Differently, the TIR domain of TLR3 binds to another adaptor protein TRIF (TIR domain-containing adapter inducing interferon-β), which binds directly to TRAF6 and RIP1 to activate NF-κB or alternatively, binds to TBK1 to activate IRF3 and IRF7. TLR4 can use both the MyD88-dependant and the MyD88-independant (TRIF-dependant) pathways to signal. The TLR signaling pathways, however, must be under tight negative regulation to maintain immune balance to prevent autoimmunity described above. The best-characterized TLR inhibitor is SIGIRR, which can directly interact with the TLR TIR domains and MyD88 TIR domains to reduce or terminate the activation of TLR signaling (detailed in chapter 5).
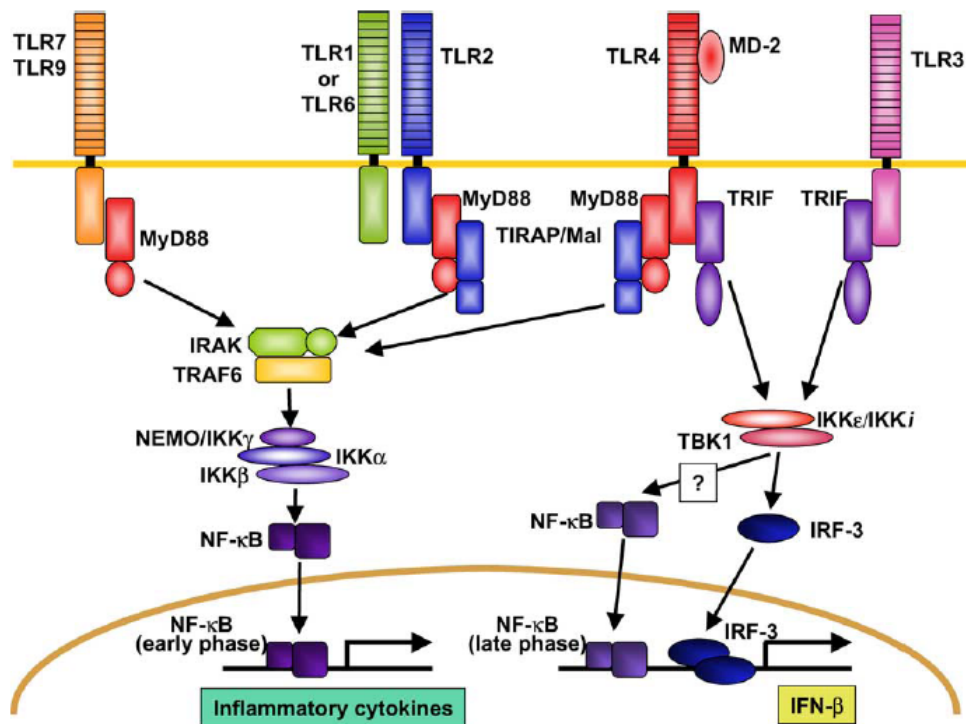
Figure 3: TLR signaling pathways. Adapted from [43] with permission from Elsevier, UK.

3. Protein Structure Prediction

3.1 Overview

Protein structure prediction refers to the effort of generating three-dimensional models from amino acid sequences using computer algorithms [44]. The importance of computational prediction of protein structures is increasing owing to the rapid growth in the number of sequenced genomes and the relatively slow growth in the number of experimentally determined protein structures by X-ray crystallography or NMR methods [45]. In many cases the predicted three-dimensional protein models are highly useful for experimentalists guiding the design of new experiments for further investigations of protein functions. This section describes important conceptions of protein structure and current algorithms of protein structure prediction and analysis.

3.2 Four Levels of Protein Structure

Proteins are polymers of amino acids also called polypeptides. Proteins are not linear molecules. Rather, they fold into intricate three-dimensional structures that are unique to one another. It is this three-dimensional structure that allows proteins to function. The protein structure can be broken down into the following four levels [46] (Figure 4):
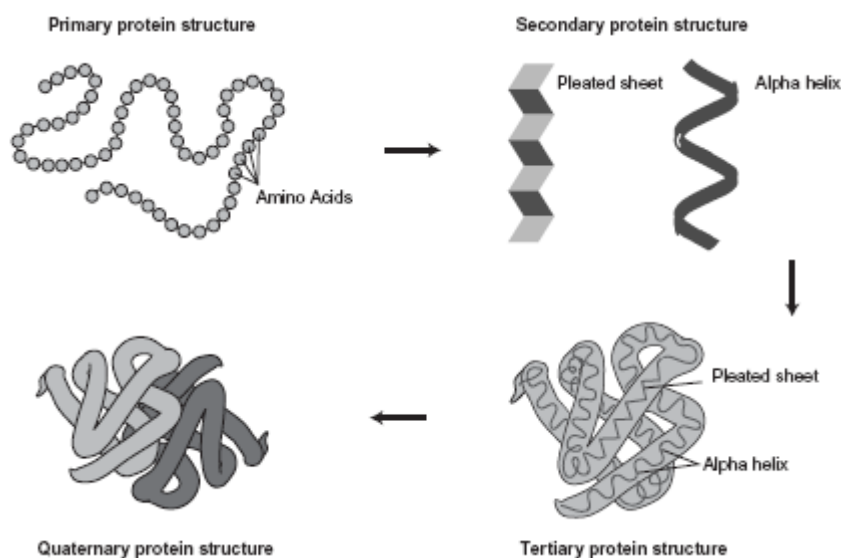
Figure 4: Four levels of protein structures. Figure taken from http://www.genome.gov/.

✧ Primary structure refers to the "linear" sequence of amino acids.

✧ Secondary structure is the "local" ordered structure brought about via hydrogen bonding mainly within the peptide backbone. The most common secondary structure elements in proteins are the α-helix and β-sheet.

◇ Tertiary structure is the "global" folding of a single polypeptide chain. A major driving force in determining the tertiary structure of globular proteins is the hydrophobic effect. The polypeptide chain folds such that the side chains of the non-polar amino acids are "hidden" within the structure, and the side chains of the polar residues are exposed on the outer surface.

◇ Quaternary structure involves the association of two or more polypeptide chains into a multi-subunit structure. Not all proteins exhibit quaternary structure. Quaternary structures are stabilized mainly by non-covalent interactions: hydrogen bonding, van der Waals interactions and ionic bonding.

3.3 Protein Structure Prediction

The prediction of the three-dimensional structure of a protein indicates the prediction of a protein's tertiary structure from its amino acid sequence. Protein structure prediction techniques fall into three categories [45]:

1) Homology modeling

Homology modeling, also called comparative modeling, exploits the fact that evolutionarily related proteins with similar sequences, as measured by sequence identity, have similar structures. The sequence identity is defined by the percentage of identical residues at each position based on an optimal sequence alignment. The sequence identity defines the branch length between two protein nodes in a phylogenetic tree (as demonstrated in Figure 2). The modeling procedure can be divided into a number of steps [47] (Figure 5). First, suitable template(s) (sequence identity ≥ 30%) related to the target sequence are selected from the Protein Data Bank (PDB) [48]. The PDB is the single worldwide repository for the processing and distribution of three-dimensional structural data of large molecules of proteins and nucleic acids. PDB accepts only experimentally derived structures. The Basic Local Alignment Search Tool (BLAST) of PDB can find sequence-similar protein structures for a query protein sequence. Second, an alignment of the target sequence to the template(s) is generated. A protein sequence alignment is an arrangement of two or more protein sequences that represents the evolutionary relationship among the sequences. Gaps are inserted between the residues so that identical or similar amino acids are aligned in successive columns. Third, coordinates of the three-dimensional model are built based on the alignment and template structures. This step can be divided into two main trends. One is to model the structure by copying the coordinates of the template in the aligned core regions. The variable regions are modeled by taking fragments with similar sequences from a database of previously observed loops. Then, the mutated side chains are replaced with rotamers that satisfy the stereochemical criteria, together with limited energy optimization. This algorithm is implemented by SWISS-MODEL [49]. The other possibility is to use the distance and torsion angles and interatomic distances from

the aligned regions of the template as modeling constraints, which permits the use of information from multiple, possibly conflicting, structures. This approach also requires the idealization of the geometry of the entire chain with constraints derived from a database of protein structures. MODELLER is a well-known program that implements this algorithm. [50]. Last, the previous steps are repeated according to the model evaluation to refine the model until acceptable results are obtained. Model evaluation tools and their working principles are detailed in section 6.2.
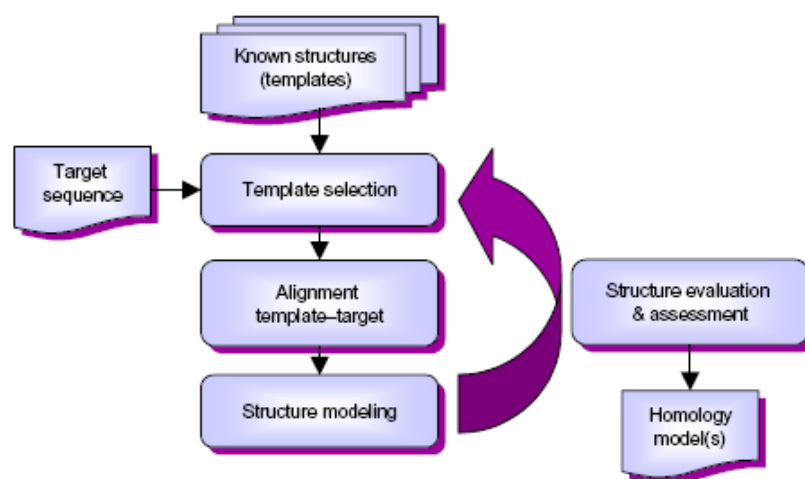

Figure 5: Flowchart of homology modeling. Adapted from [51] with permission from Future Medicine Ltd, UK.

2) Protein threading

Protein threading, also called fold recognition, uses a database of known three-dimensional protein structures (templates) to match a query protein sequence. This is accomplished by the aid of a scoring function that assesses the fit of the query sequence to a given template structure. The scoring function is usually derived from the template database and includes pairwise atom contact and solvation terms, e.g., the Z-score function. The template with the best score is assumed to be the one adopted by the sequence.

3) Ab initio modeling

The "thermodynamic hypothesis" states that the amino acid sequence perfectly determines the native three-dimensional structure of a protein, and the native structure is the one for which the free energy achieves the global minimum [52]. This inspires ab initio methods in protein structure prediction. Ab initio methods make structure predictions without using any structural information of previously solved protein structure; instead, they are entirely based on the first principles of physics. All energetics involved in the folding process of a protein are calculated by energy functions, and the structure with the lowest free energy is found.

Homology modeling is mainly used for detailed (e.g., all heavy-atoms) structure prediction when a query protein has a close homolog (sequence identity $\geq$ 30%) in the

PDB. If there is no homolog for the query protein, protein threading is used for template recognition and backbone structure prediction. If protein threading fails to detect a suitable template (i.e., no template with a Z-score better than a cutoff value), ab initio modeling should be selected. In this work, we focused mainly on the homology modeling approach. The TLR family comprises homologous TLR members as illustrated in Figure 2. The determined crystal structures of TLRs (see section 4.1) supplied useful sources of homologous templates for the TLRs with unknown structures.

3.4 Molecular Docking

Protein-protein interactions and protein-nucleic acid interactions are important for numerous biological processes. In general, the molecular interactions are driven by four kinds of forces [53]: electrostatic forces (caused by complementary charges), electrodynamic forces (van der Waals interactions), steric forces (caused by entropy) and solvent-related forces (hydrophobicity/hydrophilicity). Moreover, the interaction sites of the interacting molecules usually have a high shape complementarity [54]. Thus, the interaction sites of proteins can be theoretically predicted, given the three-dimensional structures or models of the interacting molecules. Molecular docking is a computational approach that models the quaternary structure of complexes formed by two or more interacting molecules as they would occur in a living organism. There are two categories of docking: protein-protein docking and protein-nucleic acid docking. In the protein-protein docking, if a small protein molecule ($\leq$ 30 residues) is docked onto a relative large protein receptor or enzyme, it is called protein-ligand docking. The protein-ligand docking is widely used in the rational design of drugs. If the bond angles, bond lengths and torsion angles of the components are not modified at any stage of complex generation, it is called rigid-body docking. The rigid-body docking showed success in predicting interactions between rigid globular protomers in protein complexes [55]. When substantial conformational changes occur within the components during complex formation, the rigid-body docking is inadequate. In this case a flexible docking that permits conformational changes during complexing is needed. However, to enumerate all possible conformational changes is prohibitively time-consuming. The flexible docking therefore checks only a small subset of possible conformational changes.

Docking itself produces a large number of plausible candidate interacting conformations. These candidates are evaluated and ranked by different scoring functions to identify structures that are most likely to occur in nature. A helpful way, if possible, to reduce the top-scoring false positive poses is to consider some restrictions from the known data, such as experimentally identified essential interacting residues, steric compatibility with other molecules or membranes, and residue conservation across species. A number of docking programs are described in section 6.3.

16

4. Structure Predictions of TLR Ligand-Binding Domains

4.1 Overview

Although experimental methods have provided high-resolution structures for only several TLR ligand-binding domains, computational prediction methods will provide valuable structural information for the majority of TLR sequences whose structures are not yet solved experimentally. In this section, we highlight the essentiality of structure prediction of TLRs and describe a template assembly strategy for homology modeling of a series of TLR ligand-binding domains.

4.2 Crystal Structures of TLR Ligand-Binding Domains

In 2005, Choe and co-workers and later Bell and co-workers first reported crystal structures of monomeric human TLR3 ligand-binding domains in atomic detail. They represent the first insight into the molecular basis of TLR recognition. The overall structure of TLR3 ligand-binding domain is that of a large horseshoe-shaped solenoid with an inner diameter of 42 Å, an outer diameter of 90 Å and a thickness of 35 Å [56] (Figure 6). The concave inner surface consists of a large parallel β-sheet with each β-strand roughly perpendicular to the solenoid axis and linked to the next strand by an irregular loop. The molecular surface of the TLR3 is abundantly and unevenly populated with N-linked carbohydrates. Notably, one face of the horseshoe is completely devoid of any glycosylation [57]. Later, the crystal structure of liganded TLR3 determined by Liu et al. (2008) proved that it is just the glycosylation-free face that binds to the dsRNA ligand. Until now, four crystal structures of human or mouse TLR-ligand complexes, TLR1-TLR2-lipopeptide (Pam3CSK4), TLR4-MD-2-lipopolysaccharides, TLR3-dsRNA and TLR6-TLR2-lipopeptide (Pam2CSK4) have been determined [2-5]. They provide experimental evidence for how these receptors bind to a remarkably large variety of ligands and how the agonists induce dimerization of the receptors.
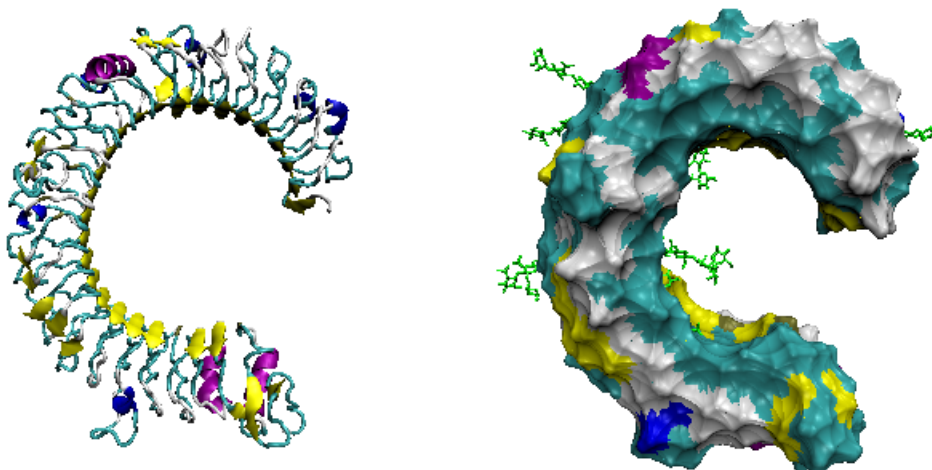
Figure 6: Overview of TLR3 ligand-binding domain structure in carton representation (left) and in secondary structure surface representation (right). The N-linked glycans are shown as green ball-and-stick (right).

In the TLR1-TLR2 complexes, the lipid chains of the triacyl-lipopeptide Pam3CSK4 bridge both receptors; two of the three lipid chains are inserted into an internal pocket in TLR2, and the remaining amide-bound lipid chain is inserted into a narrower channel in TLR1 (Figure 7A). Different from the TLR1-TLR2 complex, the TLR6-TLR2 complex recognizes diacyl-lipopeptide Pam2CSK4 which lacks the amide-bound lipid chain. The only two lipid chains of Pam2CSK4 are inserted into a large internal pocket in TLR2 (Figure 7D). The molecular interface of TLR2-TLR6 is greatly increased compared with TLR2-TLR1, which compensates for the lack of interactions between the amide-bound lipid chain and TLR6. TLR3 has multiple intermolecular contacts that stabilize the complex (Figure 7B). The dsRNA interacts with both an N-terminal and a C-terminal site on the glycan-free surface of each TLR3 ligand-binding domain, which are on opposite sides of the dsRNA, with the C-termini in contact and the N-termini outstretched at opposing ends of the linear dsRNA molecule. In the TLR4-MD2-lipopolysaccharides complexes, the lipopolysaccharide interacts with a large hydrophobic pocket in MD-2 and directly bridges the two components of the multimer (Figure 7C). Five of the six lipid chains of lipopolysaccharides are buried deep inside the pocket and the remaining chain is exposed to the surface of MD-2, forming a hydrophobic interaction with the conserved phenylalanines of TLR4.

All of these complexes reveal an M-shaped architecture. In these dimeric arrangements, the C-termini of the ectodomains of TLRs converge in the center, and such a convergence should bring the two intracellular TIR domains close together and so promote their dimerization.
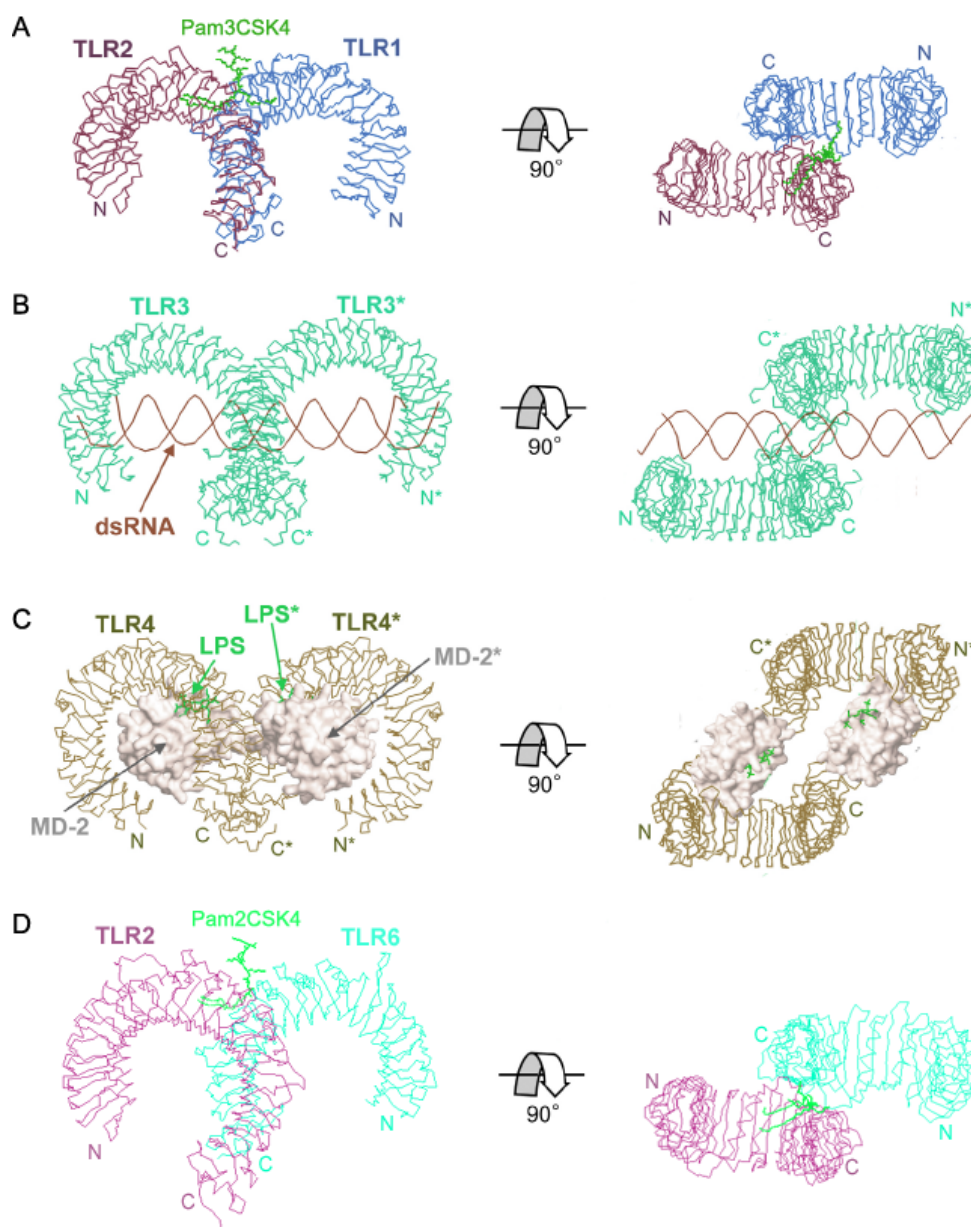
Figure 7: Crystal structures of TLR ligand-binding domains complexed with ligands.

4.3 An LRR Template Assembly Approach for Homology Modeling of TLR Ligand-Binding Domains

As described in section 3.3, the quality of the homology models strongly depends on the sequence identity between the target and template. Below 30% identity, serious errors may occur [58]. Standard homology modeling approaches search full-length templates that cover the complete or the major parts of a target protein sequence from the PDB [48]. Nevertheless, a proper full-length template with a sufficiently high sequence identity to the ligand-binding domain of TLRs is often missing due to different repeat numbers and distinct arrangements of LRRs contained in TLRs. For

instance, the full-length sequence identities between the human TLR5 ligand-binding domain (structure unknown) and the structure-known TLRs, TLR1 (PDB code: 2Z7X:B), TLR2 (2Z7X:A), TLR3 (2A0Z:A), TLR4(3FXI:A) and TLR6 (3A79:B), are 18.4%, 18.0%, 23.9%, 23.5% and 20.9%, respectively. They are much lower than the cutoff value 30%. This limitation can be overcome by assembling multiple LRR templates. In this approach, the most similar (on the sequence level) single LRR with a known structure is searched for each LRR in the target sequence as a local template. Such an LRR template may be derived from TLR structures or from other protein structures. Thereby, a suitable template may be found even for an insertion-containing irregular LRR in the target. All local template sequences are then combined to generate a multiple sequence alignment for the complete target sequence. In this way, a high-quality model can be created, even if no adequate single template is available.
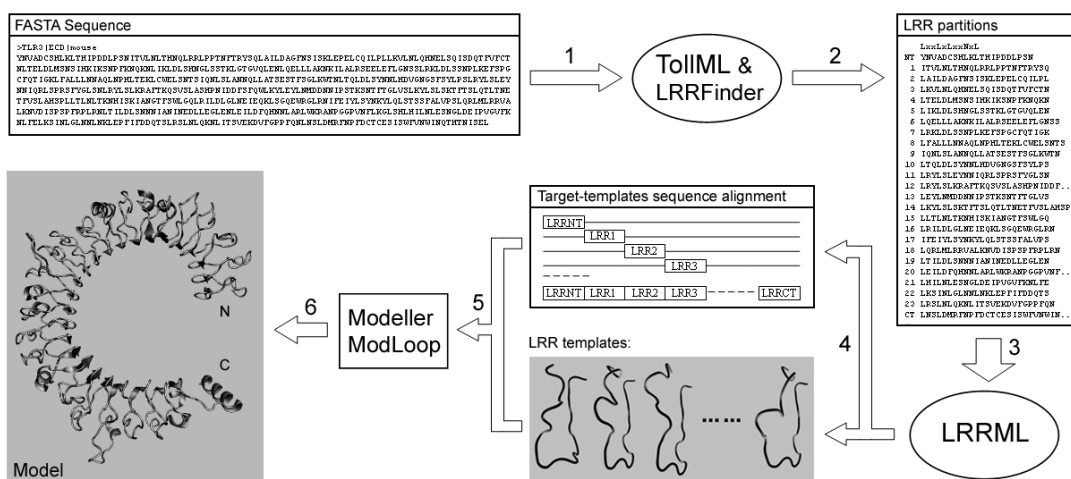

Figure 8: Flowchart of the LRR template assembly approach. A target sequence of a TLR ligand-binding domain is partitioned into LRR segments by TollML or LRRFinder. Then LRRML provides an optimal individual LRR structural template for each target LRR segment and generates target-template alignments. Next, the templates and the sequence alignments are inputted into an automatic model construction program to obtain a three-dimensional model.

To facilitate the multiple template assembly of LRR domains of TLRs, we have developed the LRRML database [59], which archives individual LRR structures manually identified from all known LRR protein structures (detailed in section 7.1). The suffix "ML" indicates that the database is supported by the extensible markup language (XML) technology (http://www.w3.org). In addition, we have developed TollML [6], a database of sequence motifs of TLRs. In TollML, all known sequences of TLR ectodomains were semi-automatically partitioned into LRR segments and are made available for query (detailed in section 7.2). For newly sequenced TLRs that are not yet archived in TollML, we have implemented an LRR prediction program named LRRFinder on the TollML webpage. It requires as input an LRR-containing amino acid sequence and returns the number and positions of LRRs in the input sequence. With the help of these two databases, LRR partitions of a TLR ectodomain can be directly obtained, and an optimal structure template for each LRR segment can be quickly found.

20

A schematic flowchart of the modeling procedure is shown in Figure 8. This LRR assembly method was successfully evaluated with the crystal structures of mouse TLR3 and 6, and was superior to a standard full-length template-based method.

4.4 Homology Models of TLR5-13 Ligand-Binding Domains

As mentioned above, 13 groups of TLRs have been found in mammalian genomes, ten in humans (TLR1-10) and 13 in mice (TLR1-13). The crystal structures of human/mouse TLR1-4 and mouse TLR6 ligand-binding domains were determined during the last six years. To enable first insight into the structural basis of receptor-ligand interactions of the structure-unknown TLRs, we modeled the human TLR5-10 and mouse TLR11-13 ligand-binding domains with our LRR template assembly method (detailed in section 7.3). Before these models were constructed, we modeled mouse TLR3 as a test case. We assumed that the structure of the TLR3 ligand-binding domain was unknown and excluded the LRRs of human and mouse TLR3 from the LRRML database before template selection. Our model was very well superimposed with the crystal structure of mouse TLR3, in particular at both of its ligand-binding sites. Moreover, we also compared our resulting model of human TLR6 with the crystal structure of mouse TLR6. They showed a high structural agreement. These values indicated that the models predicted with our method are high quality and can be used to predict potential ligand-binding sites.

TLR7, 8 and 9 are closely related and comprise a subfamily with a longer amino acid sequence than other TLRs. They are intracellularly localized and signal in response to non-self nucleic acids. They also contain an irregular segment, which is treated as an undefined region [36, 37, 60], following the LRR14. A recent study indicated that TLR7 and 9 exit the endoplasmic reticulum and travel to endolysosomes. The ectodomains of TLR7 and 9 are cleaved at the irregular segment upon arriving in the endolysosomes [61]. Only the rear parts (LRR15-26) are capable of binding ligand and recruiting MyD88 adaptor on activation. This cleavage process may also happen to TLR8 because of the high homology between TLR7/8/9 [61]. Based on this finding, we modeled the cleaved forms of TLR7/8/9 ectodomains and predicted potential ligand-binding residues and possible configurations of the receptor-ligand complex (detailed in section 3.1).

5. Models of SIGIRR Inhibiting the TLR4 and 7 Signaling Pathways

SIGIRR, also known as TIR8 (Toll/interleukin-1 receptor 8), is another TIR domain-containing transmembrane protein. Its TIR domain cannot activate NF-κB because it lacks two essential amino acids (Ser447 and Tyr536) [62]. Its small single extracellular immunoglobulin domain does not support ligand binding. SIGIRR rather acts as an endogenous inhibitor of MyD88-dependent TLR signaling because overexpression of SIGIRR in Jurkat or HepG2 cells substantially reduced the lipopolysaccharide activation of NF-κB [63-65]. Although TLRs recognize a variety of structures derived from pathogens leading to subsequent initiation of the relevant immune responses, they are also crucial in the induction and perpetuation of certain autoimmune diseases. For example, TLR7, 8 and 9 overstimulation by self RNA and DNA is an important mechanism involved in promoting systemic lupus erythematosus and psoriasis [15, 66]. In this vein, SIGIRR might contribute to the control of TLR-mediated autoimmunity. Lech et al. (2008) reported that, compared with wild type mice, *Sigirr*-deficient mice develop excessive lymphoproliferation when introduced into the context of a lupus susceptibility gene [67]. However, SIGIRR's inhibition mechanism remains unknown owing to a lack of structural information.

We constructed models for intracellular TIR domains of TLR4, TLR7, MyD88 and SIGIRR using homology modeling. Because the TIR domain is a highly conserved protein module, the determined crystal structures of TIR domains of human TLR1, 2, 10 and IL-1RAPL (interleukin-1 receptor accessory protein-like) [32, 68, 69] could serve as closely homologous full-length templates. Through protein-protein docking studies, we developed models of essential TIR complexes involved in the TLR4 and 7 signaling and the SIGIRR inhibiting processes. We suggested that SIGIRR might exert its inhibitory effect by blocking the molecular interface of TLR4, TLR7 and the MyD88 adaptor mainly via its BB-loop region (detailed in section 7.5). *In vivo* deletion experiments indicated that lack of the BB-loop completely abrogated SIGIRR's inhibitory effect on TLR7 signaling, in accordance with our hypothesis.

6. Methods

6.1 Protein Modeling

This section lists important methods that were used for the three-dimensional protein model construction and refinement.

MODELLER [70] is one of the most widely used computer programs for homology modeling of protein three-dimensional structures. In the simplest case, the input is an alignment of a sequence to be modeled with the sequence(s) of the template structure(s), and the atomic coordinates of the template(s). MODELLER then automatically calculates a model containing all non-hydrogen atoms. It implements homology modeling by satisfaction of spatial restraints, by which a set of geometrical criteria are used to create a probability density function for the location of each atom in the protein.

ModLoop [71] is a web tool for automated modeling of loops in protein structures. The inputs are the atomic coordinates of a protein structure in PDB format and the specification of the starting and ending residues of one or more segments to be modeled, containing no more than 20 residues in total. The output is the coordinates of the non-hydrogen atoms in the modeled segments. The modeling relies on a protocol consisting of a conjugate gradient minimization and a molecular dynamics simulation.

THREADER [72] is a protein fold recognition method, whereby a query sequence is fitted (threaded) directly onto the carbon backbone coordinates of non-redundant protein structures derived from the PDB. The degree of compatibility between the sequence and each proposed structure is evaluated through a set of empirical potentials derived from proteins of known structure. The specific aspect of this approach is that the matching of sequence to backbone coordinates is performed in full three-dimensional space, incorporating specific pair interactions explicitly.

pGenTHREADER [73] is a sequence profile-based structural template recognition method for protein homology modeling. It calculates sequence profiles from an input sequence and generates profile-profile alignments of the input and template sequences. The algorithm of the alignments linearly combines secondary structure-specific gap-penalties, pair potentials and solvation potentials. The output is the PDB structures that serve as candidate templates ranked by target-template similarities.

PSIPRED [74] is a protein secondary structure prediction method. It performs a PSI-BLAST search [75] for a query sequence and then feeds the resulting profiles of the query through two consecutive feed-forward neural networks (a machine learning algorithm) to predict secondary structure.

6.2 Model Evaluation

All protein model quality assessment programs used in this study are listed below.

PROCHECK [76] provides a check on the stereochemistry of a three-dimensional protein structure or model. Its outputs comprise a number of plots, such as the Ramachandran plot [77] and a comprehensive residue-by-residue listing. These provide an assessment of the overall quality of the structure compared with well-refined structures of the same resolution and also highlight regions that may need further investigation.

ProQ [78] is a neural network-based method to predict the quality of a protein model. It extracts structural features from an input model, such as the frequency of atom-atom contacts, and measures them either by LGscore [79] (for long target proteins) or MaxSub [80] (for short proteins).

ModFOLD [81] combines scores obtained from the ModSSEA method [82], the MODCHECK method and the two ProQ methods using a neural network. It can provide the following: (i) a single score and a P-value, which represents a quantitative measure of the confidence in a model related to the predicted quality of a single protein model; (ii) rankings for multiple models for the same protein target according to predicted model quality; and (iii) predictions of the local quality (per-residue errors) within multiple models.

MetaMQAP [83] is an up-to-date protein model evaluation tool. It is a meta-predictor-based on a multivariate regression model, which uses scores from eight previously published model evaluation methods. MetaMQAP predicts the absolute deviation (in Ångströms) of individual Cα atoms between the model and the unknown true structure as well as global deviations (expressed as root mean square deviations).

6.3 Docking

As described in section 3.4, there are two categories of docking: protein-protein docking and protein-nucleic acid docking. In this study, two protein-protein docking methods and five protein-nucleic acid docking methods were used.

6.3.1 Protein-Protein Docking

GRAMM-X [84] uses the correlation technique Fast Fourier Transformation (FFT) for the global search of the best rigid-body conformations. During the FFT search, the protein surface representation is smoothed to account for possible conformational changes upon binding. The search results are further refined by optimization in continuous coordinates and rescoring with several knowledge-based potential terms.

ZDOCK [85] is also an FFT search-based rigid-body docking method. An important feature of ZDOCK is that it employs a powerful scoring function, which integrates pairwise shape complementarity, desolvation and electrostatics during the FFT search.

6.3.2 Protein-Nucleic Acid Docking

BindN [86] takes an amino acid sequence as input and predicts potential DNA or RNA-binding residues using a statistics-based machine-learning model, a support vector machine (SVM) [87]. This machine was trained by protein datasets with known DNA or RNA-binding residues selected from PDB. Three sequence features from the training proteins were considered: the side chain pKa-value, hydrophobicity index and molecular mass of an amino acid.

DP-Bind [88] is a web server for predicting DNA-binding sites in a DNA-binding protein from its amino acid sequence. The web server implements three machine learning methods: SVM, kernel logistic regression (KLR) [87] and penalized logistic regression (PLR) [87]. An input can be either a sequence alone or an automatically generated profile of evolutionary conservation in the form of PSI-BLAST position-specific scoring matrix. The training data were taken from PDB.

DBS-PRED [89] makes use of two features of a query protein sequence, the amino acid composition and the sequence neighborhood/solvent accessibility, to predict the DNA-binding residues. A neural network was trained to recognize the relationship between the protein features and the DNA-binding sites. The training data were taken from the PDB and Swiss-Prot [90].

DBSPSSM [91] is a neural network-based method to utilize evolutionary information of amino acid sequences in terms of their position-specific scoring matrixes for predictions of DNA-binding site. The training data were taken from the PDB.

PreDs [92], different from the above methods, predicts DNA-binding sites from three-dimensional coordinates in PDB format instead of from an amino acid sequence. PreDs calculates the shapes (local and the global average curvatures) and the electrostatic potential of the molecular surface of the query protein. Then, the method judges whether each vertex on the molecular surface is likely to appear at a DNA-binding site or not, based on statistics derived from PDB structures of protein-DNA complexes.

6.4 Model Visualization and Analysis

Several model visualization programs with numerous built-in scripts were used in this study. They provide necessary help in displaying and analyzing protein structures and rendering figures.

VMD [93] is a molecular graphics program designed for the display and analysis of biopolymers such as proteins and nucleic acids. Molecules are displayed as one or more "representations", in which each representation embodies a particular rendering method and coloring scheme for a selected subset of atoms. VMD contains a set of tools for interactive problem solving in structural biology.

SPDBV [94] is a molecular graphics program that provides a user-friendly interface allowing to analyze several proteins simultaneously. A useful function of SPDBV is that the protein structures can be superimposed to deduce structural alignments and compare their active sites or any other relevant parts. Amino acid mutations, H-bonds, angles and distances between atoms can be obtained using the intuitive graphic and menu interface.

SuperPose [95] is a web server for both pairwise and multiple protein structure superpositions using a modified quaternion eigenvalue approach. SuperPose generates sequence alignments, structure alignments, PDB coordinates, root mean square deviation statistics and difference distance plots and images of the superimposed molecules.

PISA [96] is an interactive tool for the exploration of macromolecular (protein, DNA/RNA and ligand) interfaces, prediction of probable quaternary structures, database searches of structurally similar interfaces and assemblies and searches on various assembly and PDB entry parameters.

Additionally, **Jalview** [97] was used to view and edit multiple sequence alignments. It allows the identification of functional residues by comparison of subgroups of sequences arranged on a cluster tree. A number of color schemes were predefined to color alignments or groups.

7. Results (Extended Abstracts of Manuscripts)

7.1 Paper 1: LRRML: A Conformational Database and An XML Description of Leucine-Rich Repeats (LRRs)

(Manuscript see Appendix at page 45)

Leucine-rich repeats (LRRs) are present in more than 6,000 proteins. They play an important role in protein-ligand interactions. To date, more than 100 crystal structures of LRR proteins have been determined. This knowledge has increased our ability to use the crystal structures as templates to model the TLR ligand-binding domains and other LRR proteins with unknown structures. Because the individual three-dimensional LRR structures are not directly available from the established databases and there are only a few detailed annotations for them, a conformational LRR database useful for homology modeling of LRR proteins is desirable. We developed LRRML, a conformational database and an extensible markup language (XML) description of LRRs. The release 1.4 contains 1,475 individual LRR structures, which were identified from 130 PDB protein structures. All LRR entries are provided with three groups of manual annotations: first, classification into eight LRR types; second, partition into a highly conserved segment (HCS) and a variable segment (VS); and third, labeling of insertion segments longer than three amino acids according to LRR consensus sequences. In addition, an XML document type definition (DTD) was specified to exchange and store the LRRs. A construction pipeline is shown in Figure 9.
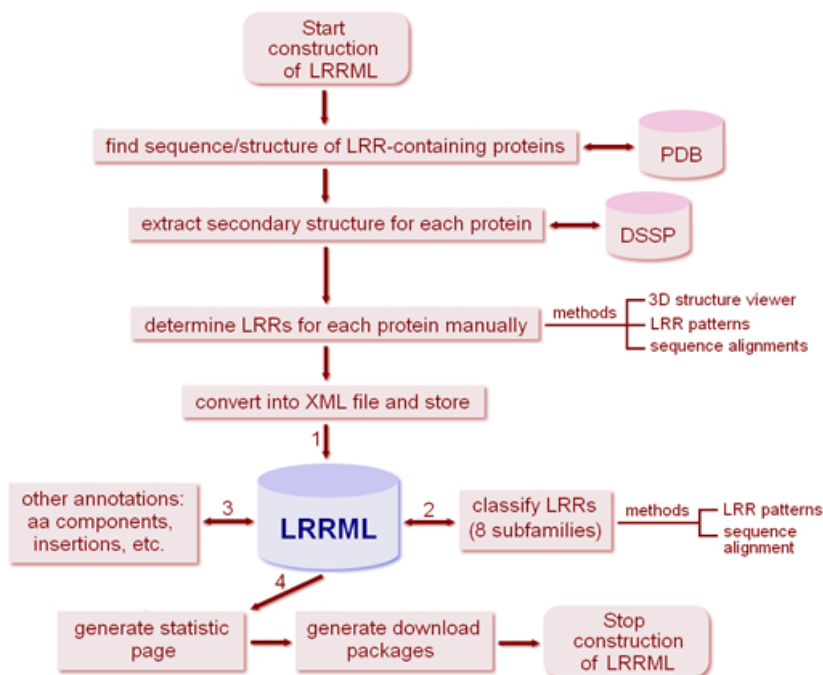

Figure 9: Construction pipeline of the LRRML database.

Through a similarity search against LRRML, the most similar individual LRR structural template can be found for each LRR segment contained in a query protein sequence. A target-template alignment will also be generated. This is a key step towards homology modeling of TLR ligand-binding domains using the LRR template assembly approach. To demonstrate the capabilities of the database, we modeled the mouse Toll-like receptor 3 ectodomain as a test case by combining multiple LRR templates obtained from LRRML. A comparison of the model with the crystal structure (PDB code: 3CIG) showed a very good structural agreement. In conclusion, LRRML provides a source for homology modeling and structural analysis of LRR proteins. This database is available at http://lrrml.lrz.de/.

7.2 Paper 2: TollML: A Database of Toll-like Receptor Structural Motifs

(Manuscript see Appendix at page 55)

Systematic and accurate motif partitions, in particular the leucine-rich repeats (LRRs) partitions, of Toll-like receptors (TLRs) are fundamental to modeling the three-dimensional structures of TLRs. Such partitions are not available in any current protein databases. In this regard, we developed the TollML database.

TLRs have become the focus of a tremendous research interest because of their crucial role in the innate immune system. A central repository for the growing amount of relevant TLR sequence information has been created. Nevertheless, structural motifs of most TLR protein sequences, such as leucine-rich repeats (LRRs), are poorly annotated in the established databases. A database that organizes the structural motifs of TLRs can be useful for developing pattern recognition programs and structural modeling of TLRs. We describe TollML, a database that integrates all of the TLR sequencing data from the NCBI protein database. Entries were first divided into TLR families (TLR1-23) and then semi-automatically subdivided into three levels of structural motif categories: (1) signal peptide (SP), ectodomain (ECD), transmembrane domain (TD) and Toll/IL-1 receptor (TIR) domain of each TLR; (2) LRRs of each ECD; (3) highly conserved segment (HCS), variable segment (VS) and insertions of each LRR. These categories can be quickly searched using an easy-to-use web interface and dynamically displayed by graphics. Additionally, all entries have hyperlinks to various sources including NCBI, Swiss-Prot, PDB, LRRML and PubMed in order to supply broad external information for users. The release 3.1 contains 2,572 TLR entries divided into 23 families. A total of 46,720 LRR motifs were recognized from these TLR entries. The database is available at http://tollml.lrz.de/.

7.3 Paper 3: A Leucine-Rich Repeat Assembly Approach for Homology Modeling of Human TLR5-10 and Mouse TLR11-13 Ectodomains

(Manuscript see Appendix at page 63)

Crystal structures are currently missing for most Toll-like receptor (TLR) ligand-binding ectodomains. Thus, their ligand recognition mechanisms are poorly understood. Computational approaches enable rapid large-scale predictions of their three-dimensional structures. The TLR ectodomains are composed of varying numbers and types of leucine-rich repeats (LRRs). Although the determined crystal structures of TLR ectodomains can provide structural templates for homology modeling of other TLR ectodomains, the quality of the predicted models that are generated from these full-length templates can be limited due to low sequence identity (< 30%) between the target and template.

To obtain better templates for modeling, we have developed an LRR template assembly approach. Individual LRR templates that are locally optimal for the target sequence are assembled into multiple templates. Two test cases underlined the feasibility and reliability of the method. First, two models of mouse TLR3 were constructed using a standard full-length template method (model 1, Figure 10a) and our LRR template assembly method (model 2, Figure 10b). Model 2 was very well superimposed with the crystal structure (PDB code: 3CIG, Figure 10c) at both of its ligand-binding regions. The backbone root mean square deviations (RMSDs) were 1.96 Å and 1.90 Å, respectively. By contrast, model 1 showed serious structural disorder spanning from LRR6 through LRR10. Second, another two models of human TLR6 were constructed using a standard full-length template method (model 3, Figure 10d) and our LRR template assembly method (model 4, Figure 10e). Both models well matched the crystal structure of mouse TLR6 (3A79, residue ID 33-474, Figure 10f), with backbone RMSDs of 1.89 Å and 1.94 Å, respectively. In the first test case, there was no proper full-length template for the target protein. Therefore, the standard method failed to produce a realistic model. In the second test case, the structure of human TLR1 (2Z7X) provided an excellent full-length template for TLR6 because TLR1 and TLR6 possess the same number of LRRs and have a high sequence identity (63.3%). Under these very good conditions, both, the standard and our approaches, provided high-quality models. These comparison results proved that our method reveals its particular strength in situations where no adequate full-length templates are available.

With this method we constructed ectodomain models of human TLR5, TLR6, TLR7, TLR8, TLR9 and TLR10, and mouse TLR11, TLR12 and TLR13 that can be used as first passes for a computational simulation of ligand-docking or to design mutation experiments. As an application example, we performed molecular electrostatics calculations of the mouse TLR11 model with a parasite profilin ligand. The results show that the entire surface of the profilin of *Plasmodium falciparum* (PDB code: 2JKF)

is predominantly negatively charged, whereas TLR11 exhibits several positively charged patches. Furthermore, protein-protein docking studies using GRAMM-X show that profilin and the positive patches on TLR11 possess compatible sizes and electrostatic complementarity.
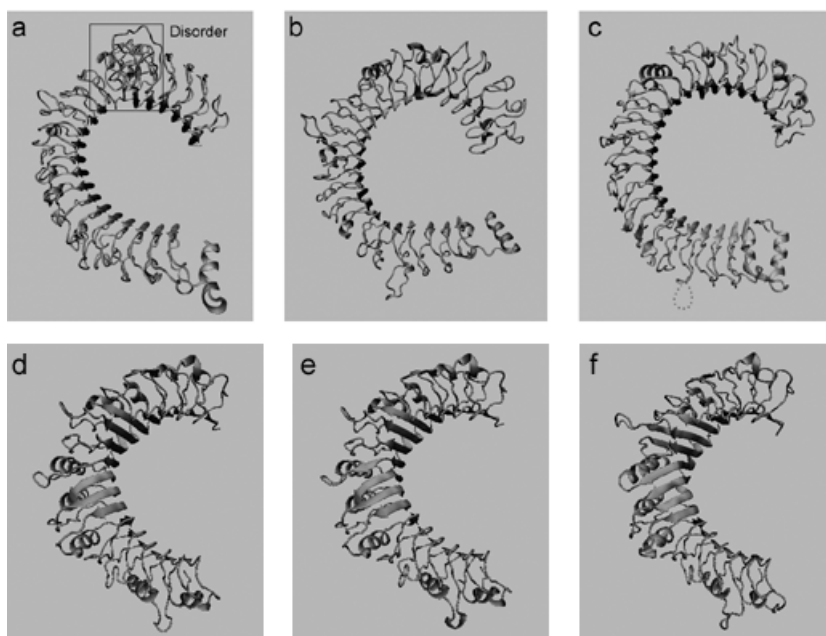

Figure 10: Homology models and crystal structures of TLR3 and six ectodomains. (a) The mouse TLR3 model based on the standard method. The framed region exhibits serious disorder. (b) The mouse TLR3 model based on the LRR template assembly method. (c) The crystal structure of mouse TLR3 (PDB code: 3CIG). (d) The human TLR6 model based on the standard method. (e) The human TLR6 model based on the LRR template assembly method. (f) The crystal structure of mouse TLR6 (3A79).

This template assembly approach can be extended to modeling of other repetitive proteins.

7.4 Paper 4: Homology Modeling of Human Toll-Like Receptors TLR7, 8 and 9 Ligand-Binding Domains

(Manuscript see Appendix at page 82)

Nucleic acid-sensing Toll-like receptors (TLRs), TLR3, 7, 8 and 9, recognize different types of microbial nucleic acids after they are transferred in the cell. Understanding their ligand-binding mechanisms is crucial for development of agonists and antagonists with therapeutic potential for infectious diseases. So far, there are no crystallographic structures for TLR7/8/9. To enable first predictions of the receptor-ligand interaction sites, we developed three-dimensional models for the ligand-binding domains of human TLR7/8/9 based on homology modeling. The predicted results can guide experimentalists to design new site-directed mutation

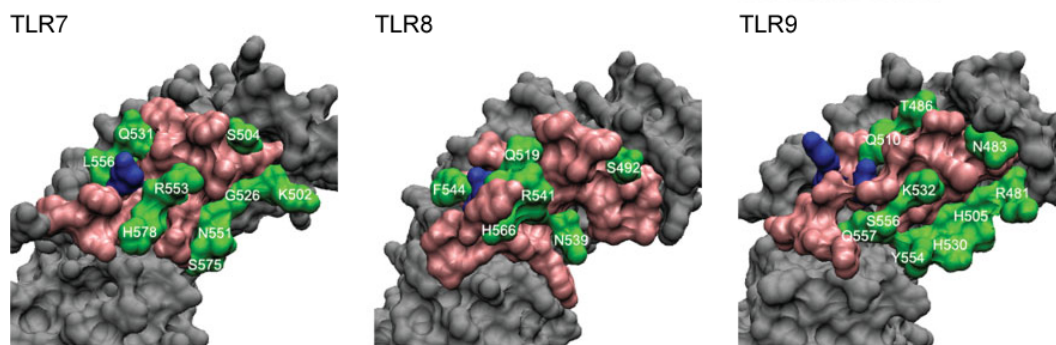experiments to unravel the ligand-binding mechanisms of these receptors.

Figure 11: Important residues in ligand-binding regions of TLR7/8/9. Blue: essential residues as reported in the literature; pink: residues close the blue ones (within two LRRs) but excluded from the potential ligand-binding residues through the four investigating processes; green: suggested potential ligand-binding residues (residue name and number are labeled).

To achieve a high sequence similarity between targets and templates, structural segments from all known TLR ectodomain structures (human TLR1/2/3/4 and mouse TLR3/4) were used as candidate templates for the modeling. Based on our models, we identified potential ligand-binding residues for TLR7/8/9 using combined procedures. Only the surface residues that fulfilled the four qualifications as follows were regarded as potential ligand-binding residues: (1) highly conserved across mammalian species; (2) non-negatively charged; (3) spatially close (within two LRRs) to the experimentally determined ligand-binding residues (Asp543 in TLR8; Asp535 and Tyr537 in TLR9); and (4) positively predicted by at least two protein-nucleic acid docking programs. Figure 11 illustrates names and locations of these residues. We suggest further investigations of these residues through mutation experiments. Moreover, we propose three potential receptor-ligand 2:1 complexing mechanisms based on the resulting models together with considerations of the potential ligand-binding residues.

7.5 Paper 5: Inhibition of the Toll-Like Receptors TLR4 and 7 Signaling Pathways by SIGIRR: A Computational Approach

(Manuscript see Appendix at page 91)

Understanding the mechanisms of negative regulation of Toll-like receptor (TLR) signaling will help to develop novel therapies to treat autoimmunity. TLRs belong to the Toll-like receptor/interleukin-1 receptor (TLR/IL-1R) superfamily, which is defined by a common cytoplasmic Toll/interleukin-1 receptor (TIR) domain. TLRs recognize pathogen-associated molecular patterns and initiate an intracellular kinase cascade to trigger an immediate defensive response. SIGIRR (single immunoglobulin interleukin-1 receptor-related molecule), another member of the TLR/IL-1R superfamily, acts as a negative regulator of MyD88-dependent TLR signaling. It attenuates the recruitment of MyD88 adaptors to the receptors with its intracellular TIR

domain. Thus, SIGIRR is a highly important molecule for the therapy of autoimmune diseases caused by TLRs. Currently, the structural mechanism of interactions between SIGIRR, TLRs and adaptor molecules is unclear. To develop a working hypothesis for this interaction, we constructed three-dimensional models for the TIR domains of TLR4, TLR7, MyD88 and SIGIRR based on computational modeling. Through a protein-protein docking analysis, we developed models of essential complexes involved in the TLR4 and 7 signaling and the SIGIRR inhibiting processes. We suggest that SIGIRR may exert its inhibitory effect by blocking the molecular interface of TLR4, TLR7 and the MyD88 adaptor mainly via its BB-loop region.

7.6 Paper 6: Lack of SIGIRR/TIR8 Aggravates Hydrocarbon Oil-Induced Systemic Lupus

(Manuscript see Appendix at page 100)

Multiple genetic factors contribute to the clinical variability of spontaneous systemic lupus erythematosus but their role in drug-induced systemic lupus erythematosus remains largely unknown. Hydrocarbon oil-induced systemic lupus erythematosus depends on mesothelial cell apoptosis and Toll-like receptor (TLR)-7-mediated induction of type interferons. Hence, we hypothesized SIGIRR/TIR8, an endogenous TLR inhibitor, prevents oil-induced systemic lupus erythematosus. *Sigirr*-deficient dendritic cells expressed higher TLR7 mRNA levels and TLR7 activation resulted in increased IL-12 production *in vitro*. *In vivo*, lack of SIGIRR increased surface CD40 expression on spleen CD11c+ dendritic cells and MX-1, TNF, IL-12, BAFF, and BCL-2 mRNA expression six months after pristane injection. Spleen cell counts of CD4-/CD8- autoreactive T cells and B220+ B cells were also increased in *Sigirr*-/- mice. Serum autoantibody analysis revealed that *Sigirr*-deficiency specifically enhanced the production of rheumatoid factor (from four months of age) and anti-snRNP IgG (from five months of age) while anti-Smith IgG or anti-dsDNA IgG were independent of the *Sigirr* genotype. This effect was sufficient to significantly aggravate lupus nephritis in *Sigirr*-deficient mice. Structure model prediction identified the BB-loop of SIGIRR's intracellular TIR domain to interact with TLR7 and MyD88. BB-loop deletion was sufficient to completely abrogate SIGIRR's inhibitory effect on TLR7 signaling. Thus, SIGIRR/TIR8 protects from hydrocarbon oil-induced lupus via suppressing the TLR7-mediated activation of dendritic cells most likely via its intracellular BB-loop.

8. Conclusions

This thesis focuses on three-dimensional structure prediction of TLR ligand-binding domains. In the view of the periodic arrangement of LRRs that comprise the TLR ligand-binding domains, an LRR template assembly approach was developed for homology modeling of these domains. The approach was implemented through two protein structure databases, TollML and LRRML. In TollML, all known TLR protein sequences (release 3.1: 2,572 entries) were semi-automatically partitioned into individual LRR sequences and are made available for query. On the other hand, LRRML archives individual LRR structures (release 0.7: 1,475 entries) manually identified from all known crystal structures of LRR proteins, with a similarity search function. The databases are available at http://tollml.lrz.de/ and http://lrrml.lrz.de/, respectively. Thus, the most similar (on the sequence level) LRR with a known structure can be found as a local template for each LRR contained in the target protein sequence. All local template sequences are then combined to generate a multiple sequence alignment for the complete target sequence. Finally, the templates (three-dimensional coordinates) and the sequence alignments are inputted into an automatic model construction program to obtain a three-dimensional model. To validate the template assembly approach, we constructed the models of TLR3 and 6 and superimposed them with the corresponding crystal structures. The high similarities (RMSDs < 2 Å) between the models and crystal structures underlined the feasibility and reliability of this method. Furthermore, the comparison of our method with a standard full-length template modeling method (pGenTHREADER) showed that our method is significantly superior in situations where no adequate full-length templates are available.

With the LRR template assembly method, a series of models of full-length TLR ligand-binding domains (human TLR5-10 and mouse TLR11-13) and the cleaved TLR7/8/9 ligand-binding domains were constructed. Model evaluation results indicated the high quality of all resulting models. The molecular surface electrostatics investigation and docking study of the mouse TLR11 model with a parasite profilin ligand demonstrated the usability of these models. Then, we identified potential ligand-binding residues for the cleaved TLR7/8/9 by combining results from four steps of investigations. The potential ligand-binding residues constitute a continuous ligand-binding region, which possesses a compatible size with the ssRNA or CpG DNA ligand and is located on the insertion-containing surface of the TLR horseshoe. The models together with the predicted ligand-binding regions could be used to derive a working hypothesis for the conformation of the receptor-ligand complex. Three models of the receptor-ligand 2:1 complexes were proposed, where the two receptor monomers sandwich the ligand at different positions. Thus, the minimum ligand size required by the three models is also different.

Inappropriate ligand recognition of TLRs can lead to autoimmune disorders. For this

reason, SIGIRR, as a negative regulator of TLRs, is highly important for the therapy of autoimmune diseases caused by TLRs. Our studies on the structural interactions between SIGIRR, TLR4, TLR7 and the TLR adaptor protein MyD88 showed that SIGIRR might block the molecular interface of TLR4, TLR7 and MyD88 mainly via the BB-loop of its intracellular TIR domain.

Still, the process of going from protein sequences to structures and to functions is far from being automated. Bioinformatic predictions become particularly helpful in an environment where the computational methods can be used in concert with experimental techniques for protein structure and function determination. Here, the predictions exercise their strengths by creating groundwork for subsequent experiments that follow up these predicted data.

References

1.   Takeda K, Akira S: **Toll-like receptors in innate immunity**. *Int Immunol* 2005, **17**(1):1-14.

2.   Jin MS, Kim SE, Heo JY, Lee ME, Kim HM, Paik SG, Lee H, Lee JO: **Crystal structure of the TLR1-TLR2 heterodimer induced by binding of a tri-acylated lipopeptide**. *Cell* 2007, **130**(6):1071-1082.

3.   Park BS, Song DH, Kim HM, Choi BS, Lee H, Lee JO: **The structural basis of lipopolysaccharide recognition by the TLR4-MD-2 complex**. *Nature* 2009, **458**(7242):1191-1195.

4.   Liu L, Botos I, Wang Y, Leonard JN, Shiloach J, Segal DM, Davies DR: **Structural basis of toll-like receptor 3 signaling with double-stranded RNA**. *Science* 2008, **320**(5874):379-381.

5.   Kang JY, Nan X, Jin MS, Youn SJ, Ryu YH, Mah S, Han SH, Lee H, Paik SG, Lee JO: **Recognition of lipopeptide patterns by Toll-like receptor 2-Toll-like receptor 6 heterodimer**. *Immunity* 2009, **31**(6):873-884.

6.   Gong J, Wei T, Zhang N, Jamitzky F, Heckl WM, Rossle SC, Stark RW: **TollML: a database of toll-like receptor structural motifs**. *J Mol Model* 2010, **16**(7):1283-1289.

7.   Tuccinardi T, Ortore G, Rossello A, Supuran CT, Martinelli A: **Homology modeling and receptor-based 3D-QSAR study of carbonic anhydrase IX**. *J Chem Inf Model* 2007, **47**(6):2253-2262.

8.   Singh N, Avery MA, McCurdy CR: **Toward Mycobacterium tuberculosis DXR inhibitor design: homology modeling and molecular dynamics simulations**. *J Comput Aided Mol Des* 2007, **21**(9):511-522.

9.   Hazai E, Bikadi Z: **Homology modeling of breast cancer resistance protein (ABCG2)**. *J Struct Biol* 2008, **162**(1):63-74.

10.   Bisson WH, Koch DC, O'Donnell EF, Khalil SM, Kerkvliet NI, Tanguay RL, Abagyan R, Kolluri SK: **Modeling of the aryl hydrocarbon receptor (AhR) ligand binding domain and its utility in virtual ligand screening to predict new AhR ligands**. *J Med Chem* 2009, **52**(18):5635-5641.

11.   Wu B, Zhang Y, Kong J, Zhang X, Cheng S: **In silico predication of nuclear hormone receptors for organic pollutants by homology modeling and molecular docking**. *Toxicol Lett* 2009, **191**(1):69-73.

12.   Savarese E, Chae OW, Trowitzsch S, Weber G, Kastner B, Akira S, Wagner H, Schmid RM, Bauer S, Krug A: **U1 small nuclear ribonucleoprotein immune complexes induce type I interferon in plasmacytoid dendritic cells through TLR7**. *Blood* 2006, **107**(8):3229-3234.

13.   Means TK, Latz E, Hayashi F, Murali MR, Golenbock DT, Luster AD: **Human lupus autoantibody-DNA complexes activate DCs through cooperation of CD32 and TLR9**. *J Clin Invest* 2005, **115**(2):407-417.

14.   Vollmer J, Tluk S, Schmitz C, Hamm S, Jurk M, Forsbach A, Akira S, Kelly KM, Reeves WH, Bauer S *et al*: **Immune stimulation mediated by autoantigen binding sites within small nuclear RNAs involves Toll-like receptors 7 and 8**. *J Exp Med* 2005, **202**(11):1575-1585.

15.   Barrat FJ, Meeker T, Gregorio J, Chan JH, Uematsu S, Akira S, Chang B, Duramad O, Coffman RL: **Nucleic acids of mammalian origin can act as endogenous ligands for Toll-like receptors and may promote systemic**

lupus erythematosus. *J Exp Med* 2005, **202**(8):1131-1139.

16. Janeway CA, Jr.: **How the immune system works to protect the host from infection: a personal view**. *Proc Natl Acad Sci U S A* 2001, **98**(13):7461-7468.

17. Janeway CA, Jr., Medzhitov R: **Innate immune recognition**. *Annu Rev Immunol* 2002, **20**:197-216.

18. Kawai T, Akira S: **Toll-like receptor and RIG-I-like receptor signaling**. *Ann N Y Acad Sci* 2008, **1143**:1-20.

19. Schwartz RS: **Advances in Immunology -- A New Series of Review Articles**. *N Engl J Med* 2000, **343**(1):61-62.

20. Hopkins PA, Sriskandan S: **Mammalian Toll-like receptors: to immunity and beyond**. *Clin Exp Immunol* 2005, **140**(3):395-407.

21. Ahmed R, Gray D: **Immunological memory and protective immunity: understanding their relation**. *Science* 1996, **272**(5258):54-60.

22. Medzhitov R, Janeway CA, Jr.: **Innate immunity: impact on the adaptive immune response**. *Curr Opin Immunol* 1997, **9**(1):4-9.

23. Jurk M, Kritzler A, Debelak H, Vollmer J, Krieg AM, Uhlmann E: **Structure-activity relationship studies on the immune stimulatory effects of base-modified CpG toll-like receptor 9 agonists**. *ChemMedChem* 2006, **1**(9):1007-1014.

24. Stein D, Roth S, Vogelsang E, Nusslein-Volhard C: **The polarity of the dorsoventral axis in the Drosophila embryo is defined by an extracellular signal**. *Cell* 1991, **65**(5):725-735.

25. Lemaitre B, Nicolas E, Michaut L, Reichhart JM, Hoffmann JA: **The dorsoventral regulatory gene cassette spatzle/Toll/cactus controls the potent antifungal response in Drosophila adults**. *Cell* 1996, **86**(6):973-983.

26. Tauszig S, Jouanguy E, Hoffmann JA, Imler JL: **Toll-related receptors and the control of antimicrobial peptide expression in Drosophila**. *Proc Natl Acad Sci U S A* 2000, **97**(19):10520-10525.

27. Medzhitov R, Preston-Hurlburt P, Janeway CA, Jr.: **A human homologue of the Drosophila Toll protein signals activation of adaptive immunity**. *Nature* 1997, **388**(6640):394-397.

28. Poltorak A, He X, Smirnova I, Liu MY, Van Huffel C, Du X, Birdwell D, Alejos E, Silva M, Galanos C *et al*: **Defective LPS signaling in C3H/HeJ and C57BL/10ScCr mice: mutations in Tlr4 gene**. *Science* 1998, **282**(5396):2085-2088.

29. Kumar H, Kawai T, Akira S: **Pathogen recognition in the innate immune response**. *Biochem J* 2009, **420**(1):1-16.

30. Brodsky I, Medzhitov R: **Two modes of ligand recognition by TLRs**. *Cell* 2007, **130**(6):979-981.

31. Weber AN, Morse MA, Gay NJ: **Four N-linked glycosylation sites in human toll-like receptor 2 cooperate to direct efficient biosynthesis and secretion**. *J Biol Chem* 2004, **279**(33):34589-34594.

32. Xu Y, Tao X, Shen B, Horng T, Medzhitov R, Manley JL, Tong L: **Structural basis for signal transduction by the Toll/interleukin-1 receptor domains**. *Nature* 2000, **408**(6808):111-115.

33. Barton GM, Kagan JC, Medzhitov R: **Intracellular localization of Toll-like receptor 9 prevents recognition of self DNA but facilitates access to viral DNA**. *Nat Immunol* 2006, **7**(1):49-56.

38

34. O'Neill LA, Bowie AG: **The family of five: TIR-domain-containing adaptors in Toll-like receptor signalling**. *Nat Rev Immunol* 2007, **7**(5):353-364.

35. Kajava AV: **Structural diversity of leucine-rich repeat proteins**. *J Mol Biol* 1998, **277**(3):519-527.

36. Bell JK, Mullen GE, Leifer CA, Mazzoni A, Davies DR, Segal DM: **Leucine-rich repeats and pathogen recognition in Toll-like receptors**. *Trends Immunol* 2003, **24**(10):528-533.

37. Matsushima N, Tanaka T, Enkhbayar P, Mikami T, Taga M, Yamada K, Kuroki Y: **Comparative sequence analysis of leucine-rich repeats (LRRs) within vertebrate toll-like receptors**. *BMC Genomics* 2007, **8**:124.

38. Roach JC, Glusman G, Rowen L, Kaur A, Purcell MK, Smith KD, Hood LE, Aderem A: **The evolution of vertebrate Toll-like receptors**. *Proc Natl Acad Sci U S A* 2005, **102**(27):9577-9582.

39. Takeda K, Kaisho T, Akira S: **Toll-like receptors**. *Annu Rev Immunol* 2003, **21**:335-376.

40. Gay NJ, Gangloff M: **Structure and function of Toll receptors and their ligands**. *Annu Rev Biochem* 2007, **76**:141-165.

41. Werling D, Piercy J, Coffey TJ: **Expression of TOLL-like receptors (TLR) by bovine antigen-presenting cells-potential role in pathogen discrimination?** *Vet Immunol Immunopathol* 2006, **112**(1-2):2-11.

42. Lang KS, Georgiev P, Recher M, Navarini AA, Bergthaler A, Heikenwalder M, Harris NL, Junt T, Odermatt B, Clavien PA *et al*: **Immunoprivileged status of the liver is controlled by Toll-like receptor 3 signaling**. *J Clin Invest* 2006, **116**(9):2456-2463.

43. Takeda K, Akira S: **TLR signaling pathways**. *Semin Immunol* 2004, **16**(1):3-9.

44. Zhang Y: **I-TASSER server for protein 3D structure prediction**. *BMC Bioinformatics* 2008, **9**:40.

45. Zaki MJ, Bystroff C: **Protein Structure Prediction**, 2 edn: Humana Press; 2008.

46. Petsko GA, Ringe D: **Protein Structure and Function**: New Science Pres; 2004.

47. Ginalski K: **Comparative modeling for protein structure prediction**. *Curr Opin Struct Biol* 2006, **16**(2):172-177.

48. Berman HM, Westbrook J, Feng Z, Gilliland G, Bhat TN, Weissig H, Shindyalov IN, Bourne PE: **The Protein Data Bank**. *Nucleic Acids Res* 2000, **28**(1):235-242.

49. Arnold K, Bordoli L, Kopp J, Schwede T: **The SWISS-MODEL workspace: a web-based environment for protein structure homology modelling**. *Bioinformatics* 2006, **22**(2):195-201.

50. Fiser A, Do RK, Sali A: **Modeling of loops in protein structures**. *Protein Sci* 2000, **9**(9):1753-1773.

51. Kopp J, Schwede T: **Automated protein structure homology modeling: a progress report**. *Pharmacogenomics* 2004, **5**(4):405-416.

52. Anfinsen CB: **Principles that govern the folding of protein chains**. *Science* 1973, **181**(96):223-230.

53. Cserhati T, Szogyi M: **Role of hydrophobic and hydrophilic forces in**

peptide-protein interaction: new advances. *Peptides* 1995, **16**(1):165-173.

54.   Zhang Q, Sanner M, Olson AJ: **Shape complementarity of protein-protein complexes at multiple resolutions**. *Proteins* 2009, **75**(2):453-467.

55.   Cheng TM, Blundell TL, Fernandez-Recio J: **Structural assembly of two-domain proteins by rigid-body docking**. *BMC Bioinformatics* 2008, **9**:441.

56.   Bell JK, Botos I, Hall PR, Askins J, Shiloach J, Segal DM, Davies DR: **The molecular structure of the Toll-like receptor 3 ligand-binding domain**. *Proc Natl Acad Sci U S A* 2005, **102**(31):10976-10980.

57.   Choe J, Kelker MS, Wilson IA: **Crystal structure of human toll-like receptor 3 (TLR3) ectodomain**. *Science* 2005, **309**(5734):581-585.

58.   Baker D, Sali A: **Protein structure prediction and structural genomics**. *Science* 2001, **294**(5540):93-96.

59.   Wei T, Gong J, Jamitzky F, Heckl WM, Stark RW, Roessle SC: **LRRML: a conformational database and an XML description of leucine-rich repeats (LRRs)**. *BMC Struct Biol* 2008, **8**(1):47.

60.   Gibbard RJ, Morley PJ, Gay NJ: **Conserved features in the extracellular domain of human toll-like receptor 8 are essential for pH-dependent signaling**. *J Biol Chem* 2006, **281**(37):27503-27511.

61.   Ewald SE, Lee BL, Lau L, Wickliffe KE, Shi GP, Chapman HA, Barton GM: **The ectodomain of Toll-like receptor 9 is cleaved to generate a functional receptor**. *Nature* 2008, **456**(7222):658-662.

62.   Thomassen E, Renshaw BR, Sims JE: **Identification and characterization of SIGIRR, a molecule representing a novel subtype of the IL-1R superfamily**. *Cytokine* 1999, **11**(6):389-399.

63.   Wald D, Qin J, Zhao Z, Qian Y, Naramura M, Tian L, Towne J, Sims JE, Stark GR, Li X: **SIGIRR, a negative regulator of Toll-like receptor-interleukin 1 receptor signaling**. *Nat Immunol* 2003, **4**(9):920-927.

64.   Polentarutti N, Rol GP, Muzio M, Bosisio D, Camnasio M, Riva F, Zoja C, Benigni A, Tomasoni S, Vecchi A *et al*: **Unique pattern of expression and inhibition of IL-1 signaling by the IL-1 receptor family member TIR8/SIGIRR**. *Eur Cytokine Netw* 2003, **14**(4):211-218.

65.   Qin J, Qian Y, Yao J, Grace C, Li X: **SIGIRR inhibits interleukin-1 receptor- and toll-like receptor 4-mediated signaling through different mechanisms**. *J Biol Chem* 2005, **280**(26):25233-25241.

66.   Gilliet M, Conrad C, Geiges M, Cozzio A, Thurlimann W, Burg G, Nestle FO, Dummer R: **Psoriasis triggered by toll-like receptor 7 agonist imiquimod in the presence of dermal plasmacytoid dendritic cell precursors**. *Arch Dermatol* 2004, **140**(12):1490-1495.

67.   Lech M, Kulkarni OP, Pfeiffer S, Savarese E, Krug A, Garlanda C, Mantovani A, Anders HJ: **Tir8/Sigirr prevents murine lupus by suppressing the immunostimulatory effects of lupus autoantigens**. *J Exp Med* 2008, **205**(8):1879-1888.

68.   Nyman T, Stenmark P, Flodin S, Johansson I, Hammarstrom M, Nordlund P: **The crystal structure of the human toll-like receptor 10 cytoplasmic domain reveals a putative signaling dimer**. *J Biol Chem* 2008, **283**(18):11861-11865.

69.   Khan JA, Brint EK, O'Neill LA, Tong L: **Crystal structure of the Toll/interleukin-1 receptor domain of human IL-1RAPL**. *J Biol Chem* 2004,

279(30):31664-31670.

70.   Eswar N, Webb B, Marti-Renom MA, Madhusudhan MS, Eramian D, Shen MY, Pieper U, Sali A: **Comparative protein structure modeling using MODELLER**. *Curr Protoc Protein Sci* 2007, **Chapter 2**:Unit 2 9.

71.   Fiser A, Sali A: **ModLoop: automated modeling of loops in protein structures**. *Bioinformatics* 2003, **19**(18):2500-2501.

72.   Jones DT, Taylor WR, Thornton JM: **A new approach to protein fold recognition**. *Nature* 1992, **358**(6381):86-89.

73.   Lobley A, Sadowski MI, Jones DT: **pGenTHREADER and pDomTHREADER: new methods for improved protein fold recognition and superfamily discrimination**. *Bioinformatics* 2009, **25**(14):1761-1767.

74.   Bryson K, McGuffin LJ, Marsden RL, Ward JJ, Sodhi JS, Jones DT: **Protein structure prediction servers at University College London**. *Nucleic Acids Res* 2005, **33**(Web Server issue):W36-38.

75.   Altschul SF, Madden TL, Schaffer AA, Zhang J, Zhang Z, Miller W, Lipman DJ: **Gapped BLAST and PSI-BLAST: a new generation of protein database search programs**. *Nucleic Acids Res* 1997, **25**(17):3389-3402.

76.   Laskowski RA, MacArthur MW, Moss DS, Thornton JM: **PROCHECK: a program to check the stereochemical quality of protein structures**. *J Appl Cryst* 1993, **26**:283-291.

77.   Ramachandran GN, Ramakrishnan C, Sasisekharan V: **Stereochemistry of polypeptide chain configurations**. *J Mol Biol* 1963, **7**:95-99.

78.   Wallner B, Elofsson A: **Can correct protein models be identified?** *Protein Sci* 2003, **12**(5):1073-1086.

79.   Cristobal S, Zemla A, Fischer D, Rychlewski L, Elofsson A: **A study of quality measures for protein threading models**. *BMC Bioinformatics* 2001, **2**:5.

80.   Siew N, Elofsson A, Rychlewski L, Fischer D: **MaxSub: an automated measure for the assessment of protein structure prediction quality**. *Bioinformatics* 2000, **16**(9):776-785.

81.   McGuffin LJ: **The ModFOLD server for the quality assessment of protein structural models**. *Bioinformatics* 2008, **24**(4):586-587.

82.   McGuffin LJ: **Benchmarking consensus model quality assessment for protein fold recognition**. *BMC Bioinformatics* 2007, **8**:345.

83.   Pawlowski M, Gajda MJ, Matlak R, Bujnicki JM: **MetaMQAP: a meta-server for the quality assessment of protein models**. *BMC Bioinformatics* 2008, **9**:403.

84.   Tovchigrechko A, Vakser IA: **GRAMM-X public web server for protein-protein docking**. *Nucleic Acids Res* 2006, **34**(Web Server issue):W310-314.

85.   Chen R, Li L, Weng Z: **ZDOCK: an initial-stage protein-docking algorithm**. *Proteins* 2003, **52**(1):80-87.

86.   Wang L, Brown SJ: **BindN: a web-based tool for efficient prediction of DNA and RNA binding sites in amino acid sequences**. *Nucleic Acids Res* 2006, **34**(Web Server issue):W243-248.

87.   Vapnik CA: **Statistical Learning Theory**: John Wiley and Sons; 1998.

88.   Hwang S, Gou Z, Kuznetsov IB: **DP-Bind: a web server for sequence-based prediction of DNA-binding residues in DNA-binding proteins**.

Bioinformatics 2007, **23**(5):634-636.

89.   Ahmad S, Gromiha MM, Sarai A: **Analysis and prediction of DNA-binding proteins and their binding residues based on composition, sequence and structural information**. *Bioinformatics* 2004, **20**(4):477-486.

90.   Boeckmann B, Bairoch A, Apweiler R, Blatter MC, Estreicher A, Gasteiger E, Martin MJ, Michoud K, O'Donovan C, Phan I *et al*: **The SWISS-PROT protein knowledgebase and its supplement TrEMBL in 2003**. *Nucleic Acids Res* 2003, **31**(1):365-370.

91.   Ahmad S, Sarai A: **PSSM-based prediction of DNA binding sites in proteins**. *BMC Bioinformatics* 2005, **6**:33.

92.   Tsuchiya Y, Kinoshita K, Nakamura H: **PreDs: a server for predicting dsDNA-binding site on protein molecular surfaces**. *Bioinformatics* 2005, **21**(8):1721-1723.

93.   Humphrey W, Dalke A, Schulten K: **VMD: visual molecular dynamics**. *J Mol Graph* 1996, **14**(1):33-38, 27-38.

94.   Guex N, Peitsch MC: **SWISS-MODEL and the Swiss-PdbViewer: an environment for comparative protein modeling**. *Electrophoresis* 1997, **18**(15):2714-2723.

95.   Maiti R, Van Domselaar GH, Zhang H, Wishart DS: **SuperPose: a simple server for sophisticated structural superposition**. *Nucleic Acids Res* 2004, **32**(Web Server issue):W590-594.

96.   Krissinel E, Henrick K: **Inference of macromolecular assemblies from crystalline state**. *J Mol Biol* 2007, **372**(3):774-797.

97.   Waterhouse AM, Procter JB, Martin DM, Clamp M, Barton GJ: **Jalview Version 2--a multiple sequence alignment editor and analysis workbench**. *Bioinformatics* 2009, **25**(9):1189-1191.

Acknowledgements

Acknowledgements

Appendix

Paper 1

LRRML: a conformational database and an XML description of leucine-rich repeats (LRRs)

Tiandi Wei, Jing Gong, Ferdinand Jamitzky, Wolfgang M. Heckl, Robert W. Stark and Shaila C. Rössle

BMC Structural Biology

LRRML: a conformational database and an XML description of leucine-rich repeats (LRRs)

Tiandi Wei[†1], Jing Gong*[†1], Ferdinand Jamitzky[1,2], Wolfgang M Heckl[1,3], Robert W Stark[1] and Shaila C Rössle[1]

Address: [1]Department of Earth and Environmental Sciences, Ludwig-Maximilians-Universität München, Theresienstr, 41, 80333 Munich, Germany, [2]Leibniz Supercomputing Centre, 85748 Garching, Germany and [3]Deutsches Museum, 80538 Munich, Germany

E-mail: Tiandi Wei - tiandi@informatik.uni-muenchen.de; Jing Gong* - gongj@informatik.uni-muenchen.de; Ferdinand Jamitzky - jamitzky@lrz.de; Wolfgang M Heckl - heckl@lmu.de; Robert W Stark - stark@lrz.uni-muenchen.de; Shaila C Rössle - shaila.roessle@lrz.uni-muenchen.de;
*Corresponding author   †Equal contributors

Abstract

Background: Leucine-rich repeats (LRRs) are present in more than 6000 proteins. They are found in organisms ranging from viruses to eukaryotes and play an important role in protein-ligand interactions. To date, more than one hundred crystal structures of LRR containing proteins have been determined. This knowledge has increased our ability to use the crystal structures as templates to model LRR proteins with unknown structures. Since the individual three-dimensional LRR structures are not directly available from the established databases and since there are only a few detailed annotations for them, a conformational LRR database useful for homology modeling of LRR proteins is desirable.

Description: We developed LRRML, a conformational database and an extensible markup language (XML) description of LRRs. The release 0.2 contains 1261 individual LRR structures, which were identified from 112 PDB structures and annotated manually. An XML structure was defined to exchange and store the LRRs. LRRML provides a source for homology modeling and structural analysis of LRR proteins. In order to demonstrate the capabilities of the database we modeled the mouse Toll-like receptor 3 (TLR3) by multiple templates homology modeling and compared the result with the crystal structure.

Conclusion: LRRML is an information source for investigators involved in both theoretical and applied research on LRR proteins. It is available at http://zeus.krist.geo.uni-muenchen.de/~lrrml.

Background

Leucine-rich repeats (LRRs) are arrays of 20 to 30 amino acid long protein segments that are unusually rich in the hydrophobic amino acid leucine. They are present in more than 6000 proteins in different organisms ranging from viruses to eukaryotes [1]. The structure of the LRRs and their arrangement in repetitive stretches of variable length generate a versatile and highly evolvable framework for the binding of manifold proteins and non-protein ligands [2]. The crystal structure of the ribonuclease inhibitor (RI) yielded the first insight into the three-dimensional molecular basis of LRRs [3]. It has a horseshoe shaped solenoid structure with parallel β-sheet lining the inner circumference and α-helices flanking its outer circumference. To date, there are over one hundred crystal structures available. All known LRR domains adopt an arc or horseshoe shape [1].

The LRR sequences can be divided into a highly conserved segment (HCS) and a variable segment (VS). The highly conserved segment consists of an 11 or 12 residue stretch with the consensus sequence LxxLxLxxN(Cx)xL. Here, the letter L stands for Leu, Ile, Val or Phe forming the hydrophobic core, N stands for Asn, Thr, Ser or Cys, and x is any amino acid. The variable segment is quite diverse in length and consensus sequence, accordingly eight classes of LRRs have been proposed [4, 5]: 'RI-like (RI)', 'Cysteine-containing (CC)', 'Bacterial (S)', 'SDS22-like (SDS22)', 'Plant-specific (PS)', 'Typical (T)', 'Treponema pallidum (Tp)' and 'CD42b-like (CD42b)'.

The discrepancy between the numbers of structure-known LRR proteins and the structure-unknown ones triggered studies focusing on the homology modeling of LRR proteins [6-8]. Homology modeling is a computational method, which is widely used to identify structural features defining molecular interactions [8-10]. The modeling results are an important input for the design of biochemical experiments. The first step of homology modeling is the selection of a structure-known protein, which serves as a template for the unknown target structure. In practice, however, it is difficult to find a complete template which has a high enough sequence identity to the target repetitive protein (single template modeling), due to different repeat numbers and varying arrangements. This limitation can be overcome by combining multiple templates. First, the most similar structure-known LRRs are found for each LRR in the target sequence as a local template. Second, all local templates are combined to generate the multiple sequence alignments for the entire target sequence. Thus, it is possible to construct a start model for further investigation, even if no adequate single template is available. Such an approach, however, requires a comprehensive database of LRRs to extract adequate template candidates. So far, the individual three-dimensional LRR structures are not directly available from the established databases and there are only a few detailed annotations for them. Additional information such as sequence insertions and types is missing. In order to consolidate this information and to provide a source for homology modeling and structural analysis of LRR proteins, we developed LRRML, a database and an extensible markup language (XML) description of LRR structures.

Construction and content

Structure-known LRR proteins were extracted from the Protein Data Bank (PDB) [11] release Sept 10, 2008. In order to ensure that all LRR proteins were found, we combined three groups of search results. First, 'leucine rich repeat', 'leucine rich repeats', 'leucine-rich repeat', 'leucine-rich repeats', 'lrr' and 'lrrs' were used as key words in the PDB quick search; second, 'SCOP classification -> Alpha and beta proteins (a/b) -> Leucine-rich repeat' was used as options in

PDB advanced search; third, 'CATH classification -> Alpha Beta -> Alpha-Beta Horseshoe -> Leucine-rich repeat' was used as options in PDB advanced search. Because of the irregularity (mutations and insertions in the sequence) of LRRs reliable identifications of LRRs contained in the LRR proteins could only be performed manually. We inspected the three-dimensional structures of the LRR proteins using molecular viewers and identified each LRR based on two criteria:

1. A LRR begins at the beginning of the highly conserved segment (HCS) and ends at the end of the variable segment (VS) (just before the HCS of the next LRR).

2. The HCS of a LRR must pose a typical conformation, i.e. a short β-sheet begins at about position 3 and a hydrophobic core is formed by the four L residues at position 1, 4, 6, and 11.

The LRRs were then manually classified according to the consensus sequences [4, 5]. In addition to the eight canonical LRR classes listed in the background section we included a new class 'other' for the N-/C-terminal LRRs and some hyper-irregular LRRs. Table 1 illustrates the consensus sequences of the eight canonical LRR classes.

During the LRR identification and classification all sequence insertions longer than 3 residues were annotated. About one tenth of entries have insertions longer than 3 residues while few entries have deletions, which suggests that the evolution of LRRs may prefer insertion to deletion.

The LRRML release 0.2 contains 1261 LRR entries from 112 PDB structures. Among them 548 LRRs are distinct on sequence level, indicating that different molecules can share identical LRRs. By superimposition, we found that they also have highly similar structures. This fact enhances the confidence in modeling LRR proteins using multiple LRR templates. A histogram of entry length distribution

Table 1: Consensus sequences of the eight canonical LRR classes [4, 5].

Classes	HCS	VS
Typical type (T)	LxxLxLxxNxL	xxLxxxxLxxLxx
Bacterial type (S)	LxxLxLxxNxL	xxLPx(x)LPxx
Ribonuclease inhibitor-like type (RI)	LxxLxLxxNxL	xxxxxxxLxxxLxxxxx
SDS22-like type (SDS22)	LxxLxLxxNxL	xxLxxLxxLxx
Cysteine-containing type (CC)	LxxLxLxxCxxL	TDxxxxxLxxxCxx
Plant-specific type (PS)	LxxLxLxxNxL	xxxLPxxLGxLxx
Treponema pallidum type (Tp)	LxxLxLPxxLxx	LxxxAFxxCxx
CD42b type (CD42b)	LxxLxLxxNxL	xxLPxxxxxxxx

L: Leu, Ile, Val, Phe; N: Asn, Thr, Ser, Cys; P: Pro; T: Thr; D: Asp; G: Gly; A: Ala; F: Phe; C: Cys; x: random residues.

(Figure 1) shows that the LRR lengths are concentrated in the interval from 20 to 29, which covers the characteristic lengths of consensus sequences of the eight canonical LRR classes. Some entries have a sequence longer than 30, because they contain large insertions. Table 2 presents the distribution of LRR entries and PDB entries over the nine classes respectively. The classification results are consistent with a previous report which showed that LRRs from different classes never occur simultaneously in the same protein and have most probably evolved independently [4]. Exceptions to this rule are the T and S types which often exist in the same protein forming the super motif 'STT' [12]. It is assumed that both evolved from a common precursor [1].

Currently, there are several protein databases containing information on LRRs, such as Pfam [13], InterPro [14], SMART [15] and Swiss-Prot [16]. These databases predict the LRR numbers and boundaries for their LRR protein entries by various computational methods, no matter whether the entries have known three-dimensional

structures or not, thereby 'false negative' occurs frequently. Table 3 lists the numbers of structure-known LRR proteins and their LRRs covered by these databases. As more detailed examples, LRR numbers of LRR proteins from different classes reported by the established databases are compared in Table 4. Additionally, the individual three-dimensional LRR structures are not directly available from these databases. In order to combine the information required for homology modeling and structural analysis, LRRML is provided with three prominent characteristics:

1. Each database entry is an individual three-dimensional LRR structure, which was identified with high accuracy.

2. Extensive annotations, such as systematic classification, secondary structures, HCS/VS partitions and sequence insertion, are provided.

3. LRRs were extracted from all structure-known LRR protein structures from PDB.
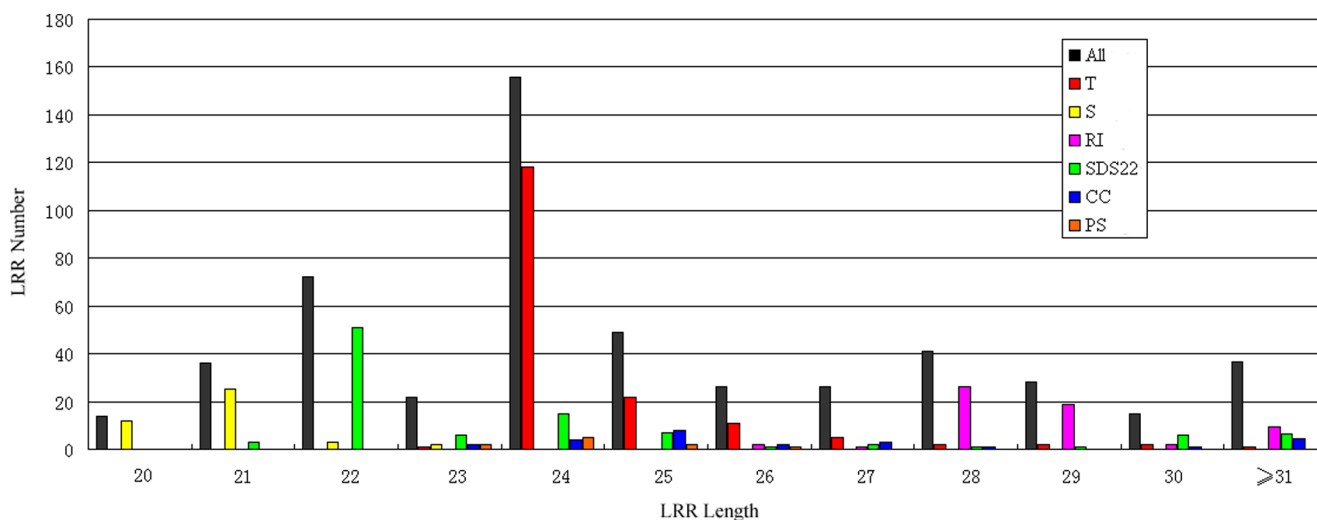
Figure 1
LRR entry length distribution. The most common entry lengths vary from 20 to 29. Each LRR class has a characteristic length distribution. Some entries have a sequence length larger than 29 due to insertions.

Table 2: Numbers of LRR and PDB entries (release 0.2) in the nine LRR classes.

	T	S	RI	SDS22	CC	PS	Tp	CD42b	Other	Total
LRR structures	272	72	151	372	184	10	0	0	200	1261
LRR entries	169	40	59	114	28	10	0	0	128	548
PDB entries		32	13	50	16	1	0	0	-	112

Up to present, no crystal structures for LRR proteins of Tp/CD42b types are determined. Different from other LRR types, the S type and T type LRRs evolved from a common precursor [1] and thus can exist in the same PDB entry simultaneously.

Table 3: Coverage of LRR proteins with PDB structures of different databases.

Databases	Numbers of LRR proteins with PDB structures	Numbers of identified LRRs
InterPro	62	325
Swiss-Prot	98	997
Pfam	48	173
SMART	84	547
LRRML	112	1261

The results were obtained on October 13, 2008.

XML description

The extensible markup language (XML) was standardized in the 90s and is well established as a format for hierarchical data. It can be queried and parsed more easily by application programs. Therefore, more and more biological databases use the XML as data saving format and database management system (DBMS) [17-19]. LRRML was designed by using eXist [20], an XML DBMS, and using XPath/XQuery [21] for processing queries and web forms. We developed a LRR markup language (LRRML) for exchanging and storing LRR structures. It consists of four blocks of information:

1. The sequence information (XML tag <l:Sequence>): amino acid sequence and sequence length.

2. The classification information (XML tag <l:Type>): class name and consensus sequences.

3. The sequence partitions (XML tag <l:Regions>): amino acid sequence, position, length and insertion of HCS and VS.

4. The corresponding PDB sources (XML tag <l:Sources>): ID, chain, LRR number and classification of the source PDB entries; serial number, position, DSSP [22] secondary structure and three-dimensional coordinates of the current LRR in these source PDB entries.

An example describing the LRR3 from PDB entry 2O6S is shown in Figure 2. The document type definition (DTD) file of LRRML is provided asAdditional file 1.

Utility
Web application
The entire database can be browsed by LRR IDs or by PDB IDs. When browsing, the entries appear in a summary table containing at first ID, type and sequence. Clicking on an ID opens an XML Stylesheet (XSLT) [21] converted HTML web page that presents the entry in detail. The original XML file and the coordinates file in PDB format can also be downloaded. The XSLT file used is provided as Additional file 2. Aside from the textual view, a LRR structure can be visualized by the online molecular viewer Jmol [23]. After loading, users can change the view settings flexibly by themselves. LRRML is provided with various search functions, including PDB ID search which returns all LRRs contained in this PDB structure, class search which returns all LRRs of this class, or length search which returns all LRRs with this sequence length. To simplify the homology modeling, the similarity search was implemented. It returns the structures of the most similar LRRs for a structure-unknown LRR. The target LRR sequence can be searched against the entire database, a certain LRR class or LRRs with a certain length. At first, a global pair wise sequence alignment with sequence identity will be generated for the target LRR and each of the LRRs in the user selected set. Then, the most similar LRRs will be returned as template candidates, ranked by sequence identity.

The DBMS provides a REST-style application programming interface (API) through HTTP, which supports GET and POST requests. A unique resource identifier (URI) 'http://zeus.krist.geo.uni-muenchen.de:8081/exist/rest/...' is treated by the server as path to a database collection. Also, request parameters can help select any required elements.

Table 4: Comparison of LRR numbers of different LRR proteins by different databases.

PDB codes	Protein functions	LRR classes	InterPro	Swiss-Prot	Pfam	SMART	LRRML
2A0Z	Immune System	T	18	22	7	20	25
1G9U	Toxin	S	7	15	1	0	15
2FT3	Structural Protein	T+S	8	8	5	9	12
1K5D	Signaling Protein	RI	2	8	0	0	11
1GWB	Glycoprotein	SDS22	6	6	4	7	8
2P1M	Signaling Protein	CC	2	16	0	6	18
1OGQ	Inhibitor	PS	7	10	2	0	10

All listed LRR numbers include N-/C-terminal LRRs. To date, only the LRRML database contains the complete set of LRRs of all LRR proteins with known structures. The results were obtained on October 13, 2008.

```
<l:LRR xmlns:l="http://zeus.krist.geo.uni-muenchen.de/~lrrml">
  <l:Sequence>
    <l:SLength>24</l:SLength>
    <l:SPrimary>LTQLYLGGNKLQSLPNGVFNKLTS</l:SPrimary>
  </l:Sequence>
  <l:Type>
    <l:TName>Typical type</l:TName>
    <l:TAbbr>T</l:TAbbr>
    <l:TPattern>
      <l:TPLen>24</l:TPLen>
      <l:TPSeq>LxxLxLxxNxLxxLxxxxLxxLxx</l:TPSeq>
      <l:TPHCS>LxxLxLxxNxL</l:TPHCS>
      <l:TPVS>xxLxxxxLxxLxx</l:TPVS>
    </l:TPattern>
  </l:Type>
  <l:Regions>
    <l:Region>
      <l:RName>Highly Conserved Segment</l:RName>
      <l:RNAbbr>HCS</l:RNAbbr>
      <l:RBegin>1</l:RBegin>
      <l:REnd>11</l:REnd>
      <l:RLength>11</l:RLength>
      <l:RSeq>LTQLYLGGNKL</l:RSeq>
    </l:Region>
    <l:Region>
      <l:RName>Variable Segment</l:RName>
      <l:RNAbbr>VS</l:RNAbbr>
      <l:RBegin>12</l:RBegin>
      <l:REnd>24</l:REnd>
      <l:RLength>13</l:RLength>
      <l:RSeq>QSLPNGVFNKLTS</l:RSeq>
    </l:Region>
  </l:Regions>
  <l:Sources>
    <l:Source>
      <l:PDBInfo>
        <l:PDBId>2O6S</l:PDBId>
        <l:PDBChain>A</l:PDBChain>
        <l:PDBLrrNum>7</l:PDBLrrNum>
        <l:PDBClass>Immune System</l:PDBClass>
      </l:PDBInfo>
      <l:LRRInfo>
        <l:LRRNumber>3</l:LRRNumber>
        <l:LRRBegin>77</l:LRRBegin>
        <l:LRREnd>100</l:LRREnd>
        <l:LRRSecStr>LLEEELLLLLLLLLLLLLLLLLLLL</l:LRRSecStr>
        <l:LRR3dStr>2O6S.A.7.3</l:LRR3dStr>
      </l:LRRInfo>
    </l:Source>
  </l:Sources>
</l:LRR>
```

Figure 2
The LRRML description of a LRR structure. This entry is a 24 residue long typical LRR. The first 11 residues compose its HCS and the last 13 residues compose its VS (no insertions). It is contained only in the chain A of PDB structure 2O6S (a protein involved in the immune system). It is the third one of the 7 LRRs of 2O6S, from position 77 to 100. Its secondary structure was extracted from DSSP and its three-dimensional coordinate file is available though the hyperlink on the corresponding web page.

Table 5: Sequence identities (%) of target-template LRR pairs.

	NT	1	2	3	4	5	6	7	8	9	10	11	12	13	14	15	16	17	18	19	20	21	22	23	CT	Avg
LRRML ID	406	65	212	465	151	177	110	259	8	203	64	293	270	357	65	152	259	316	152	239	239	92	80	101	173	—
PDB source	1XWD	2O6S	1G9U	1OZN	1XKU	1SQ0	2FT3	2V9S	1IO0	1H6U	2O6S	2Z64	2Z62	2Z81	2O6S	1XKU	2V9S	2Z7X	1XKU	1P8V	1P8V	2ID5	2O6Q	2ID5	1V8A	—
Identity (%)	47.60	45.83	41.67	50.00	50.00	46.15	41.67	41.38	42.31	50.00	50.00	33.33	41.67	42.86	50.00	40.00	37.50	38.46	50.00	45.83	50.00	41.67	40.00	39.29	44.12	

In the header line, 1–25 denote canonical LRRs; NT and CT denote N-/C-terminal LRRs.
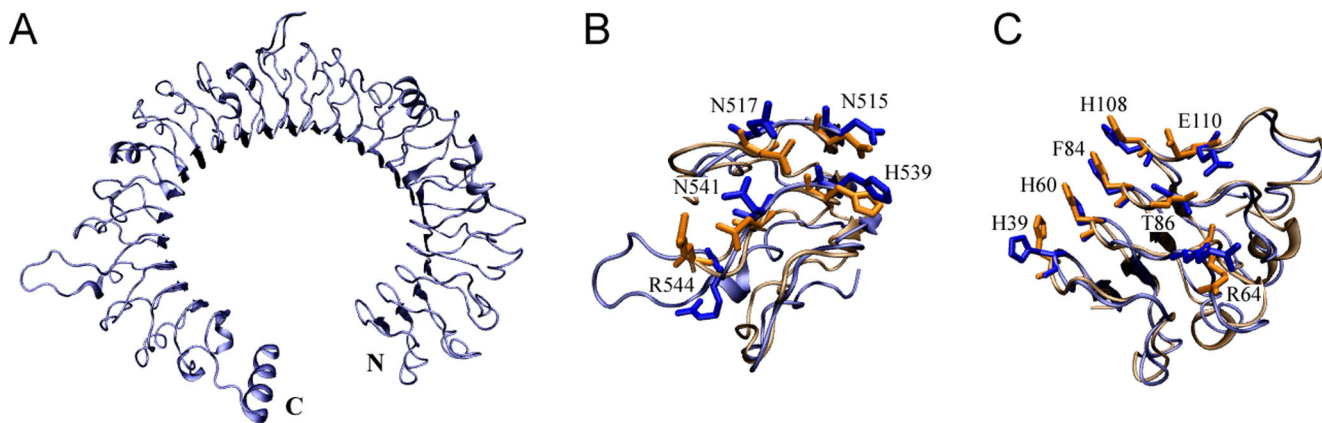
Figure 3
Comparison of model and crystal structure of mouse TLR3 ectodomain at the two ligand interaction regions. Blue: structure obtained by homology modeling; orange: crystal structure (PDB code: 3CIG). (A) The modeled backbone structure of mouse TLR3 ectodomain. (B) Model and crystal structure superimposed at the N-terminal interaction region. The root mean square deviation is 1.96 Å. (C) Superimposition at the C-terminal interaction region. The root mean square deviation is 1.9 Å. The reported interacting residues are presented with side chain and labelled with residue name and position in (B) and (C).

Figure 4
Ramachandran plot of model and crystal structure of mouse TLR3 ectodomain. (A) Predicted model of mouse TLR3 ectodomain. (B) Crystal structure of mouse TLR3 ectodomain. The different colored areas indicate 'disallowed' (white), 'generously allowed' (light yellow), 'additional allowed' (yellow), and 'most favored' (red) regions.

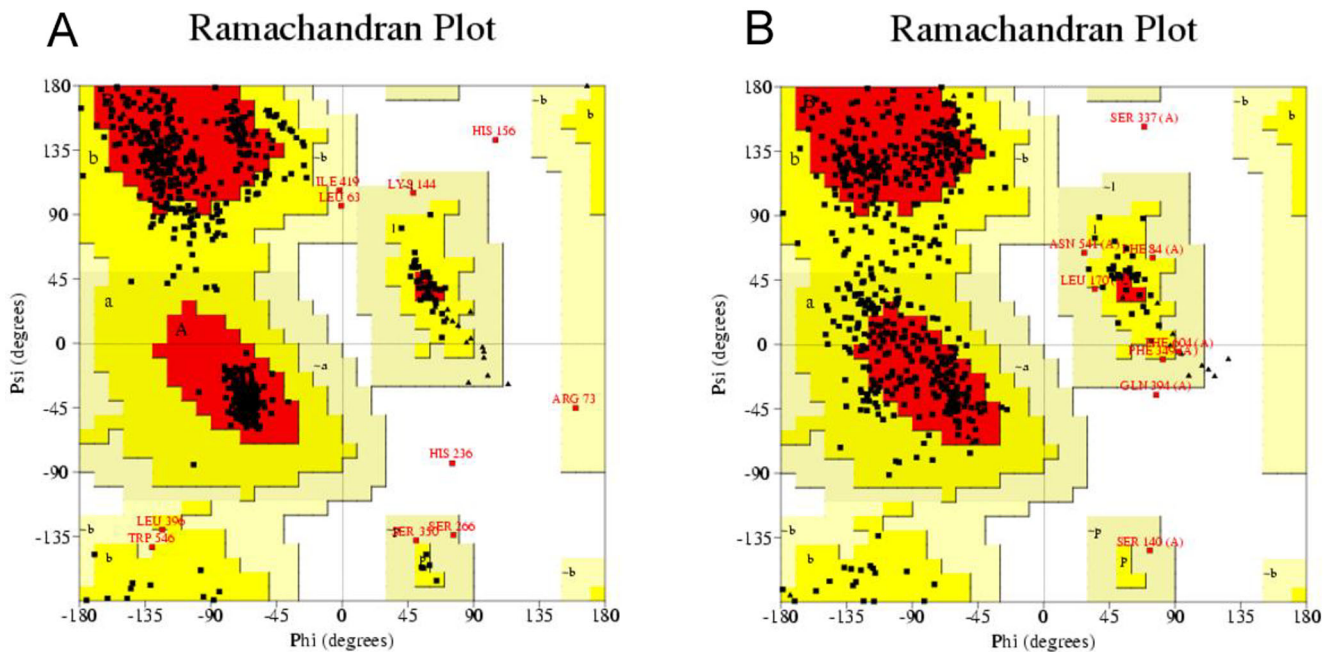For example, '_query' executes a specified XPath/XQuery; the URL "http://zeus.krist.geo.uni-muenchen.de:8081/exist/rest/db/lrrml?_query=//LRR [.//TAbbr='S']" returns all the S type LRRs.

Application in homology modeling

LRRML was designed as a tool for template selection in homology modeling of LRR proteins. Traditionally, the template used in homology modeling is one or more full length protein structures obtained via similarity search. Nevertheless, due to the different repeat numbers and arrangements of LRRs, the sequence identity between the target and the full length template is usually not high enough for homology modeling. With LRRML the most similar structure-known LRR can be found for each LRR in the target sequence as a local template. The combination of all local templates through multiple alignments helps to achieve a high sequence identity to the target.

As test case we modeled the structure of mouse Toll-like receptor 3 (TLR3) ectodomain. We assumed that the structure of mouse TLR3 ectodomain were unknown and excluded the LRRs of mouse/human TLR3 ectodomain from LRRML. Through similarity search the optimal template for each of the 25 LRRs in mouse TLR3 was found. The sequence identity between each LRR pair (target/template LRR) is listed in Table 5. Then a 26-line multiple alignment was generated by the 25 template sequences and the target sequence as the input of MODELLER 9v3 [24]. The resulting three-dimensional model (Figure 3A) was evaluated by PROCHECK [25], with 98.2% residues falling into the most favored or allowed regions of the main chain torsion angles distribution, whereas the result of the TLR3 crystal structure (PDB code: 3CIG) was 98.6% (Figure 4). The mouse TLR3 has been shown to bind double-stranded RNA ligand with both N-terminal and C-terminal sites on the lateral side of the convex surface of TLR3 [26]. The N-terminal interaction site is composed of LRRNT and LRR1-3, and the C-terminal site is composed of LRR19-21. We superimposed the resulting model onto the crystal structure of mouse TLR3 ectodomain at the two interaction sites by using SuperPose v1.0 [27]. The root mean square deviations of the structures are 1.96 Å and 1.9 Å respectively (Figure 3B/C), indicating that the predicted model sufficiently well matched the crystal structure and was useful for prediction of ligand interaction sites. These results demonstrate that homology modeling using combined multiple templates obtained from LRRML can create valuable information to trigger further biochemical research. Interpretation of structural details, however, should be done exercising due care.

Conclusion

A specialised conformational leucine-rich repeats database called LRRML has been developed. It is supported by an XML database management system and can be searched and browsed with either an easy-to-use web interface or REST like interface. The interface is suitable for most graphical web browsers and has been tested on the Windows, Mac and Linux operating systems. LRRML contains individual three-dimensional LRR structures with manual structural annotations. It presents useful sources for homology modeling and structural analysis of LRR proteins. Since the amount of structure-determined LRR proteins constantly increases, we plan to update LRRML every 2 to 3 months.

Availability and requirements

This database is freely available at http://zeus.krist.geo.uni-muenchen.de/~lrrml.

Authors' contributions

TW and JG drafted the manuscript, extracted the data, compiled the database, wrote the code for the web interface and performed the statistical analysis. FJ, WMH, RWS and SCR conceived of the study, built the database server, participated in the database design and coordination and helped to draft the manuscript. TW and JG should be regarded as joint first authors. All authors read and approved the final manuscript.

Additional material

Additional file 1
The document type definition (DTD) file of LRRML.
Click here for file
[http://www.biomedcentral.com/content/supplementary/1472-6807-8-47-S1.dtd]

Additional file 2
The XML Stylesheet (XSLT) of LRRML.
Click here for file
[http://www.biomedcentral.com/content/supplementary/1472-6807-8-47-S2.xsl]

References

1. Matsushima N, Tanaka T, Enkhbayar P, Mikami T, Taga M, Yamada K and Kuroki Y: **Comparative sequence analysis of leucine-rich repeats (LRRs) within vertebrate toll-like receptors.** *BMC Genomics* 2007, **8**:124–143.
2. Dolan J, Walshe K, Alsbury S, Hokamp K, O'Keeffe S, Okafuji T, Miller SFC, Guy Tear G and Mitchell KJ: **The extracellular Leucine-Rich Repeat superfamily; a comparative survey and analysis of evolutionary relationships and expression patterns.** *BMC Genomics* 2007, **8**:320–343.

3.　Kobe B and Deisenhofer J: **Crystal structure of porcine ribonuclease inhibitor, a protein with leucine-rich repeats.** *Nature* 1993, **366:**751–756.
4.　Kobe B and Kajava AV: **The leucine-rich repeat as a protein recognition motif.** *Curr Opin Struct Biol* 2001, **11:**725–732.
5.　Bell JK, Mullen GE, Leifer CA, Mazzoni A, Davies DR and Segal DM: **Leucine-rich repeats and pathogen recognition in Toll-like receptors.** *Trends Immunol* 2003, **24:**528–533.
6.　Kajava AV: **Structural Diversity of Leucine-rich Repeat Proteins.** *J Mol Biol* 1998, **277:**519–527.
7.　Stumpp MT, Forrer P, Binz HK and Plckthun A: **Designing Repeat Proteins: Modular Leucine-richRepeat Protein Libraries Based on the Mammalian Ribonuclease Inhibitor Family.** *J Mol Biol* 2003, **332:**471–487.
8.　Kubarenko A, Frank M and Weber AN: **Structure-function relationships of Toll-like receptor domains through homology modelling and molecular dynamics.** *Biochem Soc Trans* 2007, **35:**1515–1518.
9.　Rössle SC, Bisch PM, Lone YC, Abastado JP, Kourilsky P and Bellio M: **Mutational analysis and molecular modeling of the binding of Staphylococcus aureus enterotoxin C2 to a murine T cell receptor Vbeta10 chain.** *Eur J Immunol* 2002, **32:**2172–2178.
10.　Hazai E and Bikádi Z: **Homology modeling of breast cancer resistance protein (ABCG2).** *J Struct Biol* 2008, **162:**63–74.
11.　Berman HM, Westbrook J, Feng Z, Gilliland G, Bhat TN, Weissig H, Shindyalov IN and Bourne PE: **The Protein Data Bank.** *Nucleic Acids Res* 2000, **28:**235–242.
12.　Matsushima N, Kamiya M, Suzuki N and Tanaka T: **Super-Motifs of Leucine-Rich Repeats (LRRs) Proteins.** *Genome Inform* 2000, **11:**343–345.
13.　Finn RD, Tate J, Mistry J, Coggill PC, Sammut JS, Hotz HR, Ceric G, Forslund K, Eddy SR, Sonnhammer EL and Bateman A: **The Pfam protein families database.** *Nucleic Acids Res* 2008, **36:**D281–288.
14.　Mulder NJ and Apweiler R: **InterPro and InterProScan: tools for protein sequence classification and comparison.** *Methods Mol Biol* 2007, **396:**59–70.
15.　Schultz J, Copley RR, Doerks T, Ponting CP and Bork P: **SMART: a web-based tool for the study of genetically mobile domains.** *Nucleic Acids Res* 2000, **28:**231–234.
16.　Wu CH, Apweiler R, Bairoch A, Natale DA, Barker WC, Boeckmann B, Ferro S, Gasteiger E, Huang H, Lopez R, Magrane M, Martin MJ, Mazumder R, O'Donovan C, Redaschi N and Suzek B: **The Universal Protein Resource (UniProt): an expanding universe of protein information.** *Nucleic Acids Res* 2006, **34:**D187–191.
17.　Heida N, Hasegawa Y, Mochizuki Y, Hirosawa K, Konagaya A and Toyoda T: **TraitMap: an XML-based genetic-map database combining multigenic loci and biomolecular networks.** *Bioinformatics* 2004, **20 Suppl 1:**i152–i160.
18.　Kunz H, Derz C, Tolxdorff T and Bernarding J: **XML knowledge database of MRI-derived eye models.** *Comput Methods Programs Biomed* 2004, **73:**203–208.
19.　Jiang K and Nash C: **Application of XML database technology to biological pathway datasets.** *Conf Proc IEEE Eng Med Biol Soc* 2006, **1:**4217–4220.
20.　eXist-db: an open source database management system. http://exist-db.org.
21.　The World Wide Web Consortium. http://www.w3.org.
22.　Kabsch W and Sander C: **Dictionary of protein secondary structure: pattern recognition of hydrogen-bonded and geometrical features.** *Biopolymers* 1983, **22:**2577–2637.
23.　Jmol: an open-source Java viewer for chemical structures in 3D. http://www.jmol.org.
24.　Fiser A, Do RK and Sali A: **Modeling of loops in protein structures.** *Protein Sci* 2000, **9:**1753–1773.
25.　Laskowski RA, MacArthur MW, Moss DS and Thornton JM: **PROCHECK: a program to check the stereochemical quality of protein structures.** *J Appl Cryst* 1993, **26:**283–291.
26.　Liu L, Botos I, Wang Y, Leonard JN, Shiloach J, Segal DM and Davies DR: **Structral basis of Toll-like receptor 3 signaling with double-stranded RNA.** *Science* 2008, **320:**379–381.
27.　Maiti R, Van Domselaar GH, Zhang H and Wishart DS: **SuperPose: a simple server for sophisticated structural superposition.** *Nucleic Acids Res* 2004, **32:**W590–594.

Paper 2

TollML: a database of toll-like receptor structural motifs

Jing Gong, Tiandi Wei, Ferdinand Jamitzky, Wolfgang M. Heckl, Shaila C. Rössle and Robert W. Stark

ORIGINAL PAPER

TollML: a database of toll-like receptor structural motifs

**Jing Gong · Tiandi Wei · Ning Zhang ·
Ferdinand Jamitzky · Wolfgang M. Heckl ·
Shaila C. Rössle · Robert W. Stark**

Abstract Toll-like receptors (TLRs) play a key role in the innate immune system. TLRs recognize pathogen-associated molecular patterns and initiate an intracellular kinase cascade to induce an immediate defensive response. During recent years TLRs have become the focus of tremendous research interest. A central repository for the growing amount of relevant TLR sequence information has been created. Nevertheless, structural motifs of most sequenced TLR proteins, such as leucine-rich repeats (LRRs), are poorly annotated in the established databases. A database that organizes the structural motifs of TLRs could be useful for developing pattern recognition programs, structural modeling and understanding functional mechanisms of TLRs. We describe TollML, a database that integrates all of the TLR sequencing data from the NCBI protein database. Entries were first divided into TLR families (TLR1-23) and then semi-automatically subdivided into three levels of structural motif categories: (1) signal peptide (SP), ectodomain (ECD), transmembrane domain (TD) and Toll/IL-1 receptor (TIR) domain of each TLR; (2) LRRs of each ECD; (3) highly conserved segment (HCS), variable segment (VS) and insertions of each LRR. These categories can be searched quickly using an easy-to-use web interface and dynamically displayed by graphics. Additionally, all entries have hyperlinks to various sources including NCBI, Swiss-Prot, PDB, LRRML and PubMed in order to provide broad external information for users. The TollML database is available at http://tollml.lrz.de.

J. Gong · T. Wei · F. Jamitzky · W. M. Heckl · R. W. Stark
Center for Nanoscience,
Ludwig-Maximilians-Universität München,
80799 Munich, Germany

J. Gong · T. Wei (✉) · S. C. Rössle · R. W. Stark
Department of Earth and Environmental Sciences,
Ludwig-Maximilians-Universität München,
Theresienstr. 41,
80333 Munich, Germany
e-mail: tiandi@informatik.uni-muenchen.de

N. Zhang
Department of Informatics,
Ludwig-Maximilians-Universität München,
80333 Munich, Germany

F. Jamitzky
Leibniz Supercomputing Centre,
85748 Garching, Germany

W. M. Heckl
Deutsches Museum,
80538 Munich, Germany

W. M. Heckl
TUM School of Education, Technische Universität München,
80799 Munich, Germany

Introduction

Since the *Drosophila Toll* gene was discovered in the mid-1980s [1], genome projects have led to the identification of 13 receptors in mammalian and more than 20 receptors in non-mammalian genomes that are homologs of *Drosophila Toll*. These receptors have been termed collectively Toll-like receptors (TLRs). TLRs play a key role in innate immunity. They recognize invading microbial pathogens

and rapidly initiate intracellular signal transduction pathways to trigger expression of genes, whose products can control innate immune responses [2]. All TLRs have a common domain organization, with an extracellular ectodomain (ECD), a helical transmembrane domain (TD), and an intracellular Toll/IL-1 receptor homology (TIR) domain [3]. The ectodomain is a horseshoe-shaped solenoid structure and is directly involved in the recognition of a variety of pathogens including lipopolysaccharide, lipopeptide, cytosine-phosphate-guanine (CpG) DNA, flagellin, imidazoquinoline and dsRNA [4]. The transmembrane domain determines the subcellular localization of TLRs [5]. The TIR domain is conserved across all TLRs and IL-1 receptors, and is also shared by downstream signaling adaptor molecules. Upon receptor ligation, a TIR signaling complex is formed between the receptor and the adaptor TIR domains [6].

The TLR ectodomain contains varying numbers of leucine-rich repeat (LRR) motifs, which are arrays of 20 to 30 amino acid-long protein sequences that are enriched with the hydrophobic amino acid leucine. All LRR sequences can be divided into a highly conserved segment (HCS) and a variable segment (VS). The HCS consists of an 11 or 12 residue stretch with the consensus sequence LxxLxLxxN(Cx)xL. In this notation, the letter L represents the amino acids leucine, isoleucine, valine or phenylalanine, which form a hydrophobic core, N represents asparagine, threonine, serine or cysteine, and x is any amino acid. The variable segment can vary in both length and consensus sequence. Accordingly, several types of LRRs have been proposed [7, 8]. Of these, typical (T) type (xxLxxxxLxxLxx) and bacterial (S) type (xxLPx(x)LPxx) LRRs have been observed in TLRs [9]. All LRRs in TLRs are capped by N- and C-terminal LRRs that are usually irregular and do not match any type of LRR consensus sequences.

The atomic-detail crystal structure of the human TLR1 and TLR2 TIR domain was published in 2000 and gave the first insight into the molecular basis of TIR signaling [10]. The crystal structures of the ectodomains of human TLR1-4 and mouse TLR2-4 have also been resolved [11–16]. These structures demonstrate how the LRR-based platform is adapted to ligand recognition. Nevertheless, more than 2,000 TLR proteins have been sequenced by high-throughput genome sequencing projects. It is clear that the discrepancy between the rate at which novel protein sequences are discovered and the rate at which detailed structural information on proteins can be obtained from X-ray diffraction or nuclear magnetic resonance spectroscopy will persist for the foreseeable future. Thus, a comparative analysis at the sequence level is a useful approach to identify and characterize structural motifs of TLRs [9, 17] and to gain insight into how receptors and

ligands interact. Due to the variability of LRR motifs in TLRs, however, the indicated repeat number and positions (beginning/end of a repeating unit) for individual TLRs are quite different or missing in established databases. Currently, there is no collection of structural information for features that are contained within LRRs, such as HCS, VS and sequence insertions.

In this paper, we describe a database of TLR structural motifs called TollML. The current release (3.1) includes all known TLR sequences from the NCBI protein database [18]. Structural motifs were identified and annotated by a semi-automatic procedure that included comparison of sequences with the sequences of TLRs that have a known structure, consensus sequence matching, secondary structure prediction and multiple sequence alignments. Three levels of motif elements were generated: (1) signal peptide (SP), ectodomain (ECD), transmembrane domain (TD) and TIR domain of each TLR; (2) LRRs of each ECD; and (3) HCS, VS and insertions of each LRR. Some program application examples are presented in the last section of the paper.

Construction and content

Data extraction and pre-processing

Initial TLR sequences were extracted from the NCBI protein database. Two groups of search results were obtained using the search keys *toll** and *tlr**, where the asterisk stands for any suffix, to ensure that all TLRs were included. A manual data pre-processing step was performed before the motif identification of these sequences. We inspected the NCBI annotations of entries one-by-one to exclude TLR related molecules such as adaptors, protein kinases and transcription factors. After we performed these filtering steps, 2,572 TLR entries remained (NCBI release: 1 September 2009). We then categorized the TLRs into different families (TLR1-23) based on their original annotations. In the instances in which entries were not associated with explicit comments, we compared the sequences with well classified TLR sequences using sequence BLAST.

Motif identification

Three levels of structural motif categories were generated adapting to the structural organization of TLRs. First, each full length TLR sequence was divided into ECD, TD and TIR domain. If a sequence started with a SP, which directs the subcellular transport of a protein, the presence of a SP was also indicated. Second, the ECD of each TLR was partitioned into individual LRRs including

canonical LRRs and N/C-terminal LRRs. Third, each LRR was further divided into a highly conserved segment (HCS) and a variable segment (VS). Insertions within the VS that are longer than three residues were identified and annotated.

The procedure mentioned above was semi-automated. We first sorted the TLR sequences from each family into subgroups, so that an arbitrary pair of sequences from the same subgroup had a local sequence similarity greater than 90%. Then, the three-level structural motifs were identified manually for a selected template sequence from each subgroup. This selected template sequence was a full length sequence that had the most detailed original annotations so that the most accurate motif identifications could be performed. Finally, the other members of the subgroup received their motif partition assignments through multiple alignments with the template. More than 300 subgroups were generated for the 2,572 entries. Thus more than 300 templates were processed manually.

The manual motif identification of a template sequence combined three approaches: consensus sequence matching, secondary structure prediction and reference to original annotations or literatures. The four domains on the first level of the motif categorization (SP, ECD, TD and TIR) have characteristic sequence features, so are usually accurately divided in the original annotation of a selected template. If a template did not have clear annotations, then its sequence was compared to similar sequences with known domains to determine its domain partitions. For the second level of motif categorization, if a selected template was associated with a reliable reference such as a known crystal structure, its LRR partition was then assigned accordingly. Otherwise, we matched the LRR consensus sequence LxxLxLxxN(Cx)xL to the template sequence amino-acid-by-amino-acid and detected LRR motifs manually. In addition, protein secondary structure predictions (PredictProtein [19], NNPREDICT [20], PSIPRED [21] and SSPro [22]) helped to improve the accuracy of LRR detection because all known crystal structures of TLRs show that there is always a short β-strand (3–5 residues) beginning at approximately the third position of an LRR motif [11–15]. After an LRR was identified, consensus sequence matching was used to identify its HCS and VS motifs, as well as any insertions that were longer than three residues for the third level. Simultaneously, each LRR motif was classified into different types (detailed in Database content) according to the VS consensus sequences.

Database content

The TollML release 3.1 contains 2,572 TLR entries divided into 23 families (entry distribution shown in Table 1).

Among these, 2,350 of the sequences contain an ectodomain and thus received motif annotations that correspond to the second and third levels of motif categorization. The other entries contain only a TIR domain with or without a transmembrane domain. A total of 46,720 LRR motifs were recognized from the ectodomain containing TLRs. These LRR motifs were classified into five types: typical (T), bacterial (S), N-terminal (NT), C-terminal (CT) and irregular (I). A histogram of LRR length statistics (Fig. 1) shows the characteristic length distribution of each LRR type. The standard length of the T type LRR is 24 amino acids. A large number of T type LRRs have insertions and only some have deletions. These statistics suggest that the evolution of T type LRRs may prefer insertion over deletion. By contrast, the S type LRRs are more highly conserved. Their lengths are concentrated on 20 and 21. N-terminal LRRs vary in length and do not form a peak value in length distribution. Most C-terminal LRRs contain four cysteines that are distantly separated at the sequence level and form disulfide bonds with each other. C-terminal LRRs are generally greater than 35 amino acids in length.

Annotations for each TLR entry include:

(1) Data management information: TollML ID and access/ modification date;
(2) Primary information extracted from the NCBI and related literature: FASTA sequence, biological definition, cell information, glycosylation sites and ligands;
(3) Protein family classification;
(4) Database cross links: NCBI, Swiss-Prot [23], PDB [24], LRRML [8] and PubMed [25];
(5) Three-level motif information.

Database comparison

Currently, several protein databases, such as Pfam [26], InterPro [27], SMART [28] and Swiss-Prot, contain information about TLRs. These databases predict the LRR numbers and positions for their TLR entries by various computational methods, thus resulting in a high frequency of false negative predictions. Table 2 illustrates the LRR numbers for human TLR1–10 as reported by these databases. The manual motif identification procedure discussed here provides TollML with the most complete database of LRR motifs. Although Swiss-Prot presents more accurate results than the other three databases that we investigated (Table 2), TollML has four prominent characteristics that distinguish it from Swiss-Prot:

(1) Comprehensive entry coverage. TollML covers 2,572 TLR sequences from 121 species and all sequences are provided with detailed motif annotations. Swiss-Prot

Table 1 Entry distribution over Toll-like receptor (TLR) families for mammalian/non-mammalian groups

TLR	1	2	3	4	5	6	7	8	9	10	11	12	13	14	15	16	18	19	20–23	Total
Mammalian	85	146	108	443	132	106	109	101	124	72	10	11	9	0	0	0	0	0	0	1,456
Non-mammalian	356	276	84	77	58	3	102	11	30	0	0	1	4	6	42	2	7	5	52	1,116
Total	441	422	192	520	190	109	211	112	154	72	10	12	13	6	42	2	7	5	52	2,572

covers 636 TLR sequences from 17 species and only 59 sequences have LRR annotations (results obtained on 24 February 2009).

(2) Structural motifs within an LRR. TollML annotates the HCS, VS and insertion for each LRR. This information is not present in any other published protein databases.

(3) Uniform LRR definition. The beginning/end positions of LRRs have been defined inconsistently across researchers due to the periodicity of LRR motifs. This variation leads to non-uniform LRR assignments in Swiss-Prot. All LRR motifs in TollML start at the beginning of the HCS and end at the end of the VS, just before the HCS of the next LRR.

(4) Accessibility of motif sequences. The amino acid sequence of any available motif is directly accessible in TollML, whereas only the full length sequence is directly accessible in Swiss-Prot.

Utility

Web application

The extensible markup language (XML) was standardized in the 1990s and is well established as a format for hierarchical biological data. TollML was designed by using eXist [29], an XML database management system, and XPath/XQuery [30] for processing queries and web forms. The document type definition (DTD) file of TollML is provided in the electronic supplementary material (ESM; Supplementary file 1).

The entire database is browsable. When browsing, entries appear in a summary table containing ID, definition, family, species and links of motif partitions. Clicking on an entry opens an XML Stylesheet (XSLT) [30] converted HTML web page that describes the entry in detail. The original XML file can also be downloaded. The XSLT file that the program uses is provided in the ESM (Supplementary file 2). Aside from the textual view, the structural motifs of TLRs can be exhibited by three-level dynamic graphics. Figure 2 demonstrates the motif assignment for an example entry (ID: TLR_561).

On the *advanced search* page of TollML, users can search entries flexibly by inputting keywords, specifying search fields, and defining annotation contents of the output. After selected entries are returned, a *search within result* button allows for further term filtering. The resulting entries, or an arbitrarily selected subset thereof, can be sent to generate multiple sequence alignments supplied by the T-Coffee package [31]. In addition, a Wu-BLAST search tool [32] is available. A query sequence can be BLASTed against the entire database, against a certain TLR family, or against a collection of sequences marked by a user-defined label (available for registered users).
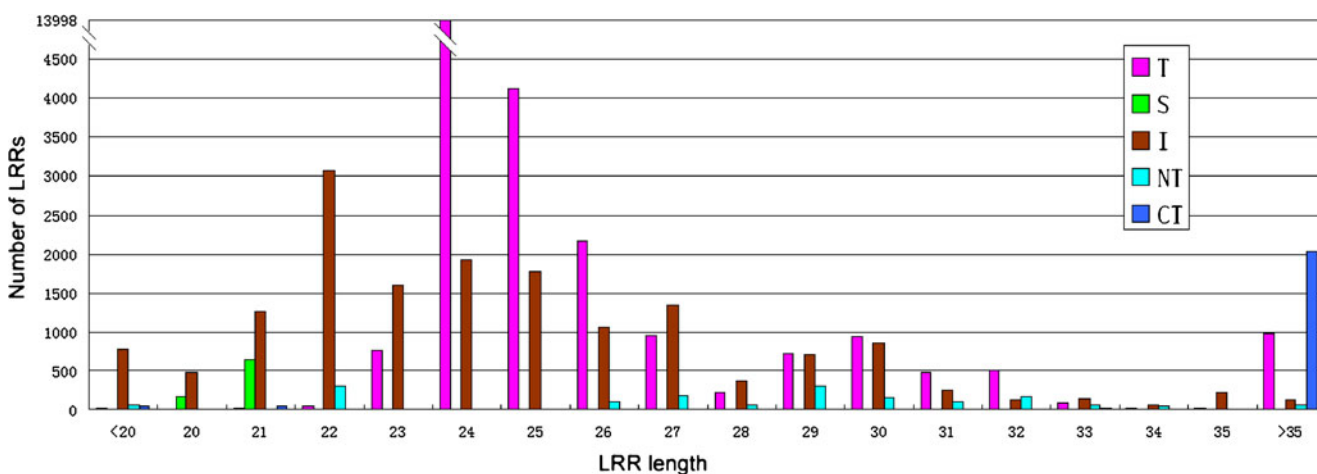

Fig. 1 Leucine-rich repeat (LRR) length distribution

Table 2 Comparison of leucine-rich repeat (LRR) numbers of human TLR1–10 in different databases (results obtained on 24 February 2009)

	TLR1	TLR2	TLR3	TLR4	TLR5	TLR6	TLR7	TLR8	TLR9	TLR10
InterPro	4	4	8	7	7	3	9	10	6	4
Pfam	4	4	7	7	8	3	8	9	6	4
SMART	6	9	19	12	10	7	16	17	19	7
Swiss-Prot	8	14	22	21	15	13	27	24	26	15
TollML	21	21	25	23	23	21	28	28	28	21

Application in LRR prediction

The automatic identification of motifs in a protein sequence is essentially a statistical pattern recognition problem. Therefore, the performance of a prediction method is thus strongly dependent on the quality and scale of the training data set. A recent program, LRRscan [17], demonstrated the feasibility of a statistics-based consensus matching algorithm applied to LRR detection. TollML supplies a large and reliable source to train LRR prediction methods of different algorithms. As an example, we developed a 20× 12 position-specific weight matrix of LRR motifs based on the LRR partitions from TollML (matrix available on the TollML webpage). A matrix element denotes the frequency probability of a certain amino acid occurring at a certain position in the LRR HCS. We have already obtained confident results through this sort of matrix scan with an appropriate cut-off score. A five-fold cross validation against all TollML entries indicates that the sensitivity and specificity are both greater than 93%. This program was implemented on the TollML webpage and has been named LRRFinder. This method can be extended to predict LRR motifs in other LRR containing proteins besides TLRs, since all LRR types possess the same HCS pattern.

Fig. 2 Online graphic display of three-level structural motifs of a database entry
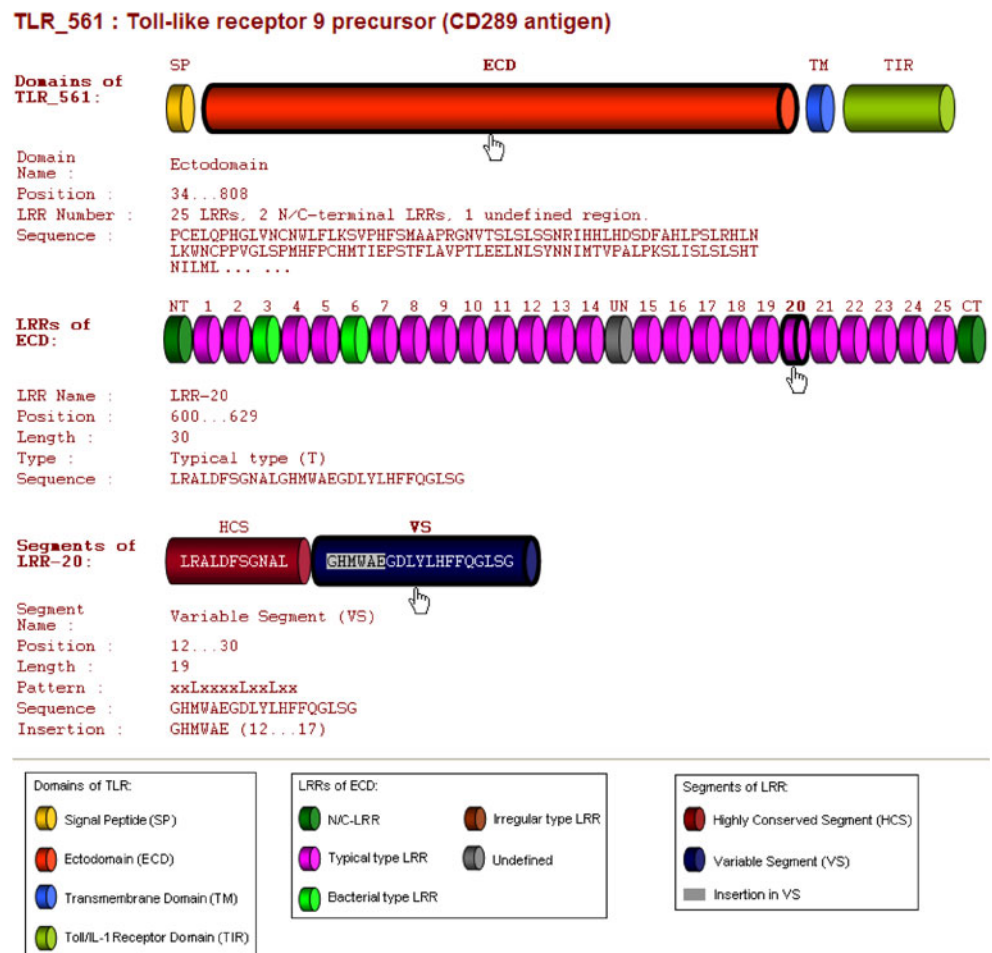
Application in homology modeling

Homology modeling is currently the most accurate computational method to predict protein structure. This system constructs a structural model for a target protein sequence from a template structure of a homologous protein. For this method to work, the target and template structures must have a sequence identity over 30%. The known crystal structures of human TLR1–4 and mouse TLR2–4 ectodomains supply valuable templates for the homology modeling of other TLR ectodomains. However, given the variability in repeat numbers and type arrangements of LRRs contained within TLRs, a full length template with a sufficient sequence identity is typically not available. This limitation can be overcome by assembling multiple LRR templates. First, all LRRs in the target sequence are identified. Then, the most similar structure-known LRR based on sequence is found for each LRR in the target sequence as a local template. Finally, all local templates are assembled to generate a multiple sequence alignment for the complete target sequence. TollML enables the direct accessibility of accurate LRR sequence partitions for the first step. The LRRML database [8] can further provide suitable LRR structural templates. This LRR template assembling approach was proven to be both feasible and significant by recent structure modeling research into human TLR7–9 [33].

Conclusions

We have developed a specialized database of TLR structural motifs called TollML. It is supported by an XML database management system and can be searched and browsed with an easy-to-use web interface. This interface is suitable for use with most graphical web browsers and has been tested on the Windows, Mac and Linux operating systems. TollML includes all TLR sequences that are published in the NCBI protein database and semi-automatically creates three levels of motif annotations. This database can help to develop motif prediction programs, to model three-dimensional structures of TLRs and to design new mutation experiments to better understand receptor–ligand or receptor–receptor interactions. We plan to update TollML every 2–3 months since the number of sequenced TLR proteins increases constantly.

Availability and requirements

This database is freely available at http://tollml.lrz.de. Any internet user can search and download data from the database, but only registered users can define and save labels for arbitrary entries.

References

1. Anderson KV, Bokla L, Nusslein-Volhard C (1985) Establishment of dorsal-ventral polarity in the Drosophila embryo: the induction of polarity by the Toll gene product. Cell 42:791–798
2. Takeda K, Akira S (2005) Toll-like receptors in innate immunity. Int Immunol 17:1–14
3. Brodsky I, Medzhitov R (2007) Two modes of ligand recognition by TLRs. Cell 130:979–981
4. Gay NJ, Gangloff M (2007) Structure and function of Toll receptors and their ligands. Annu Rev Biochem 76:141–165
5. Barton GM, Kagan JC, Medzhitov R (2006) Intracellular localization of Toll-like receptor 9 prevents recognition of self DNA but facilitates access to viral DNA. Nat Immunol 7:49–56
6. O'Neill LA, Bowie AG (2007) The family of five: TIR-domain-containing adaptors in Toll-like receptor signalling. Nat Rev Immunol 7:353–364
7. Kobe B, Kajava AV (2001) The leucine-rich repeat as a protein recognition motif. Curr Opin Struct Biol 11:725–732
8. Wei T, Gong J, Jamitzky F, Heckl WM, Stark RW, Roessle SC (2008) LRRML: a conformational database and an XML description of leucine-rich repeats (LRRs). BMC Struct Biol 8:47
9. Matsushima N, Tanaka T, Enkhbayar P, Mikami T, Taga M, Yamada K, Kuroki Y (2007) Comparative sequence analysis of leucine-rich repeats (LRRs) within vertebrate toll-like receptors. BMC Genomics 8:124
10. Xu Y, Tao X, Shen B, Horng T, Medzhitov R, Manley JL, Tong L (2000) Structural basis for signal transduction by the Toll/interleukin-1 receptor domains. Nature 408:111–115
11. Bell JK, Botos I, Hall PR, Askins J, Shiloach J, Segal DM, Davies DR (2005) The molecular structure of the Toll-like receptor 3 ligand-binding domain. Proc Natl Acad Sci USA 102:10976–10980
12. Choe J, Kelker MS, Wilson IA (2005) Crystal structure of human toll-like receptor 3 (TLR3) ectodomain. Science 309:581–585
13. Jin MS, Kim SE, Heo JY, Lee ME, Kim HM, Paik SG, Lee H, Lee JO (2007) Crystal structure of the TLR1-TLR2 heterodimer induced by binding of a tri-acylated lipopeptide. Cell 130:1071–1082
14. Kim HM, Park BS, Kim JI, Kim SE, Lee J, Oh SC, Enkhbayar P, Matsushima N, Lee H, Yoo OJ, Lee JO (2007) Crystal structure of the TLR4-MD-2 complex with bound endotoxin antagonist Eritoran. Cell 130:906–917
15. Liu L, Botos I, Wang Y, Leonard JN, Shiloach J, Segal DM, Davies DR (2008) Structural basis of toll-like receptor 3 signaling with double-stranded RNA. Science 320:379–381
16. Park BS, Song DH, Kim HM, Choi BS, Lee H, Lee JO (2009) The structural basis of lipopolysaccharide recognition by the TLR4-MD-2 complex. Nature 458:1191–1195
17. Dolan J, Walshe K, Alsbury S, Hokamp K, O'Keeffe S, Okafuji T, Miller SF, Tear G, Mitchell KJ (2007) The extracellular leucine-rich repeat superfamily; a comparative survey and analysis of evolutionary relationships and expression patterns. BMC Genomics 8:320
18. Wheeler DL, Barrett T, Benson DA, Bryant SH, Canese K, Chetvernin V, Church DM, Dicuccio M, Edgar R, Federhen S, Feolo M, Geer LY, Helmberg W, Kapustin Y, Khovayko O, Landsman D, Lipman DJ, Madden TL, Maglott DR, Miller V, Ostell J, Pruitt KD, Schuler GD, Shumway M, Sequeira E, Sherry ST, Sirotkin K, Souvorov A, Starchenko G, Tatusov RL, Tatusova TA, Wagner L, Yaschenko E (2008) Database resources of the

National Center for Biotechnology Information. Nucleic Acids Res 36:D13–D21

19. Rost B, Yachdav G, Liu J (2004) The PredictProtein server. Nucleic Acids Res 32:W321–W326

20. Kneller DG, Cohen FE, Langridge R (1990) Improvements in protein secondary structure prediction by an enhanced neural network. J Mol Biol 214:171–182

21. Bryson K, McGuffin LJ, Marsden RL, Ward JJ, Sodhi JS, Jones DT (2005) Protein structure prediction servers at University College London. Nucleic Acids Res 33:W36–W38

22. Pollastri G, Przybylski D, Rost B, Baldi P (2002) Improving the prediction of protein secondary structure in three and eight classes using recurrent neural networks and profiles. Proteins 47:228–235

23. Wu CH, Apweiler R, Bairoch A, Natale DA, Barker WC, Boeckmann B, Ferro S, Gasteiger E, Huang H, Lopez R, Magrane M, Martin MJ, Mazumder R, O'Donovan C, Redaschi N, Suzek B (2006) The Universal Protein Resource (UniProt): an expanding universe of protein information. Nucleic Acids Res 34:D187–D191

24. Berman HM, Westbrook J, Feng Z, Gilliland G, Bhat TN, Weissig H, Shindyalov IN, Bourne PE (2000) The Protein Data Bank. Nucleic Acids Res 28:235–242

25. PubMed: http://www.ncbi.nlm.nih.gov/pubmed

26. Finn RD, Tate J, Mistry J, Coggill PC, Sammut SJ, Hotz HR, Ceric G, Forslund K, Eddy SR, Sonnhammer EL, Bateman A (2008) The Pfam protein families database. Nucleic Acids Res 36: D281–D288

27. Mulder N, Apweiler R (2007) InterPro and InterProScan: tools for protein sequence classification and comparison. Methods Mol Biol 396:59–70

28. Schultz J, Copley RR, Doerks T, Ponting CP, Bork P (2000) SMART: a web-based tool for the study of genetically mobile domains. Nucleic Acids Res 28:231–234

29. eXist: http://exist-db.org

30. The World Wide Web Consortium: http://www.w3.org

31. Notredame C, Higgins DG, Heringa J (2000) T-Coffee: A novel method for fast and accurate multiple sequence alignment. J Mol Biol 302:205–217

32. WU-BLAST: http://blast.wustl.edu

33. Wei T, Gong J, Jamitzky F, Heckl WM, Stark RW, Rossle SC (2009) Homology modeling of human Toll-like receptors TLR7, 8, and 9 ligand-binding domains. Protein Sci 18:1684–1691

Paper 3

A leucine-rich repeat assembly approach for homology modeling of human TLR5-10 and mouse TLR11-13 ectodomains

Tiandi Wei, Jing Gong, Ferdinand Jamitzky, Wolfgang M. Heckl, Shaila C. Rössle and Robert W. Stark

A leucine-rich repeat assembly approach for homology modeling of human TLR5-10 and mouse TLR11-13 ectodomains

Tiandi Wei [a,b], Jing Gong [a,b,*], Shaila C. Rössle [b], Ferdinand Jamitzky [a,c], Wolfgang M. Heckl [a,d,e] and Robert W. Stark [a,b]

[a]*Center for Nanoscience, Ludwig-Maximilians-Universität München. 80799 Munich, Germany.*

[b]*Department of Earth and Environmental Sciences, Ludwig-Maximilians-Universität München. 80333 Munich, Germany.*

[c]*Leibniz Supercomputing Centre. 85748 Garching, Germany.*

[d]*Deutsches Museum. 80538 Munich, Germany.*

[e]*TUM School of Education, Technische Universität München. 80799 Munich, Germany.*

*Corresponding author:

Add: Theresienstr. 41, 80333 Munich, Germany

Email: gongj@informatik.uni-muenchen.de

Tel: +49-89-2180-4359

Fax: +49-89-2180-4334

Abstract

So far, 13 groups of mammalian Toll-like receptors (TLRs) have been identified. Most TLRs have been shown to recognize pathogen-associated molecular patterns from a wide range of invading agents and initiate both innate and adaptive immune responses. The TLR ectodomains are composed of varying numbers and types of leucine-rich repeats (LRRs). As the crystal structures are currently missing for most TLR ligand-binding ectodomains, homology modeling enables first predictions of their three-dimensional structures on the basis of the determined crystal structures of TLR ectodomains. However, the quality of the predicted models that are generated from full-length templates can be limited due to low sequence identity between the target and templates. To obtain better templates for modeling, we have developed an LRR template assembly approach. Individual LRR templates that are locally optimal for the target sequence are assembled into multiple templates. This method was validated through the comparison of a predicted model with the crystal structure of mouse TLR3. With this method we also constructed ectodomain models of human TLR5, TLR6, TLR7, TLR8, TLR9, and TLR10 and mouse TLR11, TLR12, and TLR13 that can be used as first passes for a computational simulation of ligand docking or to design mutation experiments. This template assembly approach can be extended to other repetitive proteins.

Key words

1. Introduction

Cells of the innate immune system, such as macrophages and dendritic cells, express a limited number of germline-encoded pattern-recognition receptors (PRR) that specifically recognize pathogen-associated molecular patterns (PAMPs) within microbes. These molecular patterns are unique to these microbes and are absent in the host [1]. Toll-like receptors (TLRs) are currently the best-characterized members of the PRRs [2]. The progress of genome sequencing projects has led so far to the identification of 13 groups of TLRs in mammalian genomes, ten in humans and 13 in mice [3], and more than 20 in non-mammalian genomes [4]. All TLRs have a common domain organization, with an extracellular ectodomain, a helical transmembrane domain, and an intracellular Toll/IL-1 receptor homology (TIR) domain [5]. The extracellular domain (ectodomain) is responsible for the recognition of common structural patterns in various microbial molecules. For example, lipoproteins or lipopeptides are recognized by TLR2 complexed with TLR1 or TLR6, viral double-stranded RNAs by TLR3, lipopolysaccharides by TLR4, bacterial flagellins by TLR5, single-stranded RNAs by TLR7 or TLR8, and microbial CpG DNAs by TLR9 [6, 7]. The TIR domains of TLRs are associated with the intracellular signaling cascade leading to the nuclear translocation of the transcription factor NF-κB [8].

A TLR ectodomain contains 19 to 27 consecutive leucine-rich repeat (LRR) motifs sandwiched between two terminal LRR modules (LRRNT and LRRCT) [4]. LRRs exist in more than 6000 proteins and more than 100 crystal structures of these proteins have been deposited in the Protein Data Bank (PDB) [9, 10]. In every case, the protein adopts an arc or horseshoe shape. An individual LRR motif is defined as an array of 20 to 30 amino acids that is rich in the hydrophobic amino acid leucine. All LRR sequences can be divided into a conserved segment and a variable segment. The conserved segments, LxxLxLxxNxL, generate the concave surface of the LRR arc or horseshoe by forming parallel β-strands, while the variable parts form its convex surface consisting of helices or loops. The terminal LRRNT and LRRCT modules stabilize the protein structure by shielding its hydrophobic core from exposure to solvent.

To date, only the crystal structures of the ectodomains of human TLR1 through 4 and mouse TLR2 through 4 have been determined [11-15]. High-throughput genome sequencing projects, however, have led to the identification of more than 2000 TLR sequences. Thus, the structures of most TLRs are still unknown because structure determination by X-ray diffraction or nuclear magnetic resonance spectroscopy experiments remains time-consuming. Protein structure prediction methods are powerful tools to bridge the gap between sequence determination and structure determination.

Homology modeling, also referred to as comparative modeling, is currently the most accurate computational method for protein structure prediction. This approach constructs a three-dimensional model for a target protein sequence from a three-dimensional template structure of a homologous protein. Thus, the quality of the homology model strongly depends on the sequence identity between the target and template. Below 30% identity, serious errors may occur [16]. Due to different repeat numbers and distinct arrangements of LRRs in the TLR ectodomains, a proper full-length template with a sufficiently high sequence identity to the target is often missing. This limitation can be overcome by assembling multiple LRR templates. In this approach the most similar (on the sequence level) LRR with a known structure is

searched as a local template for each LRR in the target sequence. Such an LRR template may be derived from TLRs or from other proteins. Thereby, a suitable template may be found even for an insertion-containing irregular LRR. All local template sequences are then combined to generate a multiple sequence alignment for the complete target sequence. Thus, a high-quality model can be created, even if no adequate single template is available. To facilitate a multiple template assembly of LRR proteins, we have developed the LRRML database [9], which archives individual LRR structures manually identified from all known LRR protein structures. In addition, we have developed TollML [4], a database of sequence motifs of TLRs. In TollML, all known sequences of TLR ectodomains were semi-automatically partitioned into LRR segments and are made available for query. For newly sequenced TLRs that are not yet archived in TollML, we have implemented an LRR prediction program named LRRFinder on the TollML webpage. It requires as input an LRR-containing amino acid sequence and returns the number and positions of LRRs in the input sequence. LRRFinder recognizes LRR motifs based on a position-specific weight matrix scan, with the sensitivity and specificity both higher than 93%. With the help of these two databases, LRR partitions of a TLR ectodomain can be directly obtained, and an optimal structure template for each LRR segment can be quickly found. A schematic flowchart of the modeling procedure is shown in Figure 1.

In this study, we apply the multiple template assembly approach to TLRs. To demonstrate the potential of the method we constructed two models of the mouse TLR3 ectodomain as a test case using our LRR template assembly method and a standard profile-profile alignment-aided full-length template recognition method. Both models were then compared with the crystal structure of mouse TLR3. The overall and ligand-binding site conformation of the template assembly-based model is closer to that of the crystal structure than that based on the standard method. We also modeled the human TLR5 through 10 and mouse TLR11 through 13 ectodomains, which represent mammalian TLR ectodomains with unknown structures. A comparison of the model for human TLR6 with the very recently reported crystal structure of mouse TLR6 shows a very good structural agreement.

2. Methods

2.1 Template selection and sequence alignment

Amino acid sequences of mouse TLR3, human TLR5 through 10, and mouse TLR11 through 13 ectodomains were extracted from TollML release 3.0 (IDs 627, 531, 571, 992, 575, 1022, 851, 703, 705, and 704). Their LRR partitions were annotated by TollML. For each LRR sequence contained in each target TLR, the three-dimensional LRR structure with the highest sequence identity was selected as a template from LRRML through a sequence similarity search. Then, a multiple sequence alignment of a target with all its local LRR templates was generated with each template comprising one alignment line. For instance, the mouse TLR3 has a total of 25 LRRs and accordingly required 25 templates. The associated multiple sequence alignment then has 26 lines (Figure 1). Because of the characteristic consensus sequences of LRRs, these alignments were made more accurately manually than automatically. To generate an alternate model with standard methods, the widely acknowledged template recognition program pGenTHREADER [17] was executed to find templates for mouse TLR3. This method calculates sequence profiles from an input sequence and combines profile-

profile alignments with secondary structure specific gap-penalties, pair potentials, and solvation potentials using a linear combination. The output is the complete PDB structures that serve as candidate templates ranked by P-values. Each candidate sequence is aligned with the target sequence.

2.2 Model construction and validation

The initial three-dimensional coordinates of all models were calculated by MODELLER 9v7 [18]. The above-described alignment file and the corresponding template structures of a target model were inputted into the default 'model' routine of MODELLER. A given number of three-dimensional models were calculated. The ectodomains of TLRs contain a number of insertion regions. Some of them corresponded to four to 15 amino acid-long gaps in the alignments because their templates do not contain a corresponding insertion. During modeling, these gaps produced loop structures in the model, thus deteriorating the model accuracy. ModLoop [19] was used to rebuild the coordinates of these loop regions. Finally, we used the model quality assessment programs ProQ [20] and MetaMQAP [21] to evaluate the output candidate models and select the one with the best scores as the final model. The structure superimpositions and molecular electrostatics involved in the structural analysis were carried out using SuperPose v1.0 [22] and VMD [23], respectively. The docking studies of TLR11 and its ligand profilin were performed with GRAMM-X [24].

3. Results

3.1 LRR templates

The number of LRRs in the full-length ectodomains of mouse TLR3, human TLR5 through 10, and mouse TLR11 through 13 is 25, 23, 21, 28, 28, 28, 21, 26, 25, and 27, respectively. Consequently, a total of 252 individual LRR templates sourced from 41 different PDB structures were selected from LRRML. Their sequence identities with the targets vary from 26.0% to 95.7% (43.8% on average), and similarities from 39.0% to 100% (58.2% on average). Remarkably, all cases of relatively low sequence identity (< 35%) were caused by highly irregular target LRRs. These highly irregular sequences include LRRNT/CTs, the highly mutated LRR15 of TLR7/8/9, and the insertion-containing LRRs whose templates do not include a similar insertion. The sources (LRRML IDs) and sequence identities of all LRR templates are listed in Table 1.

As the modeling of mouse TLR3 was carried out to verify our approach, we assumed that the crystal structure of the mouse TLR3 ectodomain was unknown and excluded the corresponding LRR entries of mouse and human TLR3 ectodomains from LRRML before the template search. The selected individual LRR templates for mouse TLR3 were associated with 18 PDB structures, 14 of which were from non-TLR proteins. The target-template sequence identities range from 33.3% to 50.0% (44.1% on average). By contrast, pGenTHREADER provided only complete PDB structures of LRR proteins as candidate templates, with each candidate possessing a pairwise sequence alignment with the target. Because no single template covered the entire sequence of mouse TLR3, we selected the first seven candidates by rank (except mouse and human TLR3) and combined them into a multiple alignment to avoid template gaps. These templates included PDB structures 2Z64, 2Z81, 1O6V, 3FXI, 2Z7X, 1JL5, and 3BZ5, which covered the closest homologues (mouse TLR2/4 and human TLR1/4) to mouse TLR3

among all proteins with known structures. Nevertheless, the sequence identities of the seven templates to mouse TLR3 range from 16.1% to 21.2% (18.7% on average), which fell much below the cut-off value 30% for homology modeling [16].

3.2 Structural models

3.2.1 Model of mouse TLR3

Recently, we constructed a model of mouse TLR3 with the LRR template assembly method as a test case of the LRRML database [9]. It revealed a horseshoe-shaped assembly adopting a regular solenoid structure without disordered regions. The model was superimposed with the crystal structure of mouse TLR3 ectodomain (PDB code: 3CIG) [14] at its both ligand-binding regions, LRRNT through LRR3 and LRR19 through LRR21. The backbone root mean square deviation (RMSD) is 1.96 Å and 1.90 Å, respectively [9]. To verify the improvements of the database and the modelling process, we reconstructed the mouse TLR3 model (Figure 2b) with up-to-date LRR templates. Compared with the old model, four of the 25 LRRs of TLR3 in the new model were assigned new templates with higher sequence identities (Table 1). Because these four LRRs are not involved in the TLR3 ligand-binding sites, the corresponding RMSD values of the new model were the same as for the previous model. These values indicate that the model predicted with our method well matches the crystal structure and can be used to predict potential ligand-binding sites [25].

For comparison purposes, the mouse TLR3 ectodomain was also modeled with a standard profile-profile alignment-aided full-length template recognition method. All of the ten output models obtained from MODELLER for the full-length templates-based standard alignment showed a serious structural disorder spanning from LRR6 through LRR10 (Figure 2a). The LRR6 through LRR10 on the crystal structure form a regular solenoid structure with an α-helix in the variable segment of LRR8 (Figure 2c). By contrast, the corresponding LRRs on the model completely lost the proper LRR shape and interwove with one another. The disorder was caused by mismatches or target gaps in the alignment, where only two to four template LRRs were assigned to five target LRRs (Figure 2d). The standard alignment could not create a one-to-one correspondence between the target and template LRR units due to the irregularity of the LRRs. ProQ and MetaMQAP were used to evaluate the quality of the different models of mouse TLR3 (Table 2). Both programs make an integrative assessment of the structure quality considering geometry, stereochemistry, and energy distribution of the structures. Both template assembly-based models received better scores than the model based on standard method.

3.2.2 Models of human TLR5 through 10 and mouse TLR11 through 13

With the LRR template assembly method we modeled the human TLR5 through 10 and mouse TLR11 through 13 ectodomains. All of the resulting models are provided in Supplementary File 1. Ramachandran plots of these models were created with PROCHECK [26] and are provided in Supplementary File 2. Model evaluation data by ProQ and MetaMQAP are listed in Table 2. The models reveal a horseshoe shape (Figure 3), where a longer or shorter sequence (more or less LRR units) implies a smaller or larger horseshoe opening, e.g., TLR7/8 (smaller opening) and TLR6/10 (larger opening). Their overall structural similarity reflects the phylogenetic

relationships among these TLRs. For example, TLR6 is similar to TLR10 while TLR7 is similar to TLR8, consistent with the molecular tree proposed by Roach and co-workers [27]. Mammalian TLRs are distinct from other LRR proteins in that they contain two to seven insertion-containing irregular LRRs, which may be necessary for ligand-binding and receptor dimerization. Our models show that all insertions are located on that face of the horseshoe, to which the convex site β-strands point, whereas the other face is completely insertion-free.

To highlight the availability of these models for an analysis of receptor-ligand interaction mechanisms, we performed molecular electrostatics calculations of the mouse TLR11 model with a ligand. TLR11 can recognize profilin of some apicomplexan protozoa parasites. This protein is involved in parasite motility and invasion [28]. Expression of TLR11 is suppressed in humans [29]. The electrostatic analysis (Figure 4a) shows that the entire surface of the profilin of *P. falciparum* (PDB code: 2JKF) is predominantly negatively charged, whereas TLR11 exhibits several positively charged patches (Figure 4b). Protein docking studies using GRAMM-X showed that profilin and the positive patches on TLR11 possess compatible sizes and electrostatic complementarity (Supplementary File 3).

Very recently, the crystal structure of the TLR6 ectodomain complexed with TLR2 and a Pam2CSK4 ligand was released in PDB (PDB code: 3A79). The TLR6 structure is a hybrid structure of mouse and inshore hagfish, where 18 mouse LRRs (LRRNT through LRR17) were hybridized with two hagfish LRRs (LRR18 and LRRCT) [30]. This crystal structure served as an additional benchmark for our template assembly approach. The superimposition of the mouse part of the crystal structure with our human TLR6 model yielded a backbone RMSD of 1.94 Å, which indicates that the model is very similar to the crystal structure (Figure 5). A second model of human TLR6 was generated with pGenTHREADER in a similar procedure as described for the mouse TLR3 (Supplementary File 1). The backbone RMSD between the crystal structure and this model is 1.89 Å. The only full-length template used for this model was the structure of human TLR1 (PDB code: 2Z7X). Because TLR6 and TLR1 possess the same number of LRRs and have a very high sequence identity (63.3%), the structure of TLR1 serves as an excellent full-length template. Under these very good conditions, both, the standard and the template assembly approaches, provided high-quality models.

4. Discussion

In template-based protein modeling, the overall sequence identity between the target and template is an important criterion for the selection of suitable templates [31]. For repetitive LRR proteins, however, there is often no appropriate full-length template available due to different repeat numbers and distinct arrangements. This problem can be solved by combining individual repeating units that are locally optimal for the target sequence. In the method validation with mouse TLR3, the average target-template sequence identity achieved by our method was 44.8%, which was significantly higher than that (18.7%) achieved by a standard profile-profile alignment-aided template recognition method. However, both the standard and the template assembly methods produced models of human TLR6 very well matched the crystal structure of mouse TLR6. The comparison between the models obtained with both methods highlights the potential of the template assembly approach. It can produce models with a similar quality as the standard profile-profile alignment method. The template assembly method, however, reveals its particular strength in situations where no adequate full-length

templates are available. In the case of TLR3, the standard profile-profile alignment method failed to predict a reliable model due to significant gaps in the template. Here, the template assembly method overcomes the difficulties and generates a realistic model.

In a previous work, we constructed models of human TLR7/8/9 ligand-binding domains by combining LRR segments that were extracted from all known crystal structures of TLRs [32]. The average target-sequence similarities for TLR7/8/9 were 47.7%, 47.2%, and 46.8%, respectively. The resulting models supported experimentally determined ligand-binding residues [33, 34] and provided a reliable basis to identify potential ligand-binding residues and potential receptor dimerization mechanisms. Here, we went a step further and extended the scope of the approach by searching LRR segments from all LRR-containing proteins with known structures with the LRRML database because the same type of LRRs can exist in different proteins [9]. Consequently, 33 of the 41 source PDB structures are non-TLR proteins (numbers derived from Table 1). The average target-sequence similarities for TLR7/8/9 increased to 55.9%, 58.2%, and 59.2%.

Another key issue in LRR protein modeling is the sequence-level LRR partition of the target TLR sequence. The indicated number and beginning/end positions of LRRs in TLRs vary largely across different databases or research reports due to the irregularity and periodicity of LRRs. TollML reports the most complete and accurate LRR motifs for TLRs as compared with a number of databases [4]. In addition, TollML provides a statistics-based LRR prediction program LRRFinder for new TLR entries that are not yet collected in TollML. It can recognize LRRs from an input amino acid sequence with high confidence.

In conclusion, this work depicts an LRR template assembly approach for protein homology modeling. The comparison of a mouse TLR3 model with its crystal structure underlined feasibility and reliability of the method. With this method, a series of mammalian TLR ectodomains were modeled. These models can be used to perform ligand docking studies or to design mutagenesis experiments and hence to investigate TLR ligand-binding mechanisms. Our modeling approach can be extended to other repetitive proteins.

Acknowledgements

References

[1]   Kawai T, Akira S (2008) Toll-like receptor and RIG-I-like receptor signaling. Ann N Y Acad Sci 1143:1-20.

[2]   Medzhitov R (2007) Recognition of microorganisms and activation of the immune response. Nature 449:819-826.

[3]   Kumar H, Kawai T, Akira S (2009) Pathogen recognition in the innate immune response. Biochem J 420:1-16.

[4]   Gong J, Wei T, Zhang N, Jamitzky F, Heckl WM, Rössle SC, Stark RW (2009) TollML: a database of Toll-like receptor structural motifs. J Mol Model in press.

[5]   Brodsky I, Medzhitov R (2007) Two modes of ligand recognition by TLRs. Cell 130:979-981.

[6]   West AP, Koblansky AA, Ghosh S (2006) Recognition and signaling by toll-like receptors. Annu Rev Cell Dev Biol 22:409-437.

[7]   Akira S, Hemmi H (2003) Recognition of pathogen-associated molecular patterns by TLR family. Immunol Lett 85:85-95.

[8]   Leulier F, Lemaitre B (2008) Toll-like receptors--taking an evolutionary approach. Nat Rev Genet 9:165-178.

[9]   Wei T, Gong J, Jamitzky F, Heckl WM, Stark RW, Rössle SC (2008) LRRML: a conformational database and an XML description of leucine-rich repeats (LRRs). BMC Struct Biol 8:47.

[10]   Berman HM, Westbrook J, Feng Z, Gilliland G, Bhat TN, Weissig H, Shindyalov IN, Bourne PE (2000) The Protein Data Bank. Nucleic Acids Res 28:235-242.

[11]   Jin MS, Kim SE, Heo JY, Lee ME, Kim HM, Paik SG, Lee H, Lee JO (2007) Crystal structure of the TLR1-TLR2 heterodimer induced by binding of a tri-acylated lipopeptide. Cell 130:1071-1082.

[12]   Choe J, Kelker MS, Wilson IA (2005) Crystal structure of human toll-like receptor 3 (TLR3) ectodomain. Science 309:581-585.

[13]   Bell JK, Botos I, Hall PR, Askins J, Shiloach J, Segal DM, Davies DR (2005) The molecular structure of the Toll-like receptor 3 ligand-binding domain. Proc Natl Acad Sci U S A 102:10976-10980.

[14]   Liu L, Botos I, Wang Y, Leonard JN, Shiloach J, Segal DM, Davies DR (2008) Structural basis of toll-like receptor 3 signaling with double-stranded RNA. Science 320:379-381.

[15]   Kim HM, Park BS, Kim JI, Kim SE, Lee J, Oh SC, Enkhbayar P, Matsushima N, Lee H, Yoo OJ, Lee JO (2007) Crystal structure of the TLR4-MD-2 complex with bound endotoxin antagonist Eritoran. Cell 130:906-917.

[16]   Baker D, Sali A (2001) Protein structure prediction and structural genomics. Science 294:93-96.

[17]   Lobley A, Sadowski MI, Jones DT (2009) pGenTHREADER and pDomTHREADER: new methods for improved protein fold recognition and superfamily discrimination. Bioinformatics 25:1761-1767.

[18]   Fiser A, Do RK, Sali A (2000) Modeling of loops in protein structures. Protein Sci 9:1753-1773.

[19]   Fiser A, Sali A (2003) ModLoop: automated modeling of loops in protein structures. Bioinformatics 19:2500-2501.

[20]   Wallner B, Elofsson A (2003) Can correct protein models be identified? Protein Sci 12:1073-1086.

[21]   Pawlowski M, Gajda MJ, Matlak R, Bujnicki JM (2008) MetaMQAP: a meta-server for the quality assessment of protein models. BMC Bioinformatics 9:403.

[22]   Maiti R, Van Domselaar GH, Zhang H, Wishart DS (2004) SuperPose: a simple server for sophisticated structural superposition. Nucleic Acids Res 32:W590-594.

[23]   Humphrey W, Dalke A, Schulten K (1996) VMD: visual molecular dynamics. J Mol Graph 14:33-38, 27-38.

[24]   Tovchigrechko A, Vakser IA (2006) GRAMM-X public web server for protein-protein docking. Nucleic Acids Res 34:W310-314.

[25]   Kopp J, Bordoli L, Battey JN, Kiefer F, Schwede T (2007) Assessment of CASP7 predictions for template-based modeling targets. Proteins 69 Suppl 8:38-56.

[26]   Laskowski RA, MacArthur MW, Moss DS, Thornton JM (1993) PROCHECK: a program to check the stereochemical quality of protein structures. J Appl Cryst 26:283-291.

[27]   Roach JC, Glusman G, Rowen L, Kaur A, Purcell MK, Smith KD, Hood LE, Aderem A (2005) The evolution of vertebrate Toll-like receptors. Proc Natl Acad Sci U S A 102:9577-9582.

[28]   Yarovinsky F, Zhang D, Andersen JF, Bannenberg GL, Serhan CN, Hayden MS, Hieny S, Sutterwala FS, Flavell RA, Ghosh S, Sher A (2005) TLR11 activation of dendritic cells by a protozoan profilin-like protein. Science 308:1626-1629.

[29]   Lauw FN, Caffrey DR, Golenbock DT (2005) Of mice and man: TLR11 (finally) finds profilin. Trends Immunol 26:509-511.

[30]

[31]   Kopp J, Schwede T (2004) Automated protein structure homology modeling: a progress report. Pharmacogenomics 5:405-416.

[32]   Wei T, Gong J, Jamitzky F, Heckl WM, Stark RW, Rössle SC (2009) Homology modeling of human Toll-like receptors TLR7, 8, and 9 ligand-binding domains. Protein Sci 18:1684-1691.

[33]   Rutz M, Metzger J, Gellert T, Luppa P, Lipford GB, Wagner H, Bauer S (2004) Toll-like receptor 9 binds single-stranded CpG-DNA in a sequence- and pH-dependent manner. Eur J Immunol 34:2541-2550.

[34]   Gibbard RJ, Morley PJ, Gay NJ (2006) Conserved features in the extracellular domain of human toll-like receptor 8 are essential for pH-dependent signaling. J Biol Chem 281:27503-27511.

Table 1: Source and sequence identity (%) of the LRR templates.

LRR	mTLR3 LRRML ID	Iden	hTLR5 LRRML ID	Iden	hTLR6 LRRML ID	Iden	hTLR10 LRRML ID	Iden	mTLR12 LRRML ID	Iden
NT	406	47.6	125	34.6	333	72.7	150	40.9	125	28.6
1	65	45.8	284	45.8	334	54.2	334	45.8	90	37.5
2	212	45.8	264	42.3	335	70.8	335	62.5	178	58.3
3	465	41.7	259	54.2	336	81.0	578	42.9	465	40.7
4	151	50.0	464	46.2	337	80.0	337	68.0	578	40.9
5	177	50.0	259	48.0	338	60.9	338	47.8	21	35.5
6	110	46.2	252	34.6	339	36.0	111	33.3	497	56.0
7	275	45.8	494	29.0	340	33.3	340	41.7	202	40.9
8	8	41.4	135	37.0	341	33.3	28	34.6	39	34.6
9	203	42.3	359	26.6	342	48.1	342	44.4	356	45.8
10	484	54.2	357	41.7	343	34.6	343	46.4	179	45.8
11	293	50.0	140	50.0	344	48.3	365	29.0	177	42.3
12	270	33.3	316	50.0	345	45.5	345	40.9	566	54.2
13	357	41.7	151	45.8	346	41.7	346	41.7	66	50.0
14	65	42.9	216	45.0	347	61.5	358	48.0	468	45.8
15	152	50.0	153	38.1	348	40.0	369	41.7	501	44.0
16	259	40.0	253	36.0	349	68.2	349	45.5	581	34.8
17	316	37.5	356	40.0	350	95.7	350	43.5	372	30.8
18	152	38.5	566	41.4	351	52.0	372	45.5	283	37.0
19	239	50.0	72	58.3	128	37.5	513	36.0	396	38.7
20	239	45.8	579	45.5	-	-	-	-	260	37.5
21	92	50.0	484	40.9	-	-	-	-	496	41.4
22	80	41.7	-	-	-	-	-	-	315	45.8
23	628	46.2	-	-	-	-	-	-	110	35.7
CT	575	42.9	149	31.7	149	31.7	514	29.9	149	20.0

LRR	hTLR7 LRRML ID	Iden	hTLR8 LRRML ID	Iden	hTLR9 LRRML ID	Iden	mTLR11 LRRML ID	Iden	mTLR13 LRRML ID	Iden
NT	257	40.6	250	30.0	125	29.0	125	36.7	125	26.5
1	293	45.8	509	45.8	314	41.7	76	38.5	491	54.2
2	107	36.0	573	48.0	101	41.7	191	37.5	107	50.0
3	106	52.4	581	47.6	219	55.0	288	44.0	254	54.2
4	261	45.8	509	45.8	310	41.7	559	36.4	152	50.0
5	140	44.0	564	44.0	157	41.7	557	40.0	4	53.8
6	583	47.6	106	52.4	106	47.6	238	30.4	419	52.0
7	105	45.8	509	45.8	501	41.7	463	44.0	285	44.0
8	573	45.8	573	50.0	259	37.5	271	45.8	135	41.7
9	79	45.8	494	41.7	357	50.0	157	45.8	488	52.0
10	500	46.2	573	42.3	367	37.0	506	44.0	498	36.7
11	500	52.0	316	54.2	337	40.0	237	45.8	128	33.3
12	488	40.7	261	37.0	274	31.0	509	46.2	288	48.0
13	129	44.0	92	37.5	92	33.3	500	54.2	505	45.8
14	386	37.9	259	44.0	357	34.6	7	50.0	573	54.2
15	36	33.3	300	29.6	139	15.6	111	45.8	260	50.0
16	316	41.7	494	41.7	170	37.5	38	42.3	148	36.0
17	358	46.2	158	40.0	316	40.0	484	43.5	262	45.8
18	316	41.7	314	41.7	135	45.8	360	29.2	293	50.0
19	494	50.0	296	37.5	316	44.0	73	37.5	105	45.8
20	503	41.7	128	45.8	493	40.0	403	28.6	260	48.0
21	92	41.7	77	45.8	252	41.7	102	30.4	466	46.2
22	78	48.0	573	60.0	288	44.0	121	34.5	565	41.7
23	552	45.8	169	36.0	111	37.5	316	50.0	93	50.0
24	210	50.0	283	53.8	289	41.7	35	36.0	79	50.0
25	133	40.7	271	45.8	259	45.8	-	-	573	41.7
26	274	48.3	144	42.3	357	52.0	-	-	-	-
CT	149	36.7	149	33.9	149	28.8	469	26.2	149	36.5

Table 2: Evaluation of the crystal structure and models of the TLRs. Higher ProQ_LG/MS and MetaMQAP_GDT values indicate higher model qualities; higher MetaMQAP_RMSD values indicate lower model qualities. [a] Model of Wei *et al.* (2008).

Structure/Model	ProQ_ LG/MS	MetaMQAP_ GDT/RMSD
mTLR3 crystal	7.215/0.469	69.840/1.962
mTLR3 pGenTHREADER	4.013/0.357	41.943/4.691
mTLR3 [a]	5.136/0.423	54.068/3.080
mTLR3 new	5.349/0.405	54.542/3.030
hTLR5	4.707/0.358	54.803/3.126
hTLR6	5.807/0.439	73.230/1.907
hTLR7	4.980/0.381	52.816/3.224
hTLR8	5.053/0.408	53.490/3.113
hTLR9	5.025/0.386	53.774/3.181
hTLR10	4.835/0.362	59.918/2.883
mTLR11	4.371/0.351	49.178/3.433
mTLR12	4.546/0.337	46.131/3.493
mTLR13	4.827/0.407	55.709/2.982

Figure 1: Flowchart of the LRR template assembly method.
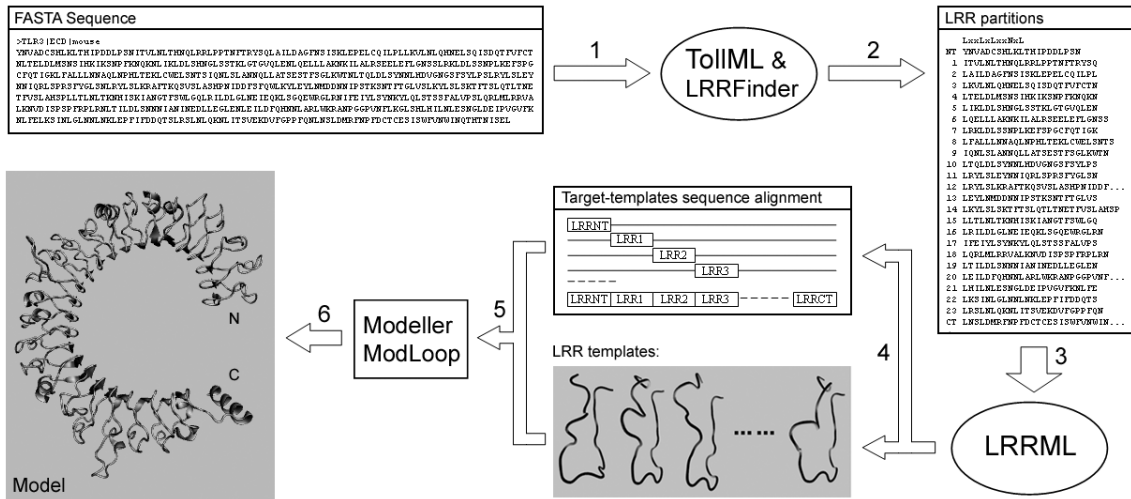
Figure 2: Homology models and crystal structure of the mouse TLR3 ectodomain. (a) The homology model based on the standard method. The framed region exhibits serious disorder. (b) The homology model based on template assembly method. (c) The crystal structure (PDB code: 3CIG). The dotted region is an insertion on LRR20 that is missing in the crystal structure. (d) The target-template sequence alignment of the disordered region of the standard method based model. The mismatches and target gaps resulted in the disorder in (a), where two to four template LRRs were wrongly assigned to five target LRRs.
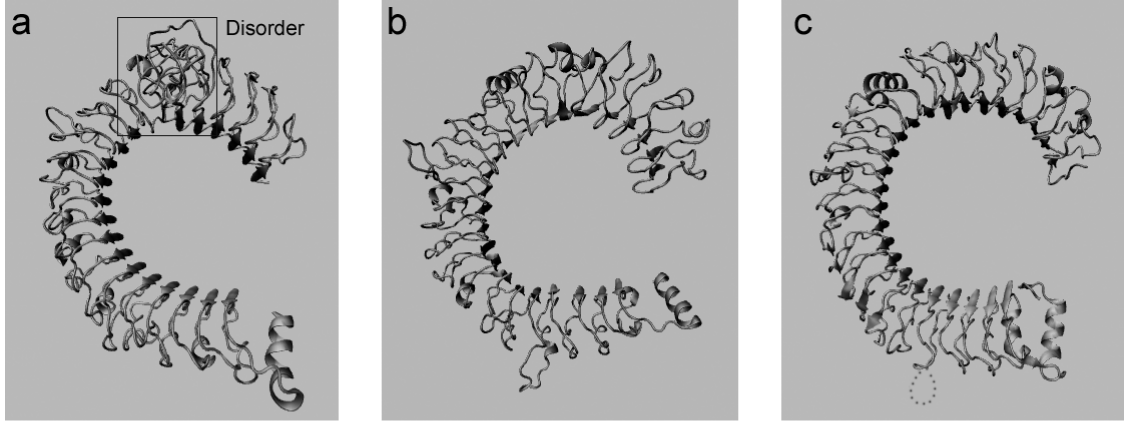

```
                    LRR6                            LRR7                            LRR8
mTLR3  |LQELLLAKNKILALRSEELEFLGNSS|LRKLDLSSNPLKEF-SPGCFQTIGK|LFALLLNNAQLNPHLTEKLCWELSNTS|
2Z64   |LVHVDLSYNYIQTITVNDLQF-----|-----LRENPQVNL-----------|--SLDMSLNPIDFIQ---------DQA|
2Z81   |--------------------------|------------------------|---------PIDFIQ---------DQA|
1O6V   |--------------------------|-------------------GSATI|TQDTPINQIFTDTALAEKMKTVLGKTN|
3FXI   |LQKLVAVETNLASLEN--FPIGHLKT|LKELNVAHNLIQSFKLPEYFSNLTN|LEHLDLSSNKIQSIYCTDLRVLHQM--|
2Z7X   |--------------------------|------------------------|---------------------------|
1JL5   |--------------------------|-----KSKTEYYNA-WSEWERNA--|-----PPGNGEQREMAVSRLRDCLDRQ|
3BZ5   |--------------------------|--------------------TLKA|GQTQSFNDWFPDDNFASEVAAAFEMQA|
                    LRR9                            LRR10
mTLR3  |IQ-------NLSLANNQLLATSESTFSGLK---------WTN|LTQLD---LSYNNLHDV-GNGSFSYLPS|
2Z64   |FQGIKLHELTLRGNFNSSNIMKTCLQNLAGLHVHRLILGEFK|---------DERNLEIF-EPSIMEGLCD|
2Z81   |TF-------SEIRRI-----------DFAG---------LTS|LNELEIKALSLRNYQS-------QSLKS|
1O6V   |VT-------DTVS--------------QTD---------LDQ|VTTLQ---ADRLGIKSI-D--GVEYLNN|
3FXI   |------------------------------------PLL|NLSLD---LSLNPMNFI-QP---GAFKE|
2Z7X   |---------KISCH--------------P---------TVN|LKHLD---LSFNAFDALPICKEFGNMSQ|
1JL5   |AH-------ELELNNLGLSSLP------EL---------PPH|LESLV---ASCNSLTEL-P----ELPQS|
3BZ5   |TD-------TISEEQLA----------------------T|LTSLD---CHNSSITDM-TG--IEKLTG|
```

Figure 3: Models of human TLR5 through 10 and mouse TLR11 through 13 ectodomains. The N-linked glycan sites of these TLRs were obtained from the NCBI protein database and are labelled with black balls.
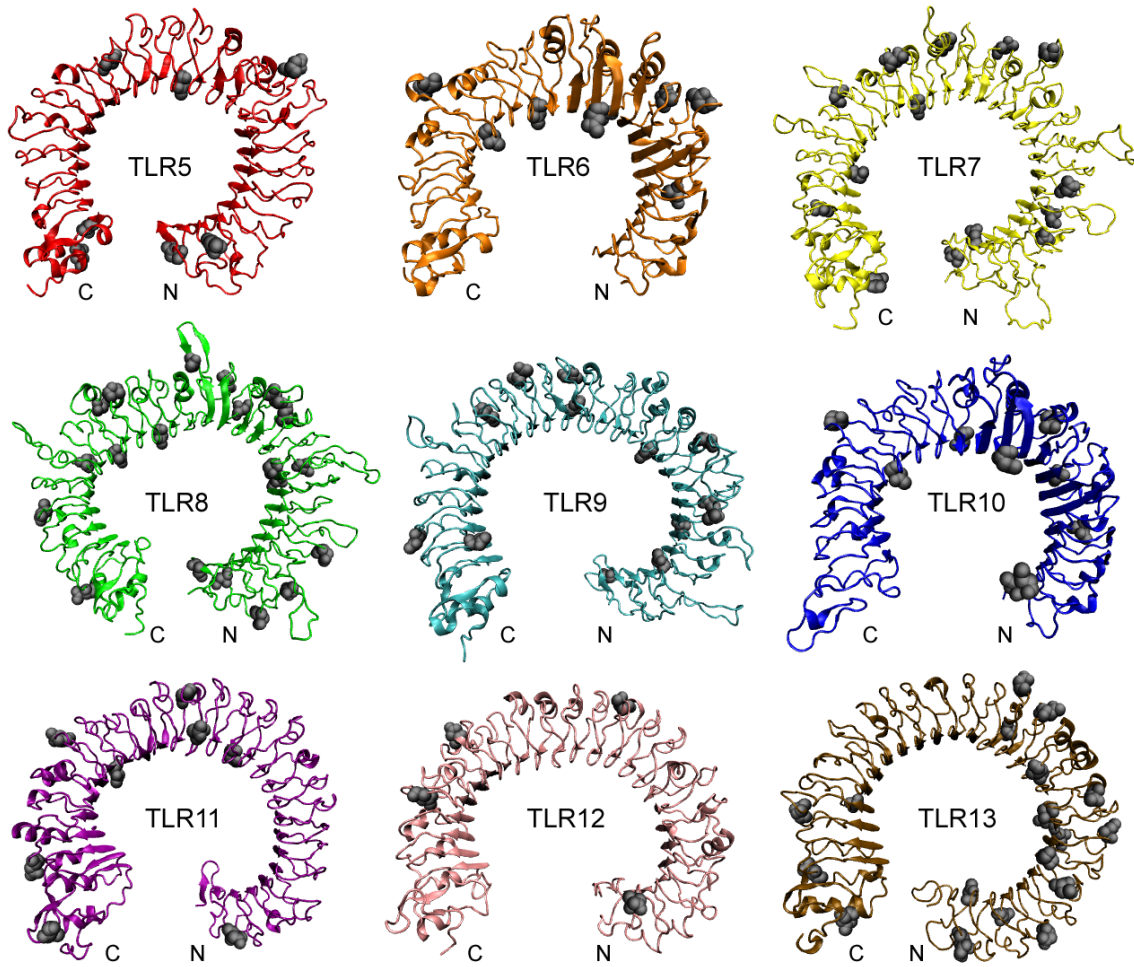
Figure 4: Surface charge analysis (APBS electrostatics) of (a) the crystal structures of profilin (PDB code: 2JKF) and (b) the model of mouse TLR11 ectodomain. Blue: positive charge; red: negative charge.
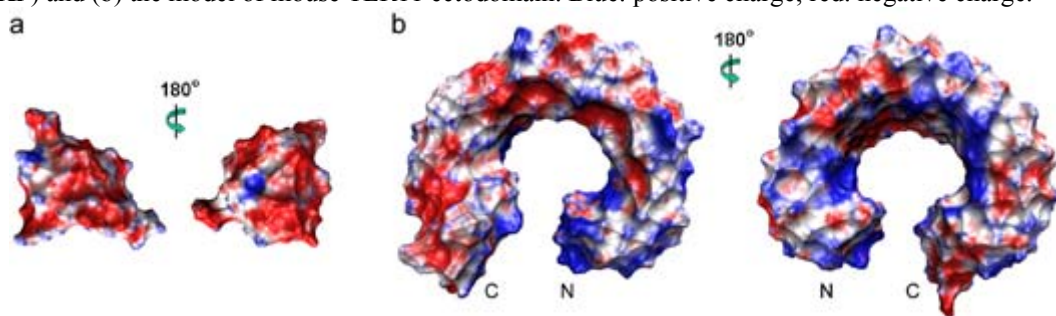
Figure 5: Superimposition of the homology model and the crystal structure of the TLR6 ectodomain. Green: homology model of human TLR6 (LRRNT through LRR17); orange: crystal structure of mouse TLR6 (LRRNT through LRR17). The Pam2CSK4 ligand-bind site is located on the variable parts of LRR10 through LRR12. The overall backbone RMSD is 1.94 Å and the backbone RMSD of the ligand-binding region is 1.18 Å.
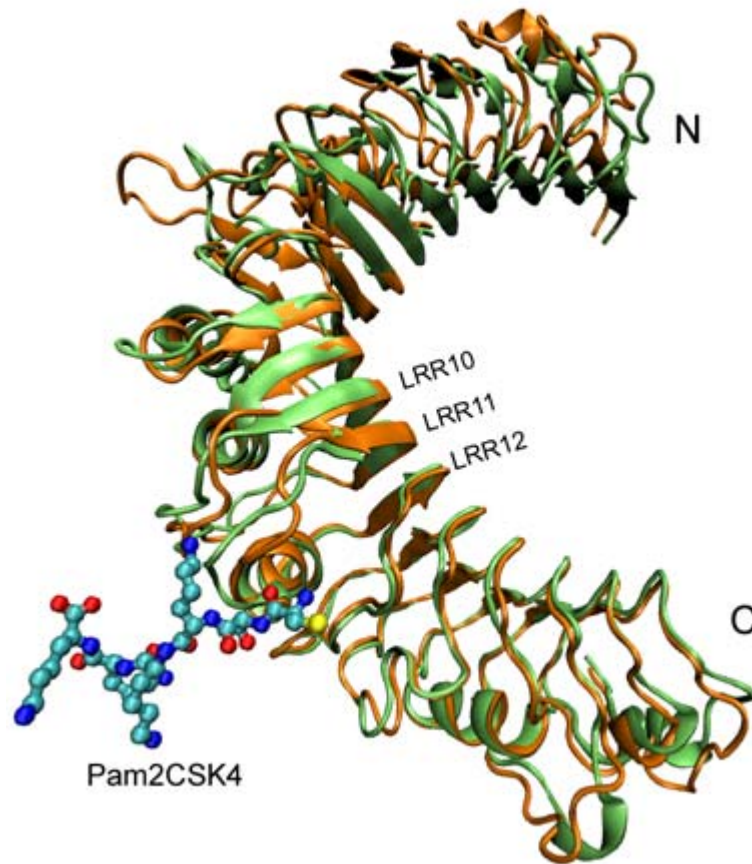
Supplementary file 1: Three-dimensional models of human TLR5-10 and mouse TLR10-13 ectodomains.

Supplementary file 2: Ramachandran plots of the models.

Supplementary file 3: Docking models of TLR11 and profiling ligand.

Paper 4

Homology modeling of human Toll-like receptors TLR7, 8 and 9 ligand-binding domains

Tiandi Wei, Jing Gong, Ferdinand Jamitzky, Wolfgang M. Heckl, Robert W. Stark and Shaila C. Rössle

Homology modeling of human Toll-like receptors TLR7, 8, and 9 ligand-binding domains

Tiandi Wei,[1] Jing Gong,[1]* Ferdinand Jamitzky,[1,2] Wolfgang M. Heckl,[1,3] Robert W. Stark,[1] and Shaila C. Rössle[1]

[1]Department of Earth and Environmental Sciences, Center for Nanoscience, Ludwig-Maximilians-Universität München, 80333 Munich, Germany

[2]Leibniz Supercomputing Centre, 85748 Garching, Germany

[3]Deutsches Museum, 80538 Munich, Germany

Abstract: Toll-like receptors (TLRs) play a key role in the innate immune system. The TLR7, 8, and 9 compose a family of intracellularly localized TLRs that signal in response to pathogen-derived nucleic acids. So far, there are no crystallographic structures for TLR7, 8, and 9. For this reason, their ligand-binding mechanisms are poorly understood. To enable first predictions of the receptor–ligand interaction sites, we developed three-dimensional structures for the leucine-rich repeat ectodomains of human TLR7, 8, and 9 based on homology modeling. To achieve a high sequence similarity between targets and templates, structural segments from all known TLR ectodomain structures (human TLR1/2/3/4 and mouse TLR3/4) were used as candidate templates for the modeling. The resulting models support previously reported essential ligand-binding residues. They also provide a basis to identify three potential receptor dimerization mechanisms. Additionally, potential ligand-binding residues are identified using combined procedures. We suggest further investigations of these residues through mutation experiments. Our modeling approach can be extended to other members of the TLR family or other repetitive proteins.

Keywords: Toll-like receptor; leucine-rich repeats; protein-nucleic acid interaction; homology modeling

Introduction

Toll-like receptors (TLRs) play an essential role in the innate immunity, recognizing invasion of microbial pathogens and initiating intracellular signal transduction pathways to trigger expression of genes, the products of which can control innate immune responses.[1] To understand how these receptors work, it is crucial to investigate them from a structural perspective. To date, only the crystal structures of the ectodomains of human TLR1/2/3/4 and mouse TLR3/4 have been determined.[2–6] The progress of genome projects, however, already led to the identification of 13 TLRs in mammalian and more than 20 TLRs in nonmammalian. A total of more than 2000 TLR proteins has been sequenced.[7] Thus, the structures of most TLRs are still unknown because structure determination by X-ray diffraction or nuclear magnetic resonance spectroscopy experiments remains time-consuming. Here, computational methods can help to bridge the gap between sequence determination and structure determination. To this end, homology modeling is a powerful tool to predict the three-dimensional structure of proteins.

Homology modeling is based on the assumption that similar sequences among evolutionarily related proteins share an overall structural similarity. The modeling procedure can be divided into a number of
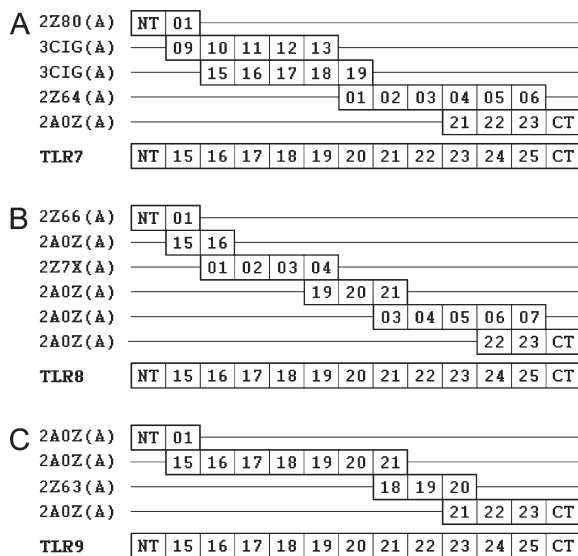
Figure 1. Models of multiple alignments between targets and templates. The numbers 01–25 denote the canonical LRRs; NT and CT denote N-/C-terminal LRRs. (A) Five segments selected from four structures (2Z80 chain A: human TLR2; 3CIG chain A: mouse TLR3; 2Z64 chain A: mouse TLR4; 2A0Z chain A: human TLR3) were used as templates for the human TLR7 ectodomain. (B) Six segments selected from three structures (2Z66 chain A: human TLR4; 2A0Z chain A: human TLR3; 2Z7X chain A: human TLR2) were used as templates for the human TLR8 ectodomain. (C) Four segments selected from two structures (2A0Z chain A: human TLR3; 2Z63 chain A: human TLR4) were used as templates for the human TLR9 ectodomain.

steps.[8,9] First, selection of suitable template(s) related to the target sequence. A template segment assembly can usually improve the model quality.[10] Second, alignment of the target sequence to the template(s). Third, building coordinates of the three-dimensional model based on the alignment. Fourth, evaluation of the model and its refinement. The resulting model can then be used to infer biological functionalities or to generate hypotheses for new experiments. A recent study on TLR4[11] highlighted the reliability and the significance of homology modeling applied to TLRs.

The structure of a TLR consists of a leucine-rich repeat (LRR) ectodomain, a helical transmembrane domain, and an intracellular Toll/IL-1 receptor homology (TIR) signaling domain.[12] The ectodomain contains varying numbers of LRRs and resembles a solenoid bent into a horseshoe shape. At both ends there is a terminal LRR that shields the hydrophobic core of the horseshoe.

These ectodomains are highly variable. They are directly involved in the recognition of a variety of pathogen-associated motifs including lipopolysaccharide, lipopeptide, cytosine–phosphate–guanine (CpG) DNA, flagellin, imidazoquinoline, and ds/ssRNA.[13] Upon receptor activation, a TIR signaling complex is formed between the receptor and adaptor TIR domains.[14]

The receptors TLR7, 8, and 9 compose a family[15] with a longer amino acid sequence than other TLRs. They are localized intracellularly and signal in response to nonself nucleic acids. They also contain an irregular segment between their LRR14 and 15. A recent study showed that the ectodomains of TLR9 and 7 are cleaved in the endolysosome to recognize ligands.[16] Only the cleaved forms can recruit MyD88 on activation. In the absence of the crystallographic structures, we developed structural models of cleaved ligand-binding domains of TLR7/8/9 by homology modeling. From the structural model we predict potential ligand-binding sites and infer possible configurations of the receptor–ligand complex.

Results

Template identification

Our target structures are the cleaved functional ectodomains of the human TLR7/8/9 comprising LRR15–25 and N/C-terminal LRRs. All the six structure-known TLR homologues were employed as template sources: human TLR1/2/3/4 and mouse TLR3/4. The TLR ectodomain is composed of strictly organized LRRs. Nevertheless, the LRR number of cleaved ligand-binding domain of human TLR7/8/9 is 13 (LRR15–25 and N/C-terminal LRR),[16] whereas the LRR number of the structure-known TLRs varies from 20 to 25. Therefore, none of the structure-known TLRs is suitable to serve as a full length template. To overcome this limitation, LRR segments with higher sequence similarity to the individual LRRs in the target were selected from the six complete homologous structures. The segments were then combined into the multiple templates. Figure 1 shows the multiple alignment models for the three proteins TLR 7/8/9, presenting the relationship between target and template segments. The sequence similarity between each LRR pair (target/template LRR) is listed in Table I. The average target–template similarities of TLR7/8/9 are 47.70, 47.20, and 46.78%, respectively.

Remarkably, the group of TLR7/8/9 has a unique structural character that is absent in other TLRs. A specific segment (26–32 residue long) is located

Table I. *Sequence Similarities (%) of Target–Template LRR Pairs*

	NT	15	16	17	18	19	20	21	22	23	24	25	CT	Avg
TRL7	28.60	58.30	60.00	41.70	47.10	58.30	46.20	52.00	50.00	33.30	46.20	48.30	50.00	47.70
TRL8	29.40	41.70	52.00	50.00	57.70	60.00	40.60	44.00	52.00	36.00	60.00	42.30	53.30	47.20
TRL9	32.30	58.30	48.00	50.00	44.40	41.70	46.90	51.90	36.00	54.20	50.00	52.00	42.40	46.78

In the header line, 15–25 denote canonical LRRs. NT and CT denote N-/C-terminal LRRs. Avg denotes the average values.

```
                                          LxxLxLxxNxL
                       ...TMGEADG GEKVWLQPGDLAPAPVDTPSSEDFRPNCSTL NFTLDLS...
     PredictProtein ...LLLLLLL LLEEELLLLLLLLLLLLLLLLLLLLLHHHHHH LLLLLLL...
          NNPREDICT ...H------ --HEEE-------------------- --EEH--...
              SSPro ...HCCCCCC CCEEEECCCCCCCCCCCCCCCCCCCCCCCCC EEEEECC...
             GOR IV ...HHHCCCC CCEEEECCCCCCCCCCCCCCCCCCCCCCCCC CEECCCC...
                        LRR14            Irregular Region          LRR15
```

Figure 2. Irregular region analysis of TLR9. Four methods (PredictProtein,[20] NNPREDICT,[21] SSPro,[22] and GOR IV[23]) were used to predict the secondary structures of the irregular region of TLR9. The results (italic letters) indicate a short β-sheet at position 3–5 of this region. Besides, this region matches the LRR pattern at three important positions (bold letters). These features support the presumption that this irregular region is a beginning N-terminal LRR after the ectodomain cleavage.

before LRR15, which was described as an undefined region.[17–19] The sequence similarity search against Protein Data Bank (PDB) provided no significant results. Thus, we carried out secondary structure predictions for this region with four different methods. As example, the results for TLR9 are shown in Figure 2. All methods indicated a short β-sheet at position 3–5 of the segment, which is a prominent characteristic of LRRs. In addition, we compared its amino acid sequence with the consensus sequence of LRRs. The most significant positions of the LRR consensus sequence, LxxLxLxxNxL, are the four L residues which form the hydrophobic core of a LRR structure. Here, the letter L not only stands for leucine but also for other highly hydrophobic residues. As illustrated in Figure 2, the specific segment of TLR9 contains three of the four highly hydrophobic residues. Also, the corresponding segment of TLR7/8 has the same features. Thus we regard this segment as an irregular LRR. Because the N-terminal LRR together with LRR1–14 of the receptor ectodomain are deleted upon arriving in endolysosome, this irregular LRR may become a new N-terminal LRR of the truncated structure. Moreover, multiple alignments of all known mammalian sequences showed that this region is very variable within each of the TLR7/8/9 groups. The structure of this LRR may be relatively relaxed, because it lacks the first L residue that participates in forming the hydrophobic core of a LRR structure and the N residue that forms hydrogen bonds between neighboring LRRs. These features also support the hypothesis that this irregular LRR is an N-terminal LRR. For this reason, a N-terminal LRR with known structure was selected as corresponding template (Fig. 1).

Structure modeling and evaluation

The three-dimensional coordinates of the models were created by MODELLER[24] and modified by ModLoop.[25] The final structures of the ectodomains of TLR7/8/9 reveal a large, arc-shaped assembly consisting of 11 canonical LRRs and two terminal LRRs, which adopted a right-handed solenoid structure (Fig. 3). The TLRs are distinct from other LRR proteins in that their LRR consensus motifs are often interrupted by extended insertions.[26] Two 4–7-residue-long insertions protuberate from the structure surface at LRR18 and LRR20, respectively. These insertions are well conserved in length and position on the sequence level in the three TLRs. The models show that the insertions are all located on one face of the arc, whereas the other face is insertion-free (Fig. 3). The convex site β-sheets are directed toward the insertion face. This feature is consistent with the known structures of TLR1/2/3/4. Because all the known ligand-binding sites of TLR1/2/3/4 are on the insertion face of the structure, the insertions suggest some functional significance. In addition, the human TLR7/8/9 are glycosylated as it is the case for other TLRs. The glycans were shown to be nonfunctional for ligand binding.[2–6] The NCBI protein database provides seven predicted N-linked glycosylation sites for TLR7/8 cleaved form and six for TLR9. All sites are located on the insertion-free faces. The PDB format files of the three final models are provided as Supporting Information Files 1–3. Evaluation of the models involved analysis of geometry, stereochemistry, and energy distributions in the models. The evaluation results (Table II) are indicative of a good quality of all three models.

Table II. *Model Evaluation*

	TLR7	TLR8	TLR9	TLR3
ProQ_LG/MS	5.340/0.461	4.613/0.402	4.355/0.339	7.923/0.526
PROCHECK	97.4%	96.2%	97.5%	99.6%
ModFOLD_Q/P	0.7588/0.01	0.7100/0.0126	0.7166/0.0121	0.7116/0.0124
MetaMQAP_GDT/RMSD	57.534/3.049 Å	53.908/3.121 Å	54.645/3.244 Å	79.322/1.566 Å

All these displayed scores indicate the models to be reliable in terms of overall packing. For comparison purpose, the values of TLR3 crystal structure (PDB code: 2A0Z) were also listed. ProQ_LG: >1.5 fairly good; >2.5 very good; >4 extremely good. ProQ_MS: >0.l, fairly good; >0.5, very good; >0.8, extremely good. PROCHECK: percentage of residues in most favored regions and additional allowed regions. ModFOLD_Q: >0.5, medium confidence; >0.75, high confidence. ModFOLD_P: <0.05, medium confidence; <0.01, high confidence. MetaMQAP_GDT/RMSD: an ideal model has a GDT score over 59 and a RMSD around 2.0 Å.
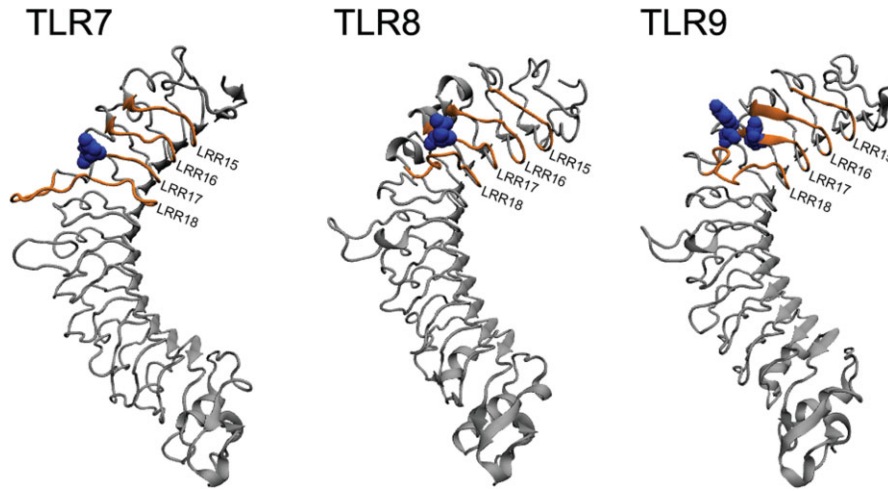
Homology Modeling of hTLR Ligand-Binding Domains

Figure 3. Structural models and ligand-binding regions of TLR7/8/9. Insertions are located on one face of the horseshoe, whereas the other face is insertion-free. The reported essential residues are located on the insertion face (labeled in blue). The orange regions are potential ligand-binding regions on the insertion face. [Color figure can be viewed in the online issue, which is available at www.interscience.wiley.com.]

Figure 4. Partial multiple sequence alignments of different mammalian TLR7/8/9. The multiple sequence alignments represent the conservation of each residue in the potential ligand-binding regions (corresponding to the orange regions in Fig. 3). In the first line below the alignments, plus signs designate important residues as reported in the literature and the asterisks designate highly conserved positions. In the second line, the number of positive docking predictions of each position is indicated. In the third line, blue squares designate important residues as reported in the literature and green squares indicate the suggested ligand-binding residues. [Color figure can be viewed in the online issue, which is available at www.interscience.wiley.com.]
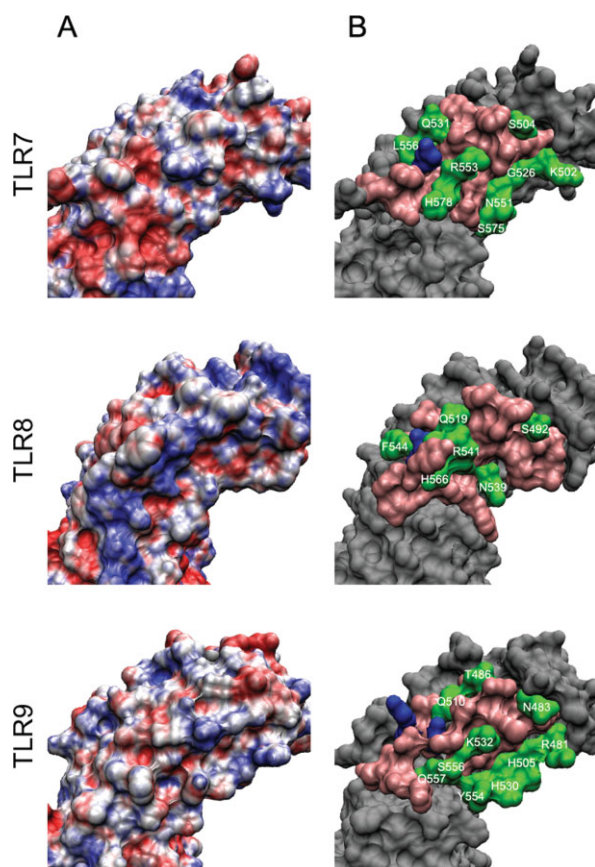
Figure 5. Surface analysis of ligand-binding regions of TLR7/8/9. (A) Surface charge distribution (APBS electrostatics) of ligand-binding regions of TLR7/8/9. Blue: positive charge; white: neutral; red: negative charge. (B) Important residues in ligand-binding regions of TLR7/8/9. Blue: important residues as reported in the literature; pink: residues close the blue ones but excluded from the potential ligand-binding residues through investigating processes; green: suggested potential ligand-binding residues (residue name and number are labeled). [Color figure can be viewed in the online issue, which is available at www.interscience.wiley.com.]

Potential ligand-binding residues

Several residues are essential for the ligand recognition: Asp543 in TLR8; Asp535 and Tyr537 in TLR9.[18,27] Our models can help to understand the biological function of these residues (Fig. 3). According to these reported residues and the sequence comparison of TLR7/8/9, we inferred a ligand-binding region for TLR7/8/9, respectively (detailed in the Discussion section). It is located at the insertion face of the ectodomain around LRR17 (Fig. 3). Because of the considerable size of the nucleic acids, the ligand-binding region should contain more interacting residues. We identified potential ligand-binding residues in the ligand-binding region aside from the experimentally determined ones. To accomplish this goal we integrated results from manual analyses and automatic docking programs.

TLR3 is closely related to the TLR7/8/9 family because of its intracellular localization and nucleic acid ligand. Therefore, we used the recently published crystal structure of the mTLR3-dsRNA 2:1 complex[6] as a guide to predict the essential interacting residues in TLR7/8/9. From all interacting residues of mTLR3, we identified three principles for the essential residues:

1. The essential residues are located on the protein surface and spatially close to each other.
2. They are highly conserved among species.
3. They create a nonnegatively charged environment.

On basis of these principles, we searched for additional residues that might be essential for ligand recognition. At first, surface residues that were spatially close (within two LRRs) to the experimentally determined essential residues were marked on the predicted models (orange regions in Fig. 3). These residues can be far from each other on the sequence level. Then, multiple alignments of all known mammalian TLR7/8/9 sequences were generated to select the highly conserved residues (columns with an asterisk in Fig. 4) from the marked ones. Notably, the L (or I, V) and N residues of the LRR consensus sequence LxxLxLxxNxL are conserved, but they cannot interact with ligands, because they are buried to form the hydrophobic core of an LRR. These residues are not labeled with asterisks in Figure 4.

Four protein-RNA docking programs and five protein-DNA docking programs (listed in the Materials and Methods section) were used to predict ligand-binding residues in TLR7/8 and TLR9. A residue from the prefiltered regions was marked as a ligand-binding residue, if it was positively predicted by at least two programs. In Figure 4, the number of positive predictions is listed for each target residue. The surface charge distributions of the regions of interest were calculated to verify the charge pattern in the predicted ligand-binding regions [Fig. 5(A)]. The resulting residues correspond to positively charged or neutral environments.

Figure 5(B) illustrates the protein surface residues from the different steps of our investigation for TLR7/8/9, respectively. All final predicted ligand-binding residues are summarized in Table III. These residues are indicated in green in both Figures 4 and 5(B).

Discussion

All three resulting models revealed similar conformations. This supports the assumption that TLR7/8/9 share

Table III. *Potential Ligand-Binding Residues of TLR7/8/9*

TLR7	K502 S504 G526 Q531 N551 R553 L556 S575 H578
TLR8	S492 Q519 N539 R541 F544 H566
TLR9	R481 N483 T486 H505 Q510 H530 K532 Y554 S556 Q557

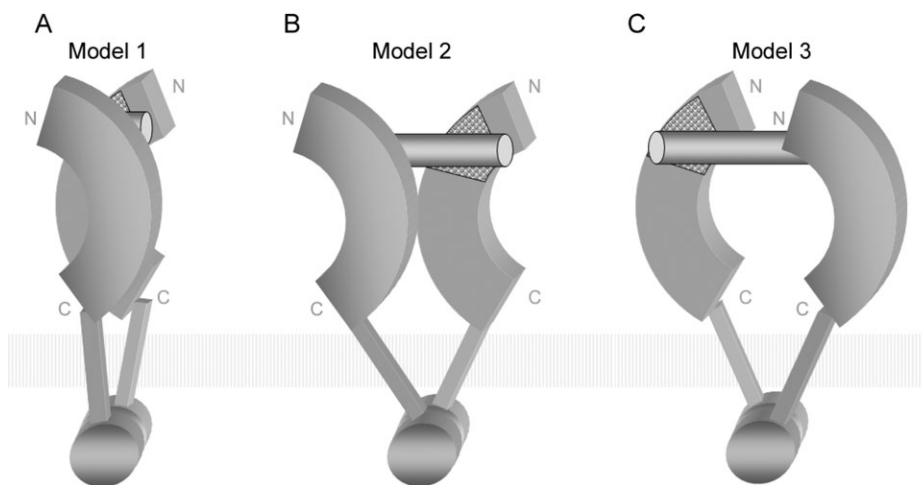Homology Modeling of hTLR Ligand-Binding Domains

Figure 6. Proposed models of receptor–ligand 2:1 complex.

a common ligand-binding and signaling mechanism.[18] We compared and analyzed the predicted structures to suggest the receptor–ligand 2:1 complex models.

Ligand-binding region

The mouse TLR9 contains a short fragment in its LRR17 that is homologous to the methyl CpG DNA binding domain protein.[27] The mutant of Asp535 and Tyr537 in this fragment abolished the TLR9 function.[27] In the human TLR8, the Asp543 that corresponds to TLR9's Asp535 was determined to be required for the TLR8 function.[18] Through sequence comparison, the Asp residue was found to be highly conserved in the TLR7/8/9 family but not in other TLRs. We considered this Asp to be significant for TLR7, because the TLR7/8/9 are highly homologous and their ligands are all pathogen-derived nucleic acids. In particular, the TLR7 and 8 are present as tandem duplication in many studied genomes discussed by Roach et al.[15] In this regard, TLR7/8/9 have a ligand-binding region located spatially around the Asp residue.

We can further exclude the necessity of other ligand-binding regions on the ectodomains, because the minimum size of stimulatory oligonucleotides is six bases.[28] These oligonucleotides are not large enough to reach another ligand-binding region on the receptor.

Receptor dimerization

The signaling mechanism of all TLRs is likely to involve dimerization of the ectodomains.[18] However, this can be achieved in various ways by using different receptors and stimuli. TLR9 is a preformed dimer. The distance between both monomers is reduced upon contact with CpG DNA.[29] TLR1/2 are activated and connected into a heterodimer by triacylated lipopeptide.[4] TLR4 recognizes lipopolysaccharide indirectly

through the coreceptor protein MD-2 and is induced to form a TLR4-MD-2 homodimer.[5] In the TLR3 homodimer the dsRNA interacts with two regions of each receptor ectodomain. Direct protein–protein interactions between both receptors occur at their C-terminal LRRs, whereas the other regions are separated by the dsRNA.[6]

The structures obtained by the homology modeling together with the identification of possible ligand-binding sites can be used to derive a working hypothesis for the structure of the receptor–ligand complex. We propose three possible receptor–ligand 2:1 complex models for the TLR7/8/9 family (Fig. 6). In all three models, the ssRNA or CpG DNA ligand interacts with the binding region on the insertion surface of both receptor ectodomains. The ectodomains are on opposite sides of the ligand. Simultaneously, the intracellular TIR domains are also in a dimer configuration. Thus the C-terminal LRRs of each monomer, which are connected to the TIR through a 20-amino-acid-long transmembrane stretch, are spatially close to each other. The main difference between the three models is the relative position of the ectodomains. In the first model [Fig. 6(A)], both C-terminal LRRs are brought into proximity, forming a protein–protein contact. Both binding regions sandwich the ligand. In the second model [Fig. 6(B)], both receptors are shifted apart along the ligand extending directions back to back. In the third model [Fig. 6(C)], both receptors are shifted in opposite directions face to face. Obviously, the minimum ligand size required by the first model is the smallest. Therefore, a CpG DNA of six bases is already long enough to stimulate TLR9.[28] The minimum size required by the second and third models is larger. These two models, however, cannot be excluded, because there is so far no evidence that TLRs have only one dimer form. Without the crystal structure of their ligands, it is difficult to determine a more precise

model for the receptor dimerization. Hence, it remains interesting to study the atomic structure of the stimulatory ssRNA/CpG DNA and to further determine the detailed interactions between ligands and receptors.

Materials and Methods

Template identification and sequence alignments

Amino acid sequences with LRR motif partitions of human TLR7/8/9 ectodomain were extracted from TollML.[7] TollML is a specialized database of TLR sequence motifs, derived from the NCBI protein database.[30] Multiple sequence alignments of all individual LRRs of TLR7/8/9 to the LRR consensus sequence are provided as Supporting Information File 4. Because the TLR ectodomain is a repetitive protein (LRRs), we selected and combined segments from all the six known TLR ectodomain structures into multiple templates to optimize the sequence similarity between targets and templates. The six candidate templates were human TLR1/2/3/4 and mouse TLR3/4 and were obtained from the PDB.[31] The PDB codes are 2Z7X, 2Z80, 2A0Z, 2Z63, 2Z66, 3CIG and 2Z64, respectively. Three steps led to the identification of structural templates. First, we partitioned the known structures into a total of 136 individual LRRs. Because of the irregularity of the LRR sequences, the partition according to the LRR consensus sequences was performed manually. Second, the LRRs were collected into the LRRML database,[32] which can return the most similar LRR for an input LRR sequence through similartiy search. Third, optimal template pieces for each target were found and combined to generate multiple alignments. Because the TLR LRRs follow common characteristic consensus sequences, target–template alignments were generated more accurately by hand than through software.

Structure construction and analysis

The initial three-dimensional coordinates of the models were generated by the fully automated program MODELLER 9v3.[24] The input files were the multiple alignment file and the coordinate files of the templates. The ligand-binding domains of TLR7/8/9 contain two 4–7-residue-long insertion regions, which correspond to gaps in the multiple alignment. During the modeling these regions became loop structures, which limited the model accuracy. ModLoop[25] was used to modify these loop regions. The resulting models were evaluated by PROCHECK,[33] ProQ,[34] ModFOLD,[35] and MetaMQAP.[36]

The detection of potential ligand-binding sites was achieved through residue conservation analysis, surface charge analysis, and several automatic docking programs. BindN,[37] DP-Bind,[38] DBS-PRED,[39] DBS-PSSM,[40] and PreDs[41] were used for protein-DNA

docking of TLR9. BindN, Pprint,[42] RNAbindR,[43] and RISP[44] were used for protein-RNA docking of TLR7/8.

Conclusions

We predicted three-dimensional structures of the closely related TLR7/8/9 ligand-binding domains by homology modeling. LRR segments were selected from known TLR structures, which are locally optimal for the target sequences. These segments were then combined into multiple templates.

To predict essential residues in the ligand-binding region, sequence conservation and charge distributions were examined. Only highly conserved nonnegative residues that are positively predicted by at least two docking programs can be considered as potential ligand-binding residues. Based on these models we also suggest three possible receptor dimerization schemes which require different minimum ligand sizes.

In summary, our models provide a structural framework that can act as a guide to develop a functional hypothesis to interpret experimental data of TLR7/8/9. They may also facilitate efforts to design further site-directed mutagenesis to learn the ligand recognition and the downstream signaling mechanisms. The presented modeling approach can be extended to other repetitive protein domains.

References

1. Takeda K, Akira S (2005) Toll-like receptors in innate immunity. Int Immunol 17:1–14.
2. Bell JK, Botos I, Hall PR, Askins J, Shiloach J, Segal DM, Davies DR (2005) The molecular structure of the Toll-like receptor 3 ligand-binding domain. Proc Natl Acad Sci USA 102:10976–10980.
3. Choe J, Kelker MS, Wilson IA (2005) Crystal structure of human toll-like receptor 3 (TLR3) ectodomain. Science 309:581–585.
4. Jin MS, Kim SE, Heo JY, Lee ME, Kim HM, Paik SG, Lee H, Lee JO (2007) Crystal structure of the TLR1-TLR2 heterodimer induced by binding of a tri-acylated lipopeptide. Cell 130:1071–1082.
5. Kim HM, Park BS, Kim JI, Kim SE, Lee J, Oh SC, Enkhbayar P, Matsushima N, Lee H, Yoo OJ, Lee JO. (2007) Crystal structure of the TLR4-MD-2 complex with bound endotoxin antagonist Eritoran. Cell 130:906–917.
6. Liu L, Botos I, Wang Y, Leonard JN, Shiloach J, Segal DM, Davies DR (2008) Structural basis of toll-like receptor 3 signaling with double-stranded RNA. Science 320: 379–381.
7. Gong J, Wei T, Jamitzky F, Heckl WM, Rössle SC (2007) TollML-a user editable database for Toll-like receptors and ligands. In: Proceedings of the Second IAPR International Workshop on Pattern Recognition in Bioinformatics, International Association of Pattern Recognition, Singapore, Paper ID 231.
8. Ginalski K (2006) Comparative modeling for protein structure prediction. Curr Opin Struct Biol 16:172–177.
9. Kopp J, Schwede T (2004) Automated protein structure homology modeling: a progress report. Pharmacogenomics 5:405–416.

10. Bujnicki JM (2006) Protein-structure prediction by recombination of fragments. Chembiochem 7:19–27.

11. Kubarenko A, Frank M, Weber AN (2007) Structure-function relationships of Toll-like receptor domains through homology modelling and molecular dynamics. Biochem Soc Trans 35:1515–1518.

12. Brodsky I, Medzhitov R (2007) Two modes of ligand recognition by TLRs. Cell 130:979–981.

13. Gay NJ, Gangloff M (2007) Structure and function of Toll receptors and their ligands. Annu Rev Biochem 76: 141–165.

14. O'Neill LA, Bowie AG (2007) The family of five: TIR-domain-containing adaptors in Toll-like receptor signalling. Nat Rev Immunol 7:353–364.

15. Roach JC, Glusman G, Rowen L, Kaur A, Purcell MK, Smith KD, Hood LE, Aderem A (2005) The evolution of vertebrate Toll-like receptors. Proc Natl Acad Sci USA 102:9577–9582.

16. Ewald SE, Lee BL, Lau L, Wickliffe KE, Shi GP, Chapman HA, Barton GM (2008) The ectodomain of Toll-like receptor 9 is cleaved to generate a functional receptor. Nature 456:658–662.

17. Bell JK, Mullen GE, Leifer CA, Mazzoni A, Davies DR, Segal DM (2003) Leucine-rich repeats and pathogen recognition in Toll-like receptors. Trends Immunol 24: 528–533.

18. Gibbard RJ, Morley PJ, Gay NJ (2006) Conserved features in the extracellular domain of human toll-like receptor 8 are essential for pH-dependent signaling. J Biol Chem 281:27503–27511.

19. Matsushima N, Tanaka T, Enkhbayar P, Mikami T, Taga M, Yamada K, Kuroki Y (2007) Comparative sequence analysis of leucine-rich repeats (LRRs) within vertebrate toll-like receptors. BMC Genomics 8:124.

20. Rost B, Yachdav G, Liu J (2004) The PredictProtein server. Nucleic Acids Res 32:W321–W326.

21. Kneller DG, Cohen FE, Langridge R (1990) Improvements in protein secondary structure prediction by an enhanced neural network. J Mol Biol 214:171–182.

22. Cheng J, Sweredoski M, Baldi P (2005) Accurate prediction of protein disordered regions by mining protein structure data. Data Min Knowl Discov 11:213–222.

23. Garnier J, Gibrat JF, Robson B (1996) GOR method for predicting protein secondary structure from amino acid sequence. Methods Enzymol 266:540–553.

24. Fiser A, Do RK, Sali A (2000) Modeling of loops in protein structures. Protein Sci 9:1753–1773.

25. Fiser A, Sali A (2003) ModLoop: automated modeling of loops in protein structures. Bioinformatics 19:2500–2501.

26. Bell JK, Askins J, Hall PR, Davies DR, Segal DM (2006) The dsRNA binding site of human Toll-like receptor 3. Proc Natl Acad Sci USA 103:8792–8797.

27. Rutz M, Metzger J, Gellert T, Luppa P, Lipford GB, Wagner H, Bauer S (2004) Toll-like receptor 9 binds single-stranded CpG-DNA in a sequence- and pH-dependent manner. Eur J Immunol 34:2541–2550.

28. He G, Patra A, Siegmund K, Peter M, Heeg K, Dalpke A, Richert C (2007) Immunostimulatory CpG oligonucleotides form defined three-dimensional structures: results from an NMR study. ChemMedChem 2:549–560.

29. Latz E, Verma A, Visintin A, Gong M, Sirois CM, Klein DC, Monks BG, McKnight CJ, Lamphier MS, Duprex WP, Espevik T, Golenbock DT. (2007) Ligand-induced conformational changes allosterically activate Toll-like receptor 9. Nat Immunol 8:772–779.

30. Wheeler DL, Barrett T, Benson DA, Bryant SH, Canese K, Chetvernin V, Church DM, Dicuccio M, Edgar R, Federhen S, Feolo M, Geer LY, Helmberg W, Kapustin Y, Khovayko O, Landsman D, Lipman DJ, Madden TL, Maglott DR, Miller V, Ostell J, Pruitt KD, Schuler GD, Shumway M, Sequeira E, Sherry ST, Sirotkin K, Souvorov A, Starchenko G, Tatusov RL, Tatusova TA, Wagner L, Yaschenko E (2008) Database resources of the national center for biotechnology information. Nucleic Acids Res 36:D13–D21.

31. Berman HM, Westbrook J, Feng Z, Gilliland G, Bhat TN, Weissig H, Shindyalov IN, Bourne PE (2000) The protein data bank. Nucleic Acids Res 28:235–242.

32. Wei T, Gong J, Jamitzky F, Heckl WM, Stark RW, Roessle SC (2008) LRRML: a conformational database and an XML description of leucine-rich repeats (LRRs). BMC Struct Biol 8:47.

33. Laskowski RA, MacArthur MW, Moss DS, Thornton JM (1993) PROCHECK: a program to check the stereochemical quality of protein structures. J Appl Crystallogr 26: 283–291.

34. Wallner B, Elofsson A (2006) Identification of correct regions in protein models using structural, alignment, and consensus information. Protein Sci 15:900–913.

35. McGuffin LJ (2008) The ModFOLD server for the quality assessment of protein structural models. Bioinformatics 24:586–587.

36. Pawlowski M, Gajda MJ, Matlak R, Bujnicki JM (2008) MetaMQAP: a meta-server for the quality assessment of protein models. BMC Bioinformat 9:403.

37. Wang L, Brown SJ (2006) BindN: a web-based tool for efficient prediction of DNA and RNA binding sites in amino acid sequences. Nucleic Acids Res 34:W243–W248.

38. Hwang S, Gou Z, Kuznetsov IB (2007) DP-Bind: a web server for sequence-based prediction of DNA-binding residues in DNA-binding proteins. Bioinformatics 23: 634–636.

39. Ahmad S, Gromiha MM, Sarai A (2004) Analysis and prediction of DNA-binding proteins and their binding residues based on composition, sequence and structural information. Bioinformatics 20:477–486.

40. Ahmad S, Sarai A (2005) PSSM-based prediction of DNA binding sites in proteins. BMC Bioinformat 6:33.

41. Tsuchiya Y, Kinoshita K, Nakamura H (2005) PreDs: a server for predicting dsDNA-binding site on protein molecular surfaces. Bioinformatics 21:1721–1723.

42. Kumar M, Gromiha MM, Raghava GP (2008) Prediction of RNA binding sites in a protein using SVM and PSSM profile. Proteins 71:189–194.

43. Terribilini M, Sander JD, Lee JH, Zaback P, Jernigan RL, Honavar V, Dobbs D (2007) RNABindR: a server for analyzing and predicting RNA-binding sites in proteins. Nucleic Acids Res 35:W578–W584.

44. Tong J, Jiang P, Lu ZH (2008) RISP: a web-based server for prediction of RNA-binding sites in proteins. Comput Methods Programs Biomed 90:148–153.

Paper 5

Inhibition of the Toll-like receptors TLR4 and 7 signaling pathways by SIGIRR: a computational approach

Jing Gong, Tiandi Wei, Robert W. Stark, Ferdinand Jamitzky, Wolfgang M. Heckl, Hans-Joachim Anders, Maciej Lech and Shaila C. Rössle

Inhibition of Toll-like receptors TLR4 and 7 signaling pathways by SIGIRR: A computational approach

Jing Gong [a,b], Tiandi Wei [a,b,*], Robert W. Stark [a,b], Ferdinand Jamitzky [a,c], Wolfgang M. Heckl [a,d,e], Hans J. Anders [f], Maciej Lech [f], Shaila C. Rössle [b]

[a] Center for Nanoscience, Ludwig-Maximilians-Universität München, 80799 Munich, Germany
[b] Department of Earth and Environmental Sciences, Ludwig-Maximilians-Universität München, 80333 Munich, Germany
[c] Leibniz Supercomputing Centre, 85748 Garching, Germany
[d] TUM School of Education, Technische Universität München, 80799 Munich, Germany
[e] Deutsches Museum, 80538 Munich, Germany
[f] Medizinische Poliklinik, Ludwig-Maximilians-Universität München, 80336 Munich, Germany

ARTICLE INFO

ABSTRACT

Toll-like receptors (TLRs) belong to the Toll-like receptor/interleukin-1 receptor (TLR/IL-1R) superfamily which is defined by a common cytoplasmic Toll/interleukin-1 receptor (TIR) domain. TLRs recognize pathogen-associated molecular patterns and initiate an intracellular kinase cascade to trigger an immediate defensive response. SIGIRR (single immunoglobulin interleukin-1 receptor-related molecule), another member of the TLR/IL-1R superfamily, acts as a negative regulator of MyD88-dependent TLR signaling. It attenuates the recruitment of MyD88 adaptors to the receptors with its intracellular TIR domain. Thus, SIGIRR is a highly important molecule for the therapy of autoimmune diseases caused by TLRs. So far, the structural mechanism of interactions between SIGIRR, TLRs and adaptor molecules is unclear. To develop a working hypothesis for this interaction, we constructed three-dimensional models for the TIR domains of TLR4, TLR7, MyD88 and SIGIRR based on computational modeling. Through protein–protein docking analysis, we developed models of essential complexes involved in the TLR4 and 7 signaling and the SIGIRR inhibiting processes. We suggest that SIGIRR may exert its inhibitory effect through blocking the molecular interface of TLR4, TLR7 and the MyD88 adaptor mainly via its BB-loop region.

1. Introduction

Toll-like receptors (TLRs) are essential for the innate immune system because they recognize molecules, such as single-stranded RNA or CpG DNA that are associated with pathogens. Such nuclear antigen-recognizing receptors are also important in the autoimmune disease systemic lupus erythematosus. The disease progresses as a consequence of the recognition of self nucleic acids by TLRs (Rahman and Eisenberg, 2006). For the future development of therapeutic approaches it is important to understand possible TLR inhibition mechanisms from a structural point of view.

TLRs belong to the Toll-like receptor/interleukin-1 receptor (TLR/IL-1R) superfamily, which is defined by the presence of a conserved cytoplasmic Toll/interleukin-1 receptor (TIR) domain (Bowie and O'Neill, 2000) connected to an ectodomain through a single transmembrane stretch. To date, 13 TLRs have been identi-

fied in mammals. Their ectodomains consist of 16–28 leucine-rich repeats (LRRs). These LRRs provide a variety of structural frameworks for the binding of protein and non-protein ligands including lipopolysaccharide (LPS), lipopeptide, CpG DNA, flagellin, imidazoquinoline and double-/single-stranded RNA (Gay and Gangloff, 2007). TLRs are capable of recognizing ligands in a dimer form (Latz et al., 2007; Liu et al., 2008; Park et al., 2009; Peter et al., 2009; Wei et al., 2009). Upon receptor activation, an intracellular TIR signaling complex is formed between the receptor and downstream adaptor TIR domains (O'Neill and Bowie, 2007). MyD88 (Myeloid differentiation primary response protein 88) was the first intracellular adaptor molecule characterized among all known adaptors in the TLR signaling (Takeda and Akira, 2004). It consists of an N-terminal death domain (DD) separated from its C-terminal TIR domain by a linker sequence. MyD88 also forms a dimer through DD-DD and TIR-TIR domain interactions when recruited to the receptor complex (Burns et al., 1998). MyD88 can recruit IRAK (IL-1RI-associated protein kinases) through its DD to continue signaling and, finally, to induce the nuclear factor-κB (NF-κB) leading to the expression of type I interferons. Although the MyD88-

dependent pathway is common to most TLRs, TLR3 exclusively uses TRIF (TIR domain-containing adapter inducing interferon-β) for signaling (MyD88-independent) while the TLR4 can signal via both pathways (Takeda and Akira, 2004).

SIGIRR (Single immunoglobulin interleukin-1 receptor-related molecule), also known as TIR8, was initially identified as an Ig domain-containing receptor of the TLR/IL-1R superfamily (Thomassen et al., 1999). Both the extracellular and intracellular domains of SIGIRR differ from those of other Ig domain-containing receptors, as its single extracellular Ig domain does not support ligand-binding. Its intracellular TIR domain cannot activate NF-κB because it lacks two crucial amino acids, Ser447 and Tyr536. Moreover, the TIR domain of SIGIRR extends that of the typical TLR/IL-1R superfamily member by more than 73 amino acids at the C-terminal (C-tail) (Thomassen et al., 1999). Instead, SIGIRR acts as an endogenous inhibitor for MyD88-dependent TLR and IL-1R signaling. This behavior was shown by over expression of SIGIRR in Jurkat or HepG2 cells which showed substantially reduced LPS, CpG DNA or IL-1-induced activation of NF-κB (Polentarutti et al., 2003; Qin et al., 2005; Wald et al., 2003). Thus, SIGIRR has attracted tremendous research interest because of its regulating function in cancer-related inflammation and autoimmunity (Lech et al., in press). For example, systemic lupus erythematosus is caused by TLR7-mediated induction of type I interferons. Compared with wild type mice *Sigirr*-deficient mice develop excessive lymphoproliferation when introduced into the context of a lupus susceptibility gene (Lech et al., 2008). Although the significance of SIGIRR has been widely acknowledged, its inhibition mechanism remains unclear owing to a lack of structural information.

Mutagenesis studies investigated three deletion mutants of SIGIRR (Qin et al., 2005): ΔN (lacking the extracellular Ig domain), ΔTIR (lacking the intracellular TIR domain) and ΔC (lacking the C-tail of the TIR domain with deletion of residues 313–410). The results showed that only the TIR domain (excluding the C-tail part) is necessary for SIGIRR to inhibit TLR4 signaling (Qin et al., 2005). Nevertheless, detailed structural interaction mechanisms of SIGIRR's TIR domain are still missing.

So far, the structures of the TIR domains of human TLR1, 2, 10 and IL-1RAPL have been determined by X-ray crystallography (Khan et al., 2004; Nyman et al., 2008; Xu et al., 2000). The TLR1 and 2 modules occur as monomers in solution and the packing of the molecules in the crystal lattice does not suggest a likely arrangement for a functional dimer. In contrast, the TLR10 and IL-1RAPL TIR domains were present as homodimers. Although they demonstrate different dimer conformations, a highly conserved BB-loop region plays a crucial role in both dimer interfaces. Using this information, we have constructed three-dimensional models for TIR domains of TLR4, TLR7, MyD88 and SIGIRR by homology modeling and protein threading. Models of essential molecular complexes involved in the TLR4 and 7 signaling pathways and the SIGIRR inhibiting process are proposed and compared based on results of protein–protein docking studies. We chose TLR4 as an additional example to elucidate the mechanisms involved in the negative regulation of the MyD88-dependent TLR signals by SIGIRR, because different mechanisms of TLR4 recognizing LPS and TLR7 recognizing single-stranded RNA may lead to different structural interactions of receptor with SIGIRR, which enables further insight into the molecular interaction.

2. Methods

2.1. Templates identification and sequence alignments

Amino acid sequences of the target proteins, human TLR4 (GenBank Accession No. O00206), TLR7 (Q9NYK1), MyD88 (AAC50954) and SIGIRR (CAG33619) were extracted from the NCBI protein database (Wheeler et al., 2008). Three-dimensional models of TLR4 (Asn672-Ala814), TLR7 (Cys889-Asp1036), MyD88 (Glu159-Pro296) and SIGIRR (Tyr165-Pro308, without the C-tail Arg309-Ser392) were constructed by homology modeling. Due to the homology of the target proteins, four common templates were obtained via BLAST search against the Protein Data Bank (PDB) (Berman et al., 2000). They were TLR1 (PDB code: 1FYV), TLR2 (1FYW), TLR10 (2J67) and IL-1RAPL (1T3G). Multiple sequence alignment of each target with the templates was generated with MUSCLE (Edgar, 2004) and analyzed with Jalview (Clamp et al., 2004). Because the secondary structure of the TIR domain is composed of well-organized alternating β-strands and α-helixes, we adjusted the alignments manually according to the secondary structure information to improve the alignment quality. The secondary structure of each target was predicted by PSIPRED (Bryson et al., 2005). In addition, the C-terminal tail of the TIR domain, which is unique to SIGIRR, has no homologue of known structure to serve as a template. In this case we employed the protein threading method THREADER 3.5 (Jones et al., 1995) to determine a template structure. The selected template was NSF-N (N-terminal domain of *N*-ethylmaleimide sensitive factor, PDB code: 1QCS).

2.2. Model construction and validation

The initial three-dimensional coordinates of the models were generated by the fully automated program MODELLER 9v3 (Fiser et al., 2000). The input files for each model were a 5-line multiple alignment file (one target and four templates) and coordinate files of the templates. During modeling, gap regions in the alignment produced 3–8 residue-long loop structures in the model, which deteriorated the model's accuracy. ModLoop (Fiser and Sali, 2003) was used to rebuild the coordinates of these loop regions. ModLoop optimizes the positions of non-hydrogen atoms of a loop (shorter than 20 residues) relying on a protocol consisting of a conjugate gradient minimization and a molecular dynamics simulation. Finally, we used the model quality assessment programs ProQ (Wallner and Elofsson, 2003), ModFOLD (McGuffin, 2008) and MetaMQAP (Pawlowski et al., 2008) to evaluate the output candidate models and select the most reliable one.

2.3. Model docking

Unrestrained pairwise model docking included eight complexes of TIR domains: TLR4-TLR4, TLR7-TLR7, MyD88-MyD88, TLR4 dimer-MyD88 dimer (tetramer), TLR7 dimer-MyD88 dimer (tetramer), TLR4-SIGIRR, TLR7-SIGIRR and MyD88-SIGIRR. We used GRAMM-X (Tovchigrechko and Vakser, 2006) and ZDOCK (Chen et al., 2003), which are widely accepted rigid-body protein–protein docking programs, to predict and assess the interactions between these complexes. Both programs rank the 10 most probable predictions out of thousands of candidates based on geometry, hydrophobicity and electrostatic complementarity of the molecular surface. We then selected the most reasonable solution from these top 10 lists in consideration of further qualifications. Briefly, these qualifications included residue conservation of the interaction sites, steric compatibility of the amino acid linker to the transmembrane helix, and knowledge from published articles (Bell et al., 2006; Loiarro et al., 2007; Nunez Miguel et al., 2007; Nyman et al., 2008; Park et al., 2009; Poltorak et al., 1998). The buried surface interaction area of dimer models were calculated with the protein interfaces, surfaces and assemblies service (PISA) at the European Bioinformatics Institute (Krissinel and Henrick, 2007).

3. Results

3.1. Molecular modeling of TIR domains

In the secondary structure-aided alignments for the homology modeling, the average target-template sequence similarity of TLR4, TLR7, MyD88 and SIGIRR was 51.7%, 50.4%, 44.5% and 42.7%, respectively (detailed in Table 1). The resulting structures exhibit a typical TIR domain conformation in which a central five-stranded parallel β-sheet (βA-βE) is surrounded by a total of five α-helixes (αA–αE) on both sides (Fig. 1A). The loops are named by the letters of the secondary structure elements that they connect. For example, the BB-loop connects β-strand B and α-helix B. The structure of NSF-N was identified as a template for SIGIRR's C-tail through protein threading. This template was first-ranked by THREADER according to the energy Z-score (Z = 2.7: borderline significant (Jones et al., 1995)). The C-tail contains a four-stranded parallel β-sheet with an α-helix and several loop structures on one side, while the other side points to SIGIRR's TIR (Fig. 1A). These results suggest that the TIR domain and the C-tail of SIGIRR are not an integrative structure, but two interconnected individual modules. There is a 3 residue-long short linker (Leu307-Arg309) between the last secondary structure αE of SIGIRR's TIR and the first secondary structure βA of SIGIRR's C-tail. Therefore, the C-tail can only be situated next to the αE of the TIR domain. Further evaluation of the models involved analysis of geometry, stereochemistry and energy distributions of the molecules. The evaluation results (Table 2) indicate high quality for all models in terms of overall packing.

Multiple sequence alignment of TIR domains from different molecules detected seven conserved boxes in the TIR domain (Fig. 1B). Our models show that they correspond to β-strand A (βA), β-strand B (βB), BB-loop, β-strand C (βC), β-strand D (βD), β-strand E (βE) and α-helix E (αE). Functional significance can usually be observed in conserved regions. Nevertheless, the five β-strands (boxes 1, 2, 4–6) are embedded structures that form a hydrophobic core of the TIR domain and hence are not likely to interact with other molecules. Also, the αE (box 7) of SIGIRR is blocked because it is linked to the C-tail. In this vein, the BB-loop (box 3) and αE of TLR4, TLR7 and MyD88, along with the BB-loop of SIGIRR, may be

Table 1
Protein sequence similarities (%) between targets and templates.

	TLR1	TLR2	TLR10	IL-1RAPL	Avg
TLR4	53.4	57.8	51.4	44.2	51.7
TLR7	51.0	55.8	49.3	45.6	50.4
MyD88	44.5	45.3	40.6	47.4	44.5
SIGIRR	41.8	42.3	37.7	49.0	42.7
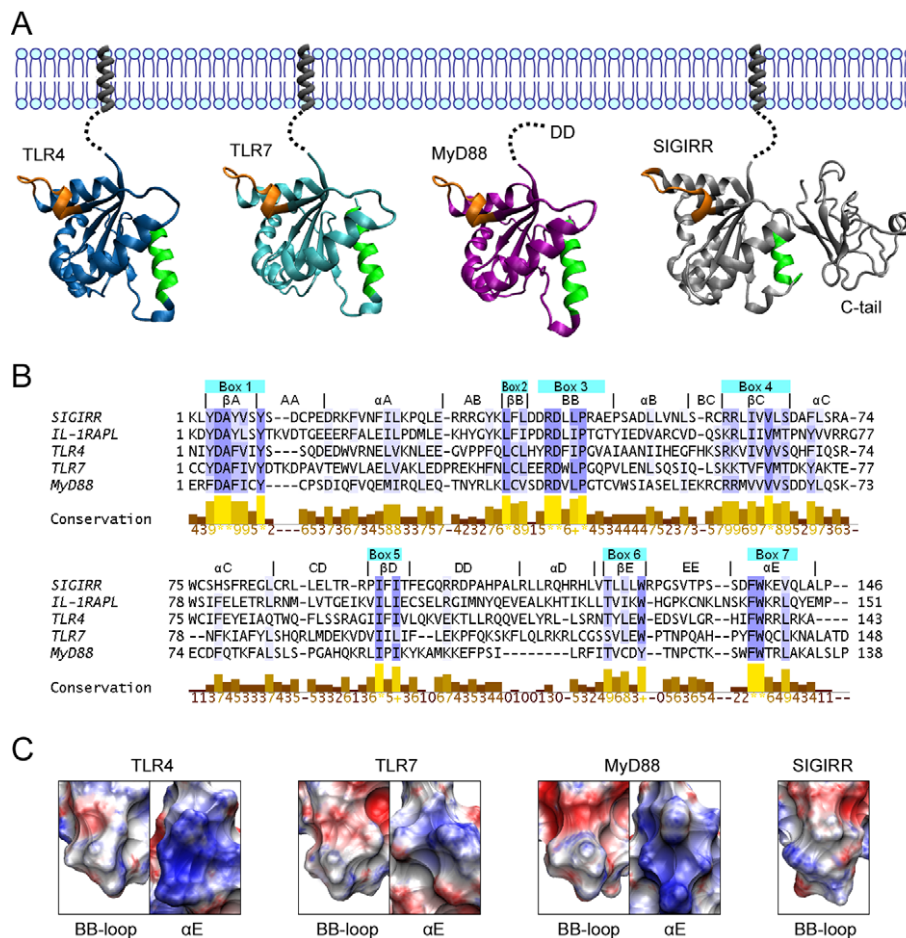
Fig. 1. Three-dimensional structures and conserved regions of TIR domains of TLR4, TLR7, MyD88 and SIGIRR. (A) The BB-loop and αE regions are highlighted in orange and green respectively. As there is a three residue-long linker between the two modules of SIGIRR's TIR, the orientation of the C-tail as shown here is speculative. (B) Multiple sequence alignment of different TIRs indicates seven conserved boxes. (C) Surface charge distribution (APBS electrostatics) of BB-loop and αE with red indicating areas of negative charge and blue indicating positive charge. (For interpretation of the references to colour in this figure legend, the reader is referred to the web version of this article.)

Table 2

Model evaluation. ProQ_LG: >1.5 fairly good; >2.5 very good; >4 extremely good. ProQ_MS: >0.l fairly good; >0.5 very good; >0.8 extremely good. ModFOLD_Q: >0.5 medium confidence; >0.75 high confidence. ModFOLD_P: <0.05 medium confidence; <0.01 high confidence. MetaMQAP_GDT/RMSD: an ideal model has a GDT score over 59 and a RMSD around 2.0 Å.

	ProQ_LG/MS	ModFOLD_Q/P	MetaMQAP_GDT/RMSD
TLR4	4.764/0.705	0.6177/0.022	76.923/2.123 Å
TLR7	4.374/0.579	0.6199/0.022	71.791/2.138 Å
MyD88	3.966/0.628	0.5749/0.027	73.188/2.202 Å
SIGIRR	3.783/0.438	0.7589/0.010	65.068/2.737 Å
C-tail	2.018/0.300	0.7731/0.009	52.083/3.023 Å

important to ensure binding specificity achieved by different combinations of TIRs during signaling (Fig. 1A). Fig. 1C illustrates the electrostatic surface potential of these BB-loops and αEs. Accordingly, all BB-loops can be divided into two self-complementary parts. The N-terminal (upper region of BB-loops in Fig. 1C) is negatively charged, whereas the C-terminal (lower region of BB-loops in Fig. 1C) is positively charged. The αEs, by contrast, are predominantly positive.

3.2. Pairwise docking of TIR domains

The procedure of protein–protein docking is highly computationally oriented. The reliability of docking results strongly depends on the quality of docking methods. In order to verify the prediction confidence of TIR-TIR interaction of both methods GRAMM-X and ZDOCK, we unrestrainedly inputted as test case the TIR domains of human TLR10 as test case, for which the dimeric crystal structure is known. The native dimerization geometry of TLR10 was present in the top 10 solutions of both GRAMM-X and ZDOCK and was first-ranked by GRAMM-X and sixth-ranked by ZDOCK. The incompleteness of TLR10's crystal structure led to the first five incorrect predictions of ZDOCK, in which large structural gaps were involved in the dimer interfaces. It was therefore straightforward to exclude these five solutions. This test highlights the feasibility and reliability of GRAMM-X and ZDOCK applied in TIR-TIR docking.

As noted above, TIR domains are able to interact heterotypically with each other. To elucidate how SIGIRR disturbs the MyD88-dependent TLR4 and 7 signals, an understanding of the interaction mode of the TLR4 and 7 signaling complexes without the presence of SIGIRR is indispensable. We thus performed unrestrained rigid-body docking for eight TIR complexes. Each docking method returned the 10 most probable models for an input. Thus each complex received a total of 20 candidate models separated into two sets. Some models from the same set had similar conformations whereas most differed considerably from one another. There were some shared models (intersection) across both sets for each complex. These shared models were considered as more confident solutions than others. The optimal docking solution was selected for each complex from the 20 candidates based on three criteria, as follows:

1. Exclude models that do not exist in the intersection of both resulting sets.
2. Exclude models that contain a steric incompatibility of the amino acid liker to the transmembrane helix.
3. Include only those models in which the dimerization geometry is supported by reported experimental data or the dimerization interface is associated with highly conserved boxes as described in Fig. 1B.

For most complexes this three-step filtering led to a unique solution. In the case of the TLR4-TLR4 and the TLR7 dimer-

MyD88 dimer, where these three rules did not yield a unique solution, a further qualification had to be considered. The highest-ranked model by ZDOCK/GRAMM-X ranking was then accepted as the optimal model. The ZDOCK/GRAMM-X ranking and the buried surface interaction area of all optimal models are detailed in Table 3. All resulting docking models are provided in Supplementary file 1.

3.2.1. TLR4–TLR4

The signaling mechanism of TLR4 involves receptor dimerization (Park et al., 2009). After the three-step filtering two candidate models remained. Their ZDOCK/GRAMM-X rankings were 1/6 and 9/2. The first model was accepted because it was best ranked on average and ZDOCK provided a clear-cut ranking. TLR4's TIR reveals an axially symmetric dimer (Fig. 2A) with the BB-loop (involved residues: Pro714-Ala717) of one monomer protruding into a groove formed by the αC (Cys747-Ile748) and DD-loop (Gln782) of the other. The αB (Ala719) of each monomer interacts tightly with each other in the middle of both BB-loop connections. In this model, the Pro714 of one monomer and the Gln782 of the other are connected by a hydrogen bond, which supports Poltorak's (1998) conclusion that the corresponding residue Pro712 is essential to mouse TLR4's function.

3.2.2. TLR7–TLR7

TLR7's TIR forms a *face-to-tail* conformation. The BB-loop (*face*, Glu930–Pro938) of one monomer is preceded by the αE (*tail*, Tyr1024–Ala1032) of the other (Fig. 2B). The BB-loop also interacts with some other regions close to the αE, including: CD-loop (Lys982–Val983), βD (Ile986–Leu988), αD (Gly1009), DE-loop (Ser1010–Ser1011), βE (Val1012–Pro1016) and EE-loop (Thr1017 and Ala1021). Aside from this connection, the EE-loop (Thr1017–Ala1021) of the frontal monomer approximates the αA (Thr905–Glu917) of the posterior. Since the BB-loop and αE are located on opposite sides of a TIR domain, such a *face-to-tail* dimer can be extended by additional TIRs. This dimer model may be relevant for a possible oligomerization of nucleic acid-recognizing TLRs. As discussed by Bell et al. (2006), oligomers might be formed if a nucleic acid ligand is sufficiently long to aggregate several receptors.

3.2.3. MyD88–MyD88

MyD88 forms a dimer when it is incorporated into a receptor complex (Burns et al., 1998). In this model, the BB-loops (Asp195–Cys203) from both monomers were docked together in an antiparallel self-complementary packing (Fig. 2A). Additionally, both αCs (Cys233–Lys238) were brought into contact next to the BB-loop connection. The model is axially symmetric similar to the dimeric crystal structure of human TLR10 (Nyman et al., 2008). Our model is consistent with Loiarro's (2007) conclusion that a heptapeptide, which mimics the BB-loop of MyD88's TIR domain, strongly interferes with dimerization of MyD88.

Table 3

Ranking and interaction area of the selected docking models.

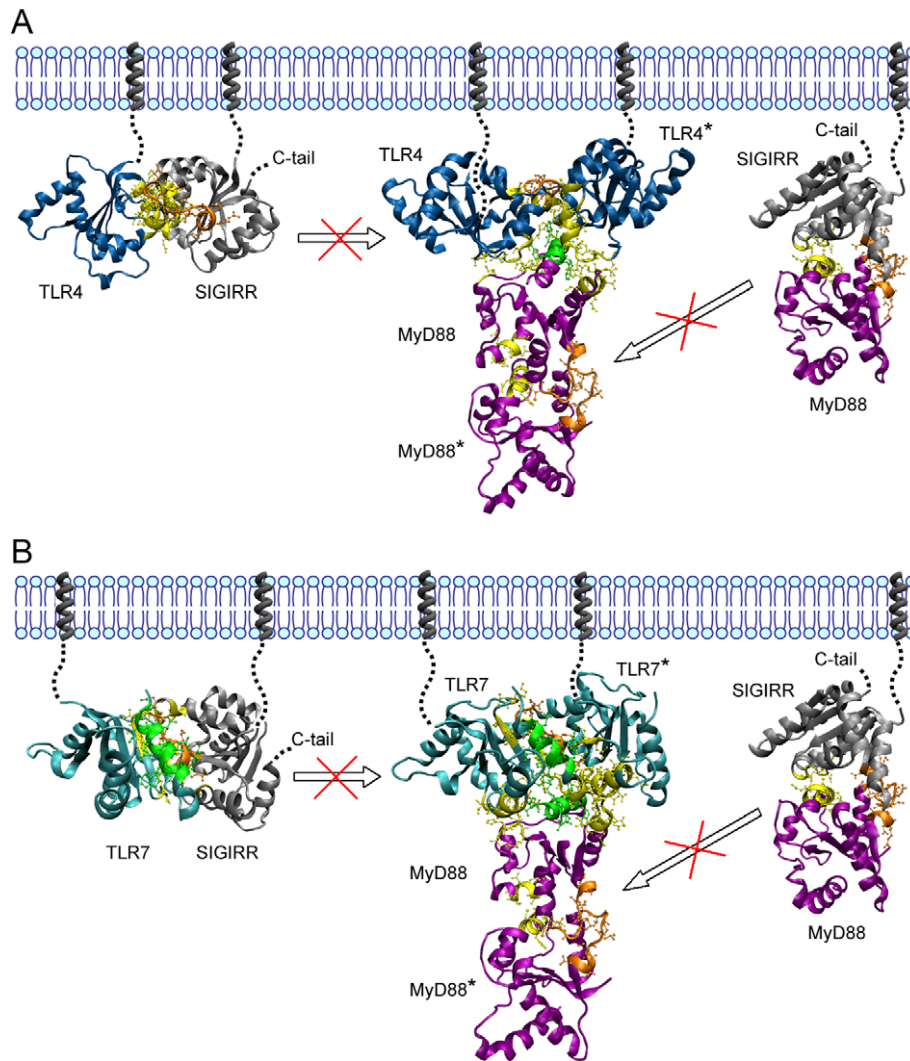|	ZDOCK	GRAMM-X	Interaction area (Å²)
TLR4–TLR4	1	6	639.0
TLR7–TLR7	1	3	965.3
MyD88–MyD88	1	7	737.2
TLR4 × 2-MyD88 × 2	4	1	1395.1
TLR7 × 2-MyD88 × 2	1	5	1249.3
TLR4–SIGIRR	1	6	1092.4
TLR7–SIGIRR	4	1	1055.2
MyD88–SIGIRR	2	9	818.1

Fig. 2. Models of SIGIRR inhibiting the MyD88-dependent TLR4 and 7 signaling. Interacting regions of BB-loop and αE are labeled in orange and green respectively. Other interacting regions are labeled in yellow. All interacting residues (orange/green/yellow) are represented using CPK (Corey, Pauling & Kultun) convention. (A) Models of SIGIRR inhibiting the TLR4 signaling. (B) Models of SIGIRR inhibiting the TLR7 signaling.

3.2.4. TLR4 dimer–MyD88 dimer

The receptor dimers and MyD88 dimer described above were assembled into tetramers. The TLR4 dimer provides a negatively charged binding pocket adjacent to its interface (Fig. 3). This pocket is constituted by the αC (Gln755) of one TLR4 monomer as well as the αB (Ala719–His724) and αC (Tyr751–Thr756) of the other monomer (TLR4*). The highly conserved, positively charged αE (Cys280–Arg288) of a MyD88 monomer just fills the pocket and makes interactions with the above described residues of TLR4 (Fig. 2A). This connection is further stabilized by three surrounding links: MyD88's DE-loop (Ile271) to TLR4's CD-loop (Arg763–Ala764); MyD88's EE-loop (Asp275–Thr277) to TLR4's CD-loop (Thr756–Gln758); and MyD88's αA (Gln181–Asn186) to TLR4*'s CD-loop (Trp757–Leu760).

3.2.5. TLR7 dimer–MyD88 dimer

After the three-step filtering, two candidate models remained for this dimer. Their ZDOCK/GRAMM-X rankings were 1/5 and 4/6, respectively. The first model obtained the higher ranking in both programs and was thus accepted as optimal. Although TLR7 dimerizes in a different manner as compared to TLR4, it also generates a negatively charged αE-binding pocket for MyD88 at the corresponding location (Figs. 2B and 3). The pocket is composed of αA

(Glu906–Glu911) and EE-loop (Trp1015–Pro1019) of one TLR7 monomer, and AA-loop (Thr899–Val904) and αA (Thr905–Glu906) of the other monomer (TLR7*). This pocket connection is further stabilized by three surrounding links: TLR7's αA (Glu906) and AA-loop (Thr899–Pro902) to MyD88's CD-loop (His248–Arg251); TLR7's EE-loop (Pro1019–Ala1021) to MyD88's AB-loop (Asn186–Arg188) and βB (Leu189); and TLR7*'s αA (Glu906–Ala914) to MyD88's AB-loop (Thr185–Asn186) and αA (Gln181–Gln184). Both TLR4–MyD88 and TLR7–MyD88 tetramers show a T-shaped conformation, where the highly conserved αE of MyD88 plays a central role (Fig. 2).

3.2.6. TLR4-sigirr

SIGIRR heterodimerizes with TLR4 and acts as an inhibitor of TLR signaling (Qin et al., 2005). Our docking model exhibits an extensive interface that is composed of three patches, which indicates a strong molecular affinity (Fig. 2A). First, a consecutive stretch containing SIGIRR's BB-loop (Asp200–Glu209) and αB (Pro210–Ser211) interacts with TLR4's CD-loop (Trp757–Leu760). Second, SIGIRR's αC (Arg235–Arg243) protrudes into the groove formed by TLR4's αB (Ala719–His728) and αC (Tyr751–Gln755). Third, SIGIRR's αD (Pro268–Ala269) interacts with TLR4's BB-loop (Val716–Ala717). Fig. 3 shows that the proper MyD88's αE-binding
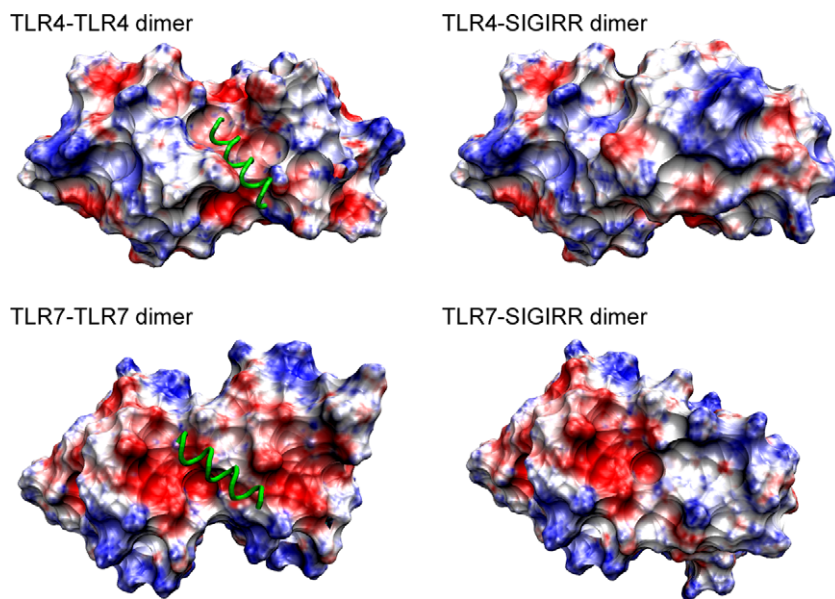
Fig. 3. Surface charge distribution of TIR dimers.Both TLR4-TLR4 and TLR7-TLR7 dimers generate a negatively charged (red) pocket adjacent to their dimer interface to hold the positively charged (blue) αE of MyD88 (charge of αE shown in Fig. 1C). The incorporation of SIGIRR completely disturbed the proper shape and electric environment of the pocket. The αE is represented by a green tube and the other part of MyD88 is omitted for better view. (For interpretation of the references to colour in this figure legend, the reader is referred to the web version of this article.)

pocket presented by the TLR4–TLR4 dimer does not persist in the TLR4-SIGIRR dimer. Notably, the C-tail of SIGIRR is located on the opposite side of SIGIRR's interacting surface. Therefore, it may not participate in the dimer interface (Qin et al., 2005).

3.2.7. TLR7–SIGIRR

Similar to TLR7–TLR7, the TLR7–SIGIRR model is *face-to-tail*, with SIGIRR replacing the rear TLR7 monomer as shown in Fig. 2B. The molecular interface between TLR7 and SIGIRR is larger than that between TLR7 and TLR7. SIGIRR's BB-loop (Asp200–Ala208) together with the beginning of the adjacent αB (Pro210–Ser211) interacts with TLR7's αE (Tyr1024–Thr1035), CD-loop (Lys982–Asp984), βD (Val985–Leu988), DE-loop (Ser1010–Ser1011) and βE (Val1012–Glu1014). Simultaneously, TLR7's DD-loop (Lys993–Phe995) interacts with SIGIRR's AA-loop (Asp173) and αA (Asn182). Likewise, there is no MyD88 αE-binding pocket on this dimer (Fig. 3) and SIGIRR's C-tail does not seem to play any role (Qin et al., 2005).

3.2.8. MyD88–SIGIRR

SIGIRR interferes with the functional dimer conformation of MyD88 by heterodimerization with MyD88 (Qin et al., 2005). The molecular interface between MyD88 and SIGIRR is also quite large (Fig. 2A). SIGIRR's BB-loop (Asp201–Ala208) complements MyD88's BB-loop (Asp195–Val204) by substituting the other BB-loop in the customary MyD88 homodimer. Furthermore, SIGIRR's AA-loop (Ser172–Cys174) and αC (Arg235–Ala236) interacts with MyD88's αC (Gln229–Thr237) under the BB-loops. This model is similar to the dimeric crystal structure of human TLR10 (Nyman et al., 2008), where the BB-loop was identified as a main component of interactions. Likewise, SIGIRR's C-tail does not seem to affect the dimer (Qin et al., 2005).

4. Discussion

So far, the only crystallized dimer structure of TLR's TIR domain is the TLR10 dimer (Nyman et al., 2008), where the BB-loop and αC of each monomer constitute the major part of the symmetric dimer interface. Nunez Miguel et al. (2007) assumed that TLR4 dimerizes in a manner identical to that of TLR10 despite

having no direct evidence. However, we do not consider them to be necessarily identical, because the TIR domain has various inherent dimer conformations (Khan et al., 2004; Nyman et al., 2008; Tao et al., 2002) and TLR4 has different ligand-binding and signaling mechanisms than TLR10. Poltorak et al. (1998) reported that a single point mutation (Pro712His) of the TIR domain of murine TLR4 abolished the TLR4 response to LPS. Our human TLR4 dimer model supports their results. The corresponding residue Pro714 is located at the very tip of the BB-loop and interacts tightly with Gln782 of the other monomer. In contrast to the intensively studied TLR4, structural information about the TIR domain of TLR7 is missing. We thus propose a dimer model of the TLR7 TIR domain. The dimer interaction is maintained mainly by the BB-loop and αE, which are highly conserved among TIRs of different molecules (Fig. 1B).

Triggering of the TLR causes the adaptor protein MyD88 to be recruited to the receptor complex, which in turn promotes association with kinases IRAK4/1. Mal (MyD88-adaptor-like) is another TIR domain-containing adapter protein specifically required by the TLR2 and 4 signaling (Gray et al., 2006). A previous study indicated that Mal promotes the recruitment of MyD88 to TLR4 as a bridging factor and there is no direct interaction between MyD88 and TLR4 (Brown et al., 2006). However, Mal has been shown to be dispensable for TLR4 signaling when MyD88 is fused to a PIP2 targeting domain (Kagan and Medzhitov, 2006). Therefore, direct interactions between TIR domains of MyD88 and TLR4 may mediate signal transduction. This alternate Mal-independent pathway could contribute to signaling as discussed recently (Monie et al., 2009; Ohnishi et al., 2009). Dunne et al. (2003) modeled the TLR4-MyD88 heterodimer using TLR4 and MyD88 monomers. This monomer to monomer model, however, may not fully reflect the molecular interactions. Our model of the receptor dimer docking to the MyD88 dimer provides additional information for a structural interpretation. In particular, both tetramers (TLR4 dimer-MyD88 dimer and TLR7 dimer-MyD88 dimer) exposed in our study demonstrate that the stimulus-induced dimerization of TIR domains creates a new negatively charged molecular pocket for the binding of the positively charged αE of the MyD88 adaptor (Fig. 3). In the presence of SIGIRR, the proper shape and electric

environment of the MyD88-binding pocket are completely disturbed (Fig. 3).

The results from the pairwise docking studies presented here could be assembled to derive a working hypothesis for the TLR4 and 7 signaling transductions and the SIGIRR inhibition mode (Fig. 2). Receptor activation would trigger the formation of TLR4 and 7 TIR dimers recruiting MyD88 TIR dimers resulting in a signaling tetramer. Model predictions including SIGIRR reveal that SIGIRR binds to TLR4 and 7 by occupying their self-interacting sites. On the other hand, the MyD88-SIGIRR dimer shows a resemblance to the MyD88 homodimer. That is, SIGIRR replaces a MyD88 monomer, interrupting the MyD88 homodimer formation. In all cases the BB-loop of SIGIRR plays a key role in binding. The relative positions of all these TIR complexes to the cell/endosome membrane are difficult to expatiate because MyD88 is dissociated from the membrane, and TIR domains of TLR4, TLR7 and SIGIRR are connected to their transmembrane helix by a 20–30 amino acid-long loop stretch which endows the TIR domain with flexible depth and orientation in a cell. Remarkably, TLR4, TLR7 and MyD88 possess a more extensive molecular interface with SIGIRR (heterodimer) than with themselves (homodimer) (Table 3). Fig. 3 also shows that the spatial approximation of receptor-SIGIRR is closer than that of receptor-receptor. These observations highlight the strong molecular affinity of SIGIRR as an inhibitor. In addition, according to our model, SIGIRR's unique C-tail is distant from the active BB-loop consistent with the observation that this tail is not required for SIGIRR's inhibitory effect on TLR signaling (Qin et al., 2005).

In summary, we propose a residue-detailed structural framework of SIGIRR inhibiting the TLR4 and 7 signaling pathways. These results were obtained by computer modeling and are expected to facilitate efforts to design further site-directed mutagenesis experiments to clarity the regulatory role of SIGIRR in inflammatory and innate immune responses.

Acknowledgments

Appendix A. Supplementary data

Supplementary data associated with this article can be found, in the online version, at doi:10.1016/j.jsb.2009.12.007.

References

Bell, J.K., Askins, J., Hall, P.R., Davies, D.R., Segal, D.M., 2006. The dsRNA binding site of human Toll-like receptor 3. Proc. Natl. Acad. Sci. USA 103, 8792–8797.

Berman, H.M., Westbrook, J., Feng, Z., Gilliland, G., Bhat, T.N., Weissig, H., Shindyalov, I.N., Bourne, P.E., 2000. The protein data bank. Nucl. Acids Res. 28, 235–242.

Bowie, A., O'Neill, L.A., 2000. The interleukin-1 receptor/Toll-like receptor superfamily: signal generators for pro-inflammatory interleukins and microbial products. J. Leukoc. Biol. 67, 508–514.

Brown, V., Brown, R.A., Ozinsky, A., Hesselberth, J.R., Fields, S., 2006. Binding specificity of Toll-like receptor cytoplasmic domains. Eur. J. Immunol. 36, 742–753.

Bryson, K., McGuffin, L.J., Marsden, R.L., Ward, J.J., Sodhi, J.S., Jones, D.T., 2005. Protein structure prediction servers at University College London. Nucl. Acids Res. 33, W36–38.

Burns, K., Martinon, F., Esslinger, C., Pahl, H., Schneider, P., Bodmer, J.L., Di Marco, F., French, L., Tschopp, J., 1998. MyD88, an adapter protein involved in interleukin-1 signaling. J. Biol. Chem. 273, 12203–12209.

Chen, R., Li, L., Weng, Z., 2003. ZDOCK: an initial-stage protein-docking algorithm. Proteins 52, 80–87.

Clamp, M., Cuff, J., Searle, S.M., Barton, G.J., 2004. The Jalview Java alignment editor. Bioinformatics 20, 426–467.

Dunne, A., Ejdeback, M., Ludidi, P.L., O'Neill, L.A., Gay, N.J., 2003. Structural complementarity of Toll/interleukin-1 receptor domains in Toll-like receptors and the adaptors Mal and MyD88. J. Biol. Chem. 278, 41443–41451.

Edgar, R.C., 2004. MUSCLE: multiple sequence alignment with high accuracy and high throughput. Nucl. Acids Res. 32, 1792–1797.

Fiser, A., Sali, A., 2003. ModLoop: automated modeling of loops in protein structures. Bioinformatics 19, 2500–2501.

Fiser, A., Do, R.K., Sali, A., 2000. Modeling of loops in protein structures. Protein Sci. 9, 1753–1773.

Gay, N.J., Gangloff, M., 2007. Structure and function of Toll receptors and their ligands. Annu. Rev. Biochem. 76, 141–165.

Gray, P., Dunne, A., Brikos, C., Jefferies, C.A., Doyle, S.L., O'Neill, L.A., 2006. MyD88 adapter-like (Mal) is phosphorylated by Bruton's tyrosine kinase during TLR2 and TLR4 signal transduction. J. Biol. Chem. 281, 10489–10495.

Jones, D.T., Miller, R.T., Thornton, J.M., 1995. Successful protein fold recognition by optimal sequence threading validated by rigorous blind testing. Proteins 23, 387–397.

Kagan, J.C., Medzhitov, R., 2006. Phosphoinositide-mediated adaptor recruitment controls Toll-like receptor signaling. Cell 125, 943–955.

Khan, J.A., Brint, E.K., O'Neill, L.A., Tong, L., 2004. Crystal structure of the Toll/interleukin-1 receptor domain of human IL-1RAPL. J. Biol. Chem. 279, 31664–31670.

Krissinel, E., Henrick, K., 2007. Inference of macromolecular assemblies from crystalline state. J. Mol. Biol. 372, 774–797.

Latz, E., Verma, A., Visintin, A., Gong, M., Sirois, C.M., Klein, D.C., Monks, B.G., McKnight, C.J., Lamphier, M.S., Duprex, W.P., Espevik, T., Golenbock, D.T., 2007. Ligand-induced conformational changes allosterically activate Toll-like receptor 9. Nat. Immunol. 8, 772–779.

Lech, M., Kulkarni, O.P., Pfeiffer, S., Savarese, E., Krug, A., Garlanda, C., Mantovani, A., Anders, H.J., 2008. Tir8/Sigirr prevents murine lupus by suppressing the immunostimulatory effects of lupus autoantigens. J. Exp. Med. 205, 1879–1888.

Lech, M., Skuginna, V., Kulkarni, O.P., Gong, J., Wei, T., Stark, R.W., Garlanda, C., Mantovani, A., Anders, H.J., in press. Lack of SIGIRR/TIR8 aggravates hydrocarbon oil-induced systemic lupus nephritis. J. Pathol. doi:10.1002/path.2678.

Liu, L., Botos, I., Wang, Y., Leonard, J.N., Shiloach, J., Segal, D.M., Davies, D.R., 2008. Structural basis of toll-like receptor 3 signaling with double-stranded RNA. Science 320, 379–381.

Loiarro, M., Capolunghi, F., Fanto, N., Gallo, G., Campo, S., Arseni, B., Carsetti, R., Carminati, P., De Santis, R., Ruggiero, V., Sette, C., 2007. Pivotal Advance. Inhibition of MyD88 dimerization and recruitment of IRAK1 and IRAK4 by a novel peptidomimetic compound. J. Leukoc. Biol. 82, 801–810.

McGuffin, L.J., 2008. The ModFOLD server for the quality assessment of protein structural models. Bioinformatics 24, 586–587.

Monie, T.P., Moncrieffe, M.C., Gay, N.J., 2009. Structure and regulation of cytoplasmic adapter proteins involved in innate immune signaling. Immunol. Rev. 227, 161–175.

Nunez Miguel, R., Wong, J., Westoll, J.F., Brooks, H.J., O'Neill, L.A., Gay, N.J., Bryant, C.E., Monie, T.P., 2007. A dimer of the Toll-like receptor 4 cytoplasmic domain provides a specific scaffold for the recruitment of signalling adaptor proteins. PLoS ONE 2, e788.

Nyman, T., Stenmark, P., Flodin, S., Johansson, I., Hammarstrom, M., Nordlund, P., 2008. The crystal structure of the human toll-like receptor 10 cytoplasmic domain reveals a putative signaling dimer. J. Biol. Chem. 283, 11861–11865.

O'Neill, L.A., Bowie, A.G., 2007. The family of five: TIR-domain-containing adaptors in Toll-like receptor signalling. Nat. Rev. Immunol. 7, 353–364.

Ohnishi, H., Tochio, H., Kato, Z., Orii, K.E., Li, A., Kimura, T., Hiroaki, H., Kondo, N., Shirakawa, M., 2009. Structural basis for the multiple interactions of the MyD88 TIR domain in TLR4 signaling. Proc. Natl. Acad. Sci. USA. 106, 10260–10265.

Park, B.S., Song, D.H., Kim, H.M., Choi, B.S., Lee, H., Lee, J.O., 2009. The structural basis of lipopolysaccharide recognition by the TLR4-MD-2 complex. Nature 458, 1191–1195.

Pawlowski, M., Gajda, M.J., Matlak, R., Bujnicki, J.M., 2008. MetaMQAP: a meta-server for the quality assessment of protein models. BMC Bioinform. 9, 403.

Peter, M.E., Kubarenko, A.V., Weber, A.N., Dalpke, A.H., 2009. Identification of an N-terminal recognition site in TLR9 that contributes to CpG-DNA-mediated receptor activation. J. Immunol. 182, 7690–7697.

Polentarutti, N., Rol, G.P., Muzio, M., Bosisio, D., Camnasio, M., Riva, F., Zoja, C., Benigni, A., Tomasoni, S., Vecchi, A., Garlanda, C., Mantovani, A., 2003. Unique pattern of expression and inhibition of IL-1 signaling by the IL-1 receptor family member TIR8/SIGIRR. Eur. Cytokine Netw. 14, 211–218.

Poltorak, A., He, X., Smirnova, I., Liu, M.Y., Van Huffel, C., Du, X., Birdwell, D., Alejos, E., Silva, M., Galanos, C., Freudenberg, M., Ricciardi-Castagnoli, P., Layton, B., Beutler, B., 1998. Defective LPS signaling in C3H/HeJ and C57BL/10ScCr mice. Mutations in TLR4 gene. Science 282, 2085–2088.

Qin, J., Qian, Y., Yao, J., Grace, C., Li, X., 2005. SIGIRR inhibits interleukin-1 receptor- and toll-like receptor 4-mediated signaling through different mechanisms. J. Biol. Chem. 280, 25233–25241.

Rahman, A.H., Eisenberg, R.A., 2006. The role of toll-like receptors in systemic lupus erythematosus. Springer Semin. Immunopathol. 28, 131–143.

Takeda, K., Akira, S., 2004. TLR signaling pathways. Semin. Immunol. 16, 3–9.

Tao, X., Xu, Y., Zheng, Y., Beg, A.A., Tong, L., 2002. An extensively associated dimer in the structure of the C713S mutant of the TIR domain of human TLR2. Biochem. Biophys. Res. Commun. 299, 216–221.

Thomassen, E., Renshaw, B.R., Sims, J.E., 1999. Identification and characterization of SIGIRR, a molecule representing a novel subtype of the IL-1R superfamily. Cytokine 11, 389–399.

Tovchigrechko, A., Vakser, I.A., 2006. GRAMM-X public web server for protein-protein docking. Nucl. Acids Res. 34, W310–314.

Wald, D., Qin, J., Zhao, Z., Qian, Y., Naramura, M., Tian, L., Towne, J., Sims, J.E., Stark, G.R., Li, X., 2003. SIGIRR, a negative regulator of Toll-like receptor-interleukin 1 receptor signaling. Nat. Immunol. 4, 920–927.

Wallner, B., Elofsson, A., 2003. Can correct protein models be identified? Protein Sci. 12, 1073–8106.

Wei, T., Gong, J., Jamitzky, F., Heckl, W.M., Stark, R.W., Rossle, S.C., 2009. Homology modeling of human Toll-like receptors TLR7, 8, and 9 ligand-binding domains. Protein Sci. 18, 1684–1691.

Wheeler, D.L., Barrett, T., Benson, D.A., Bryant, S.H., Canese, K., Chetvernin, V., Church, D.M., Dicuccio, M., Edgar, R., Federhen, S., Feolo, M., Geer, L.Y., Helmberg, W., Kapustin, Y., Khovayko, O., Landsman, D., Lipman, D.J., Madden, T.L., Maglott, D.R., Miller, V., Ostell, J., Pruitt, K.D., Schuler, G.D., Shumway, M., Sequeira, E., Sherry, S.T., Sirotkin, K., Souvorov, A., Starchenko, G., Tatusov, R.L., Tatusova, T.A., Wagner, L., Yaschenko, E., 2008. Database resources of the National Center for Biotechnology Information. Nucl. Acids Res. 36, D13–21.

Xu, Y., Tao, X., Shen, B., Horng, T., Medzhitov, R., Manley, J.L., Tong, L., 2000. Structural basis for signal transduction by the Toll/interleukin-1 receptor domains. Nature 408, 111–115.

Paper 6

Lack of SIGIRR/TIR8 aggravates hydrocarbon oil-induced systemic lupus

Maciej Lech, Veronika Skuginna, Onkar P. Kulkarni, Jing Gong, Tiandi Wei, Robert W. Stark, Cecilia Garlanda, Alberto Mantovani and Hans-Joachim Anders

Original Paper

Lack of SIGIRR/TIR8 aggravates hydrocarbon oil-induced lupus nephritis

Maciej Lech,[1] Veronika Skuginna,[1] Onkar P. Kulkarni,[1] Jing Gong,[2] Tiandi Wei,[2] Robert W. Stark,[2] Cecilia Garlanda,[3] Alberto Mantovani[3] and Hans-Joachim Anders[1]*

[1] *Medizinische Poliklinik, University of Munich, Germany*
[2] *Centre for NanoScience and Department for Earth and Environmental Sciences, University of Munich, Germany*
[3] *Istituto Clinico Humanitas and Fondazione Humanitas per la Ricerca, Rozzano, Italy*

Correspondence to:
Hans-Joachim Anders,
Medizinische Poliklinik,
Universität München,
Pettenkoferstrasse 8a, 80336
Munich, Germany.
E-mail:
hjanders@med.uni-muenchen.de

No conflicts of interest were
declared.

Abstract

Multiple genetic factors contribute to the clinical variability of spontaneous systemic lupus erythematosus (SLE) but their role in drug-induced SLE remain largely unknown. Hydrocarbon oil-induced SLE depends on mesothelial cell apoptosis and Toll-like receptor (TLR)-7-mediated induction of type I interferons. Hence, we hypothesized that TIR8/SIGIRR, an endogenous TLR inhibitor, prevents oil-induced SLE. *Sigirr*-deficient dendritic cells expressed higher *TLR7* mRNA levels and TLR7 activation resulted in increased IL-12 production *in vitro*. *In vivo*, lack of SIGIRR increased surface CD40 expression on spleen CD11c+ dendritic cells and *MX-1, TNF, IL-12, BAFF* and *BCL-2* mRNA expression 6 months after pristane injection. Spleen cell counts of CD4−/CD8− 'autoreactive' T cells and B220+ B cells were also increased in *Sigirr*−/− mice. Serum autoantibody analysis revealed that *Sigirr* deficiency specifically enhanced the production of rheumatoid factor (from 4 months of age) and anti-snRNP IgG (from 5 months of age), while anti-Smith IgG or anti-dsDNA IgG were independent of the *Sigirr* genotype. This effect was sufficient to significantly aggravate lupus nephritis in *Sigirr*-deficient mice. Structure model prediction identified the BB loop of SIGIRR's intracellular TIR domain to interact with TLR7 and MyD88. BB loop deletion was sufficient to completely abrogate SIGIRR's inhibitory effect on TLR7 signalling. Thus, TIR8/SIGIRR protects from hydrocarbon oil-induced lupus by suppressing the TLR7-mediated activation of dendritic cells, via its intracellular BB loop. Copyright © 2009 Pathological Society of Great Britain and Ireland. Published by John Wiley & Sons, Ltd.

Introduction

Genetic and environmental factors drive both the onset and the progression of autoimmune diseases [1]. As such, a number of variants in immunoregulatory genes increase the risk for systemic lupus erythematosus (SLE) [2–4]. In mice, lack of single genes, such as *TGFβ1, DNAse1, Lyn, Fas* or *C1q*, is sufficient to cause late-onset lupus-like autoimmunity [5–9]. Mutant *Sle1* or *TLR9* can trigger lupus in C57BL/6 mice only in the presence of a second genetic factor, eg the *lpr* mutation [10,11]. Weaker modifier genes, such as IL-10 or IL-27R, enhance lupus only in a genetic context of multiple susceptibility genes, eg being provided by the specific genetic background of MRL mice [12,13].

The *TIR8* gene encodes for single immunoglobulin IL-1-related receptor (SIGIRR), a member of the Toll-like receptor (TLR)/IL-1 receptor family [14,15].

Over-expression of SIGIRR in Jurkat or HepG2 cells suppresses LPS or IL-1-induced activation of NF-κB, hence SIGIRR is an endogenous inhibitor of TLR and IL-1 signalling [14,16,17]. *Sigirr*-deficient mice develop severe immunity-mediated tissue damage upon pathogen challenge or dextran-induced damage of the intestinal epithelium [16,18–21]. Lack of SIGIRR also enhances spontaneous autoimmunity in C57BL/6*lpr/lpr* mice [22]. These mice suffer from defective Fas-induced apoptosis of autoreactive lymphocytes, which massively increases the exposure of nuclear autoantigens to the immune system [23]. Hence, the aggravated phenotype of *Sigirr*-deficient C57BL/6*lpr/lpr* mice could best be explained by a suppressive effect of Sigirr on self-RNA and -DNA-mediated activation of dendritic cells and B cells, a process known to involve TLR7 and TLR9 [10,24–27]. For example, plasmacytoid dendritic cells are the major source of type I interferons upon recognition of RNA via TLR7 [25],

whereas conventional dendritic cells produce interferon mainly upon cytosolic RNA recognition receptors [28].

Whether SIGIRR also suppresses environmentally-induced autoimmunity is unknown. To address this question would require SLE-like disease to be induced in genetically unaltered mice without a predisposing autoimmune genetic background. We therefore used the hydrocarbon oil 2,6,10,14-tetramethyl-pentadecane (pristane) to induce SLE in $Sigirr^{-/-}$ and $Sigirr^{+/+}$ mice of an identical C57BL/6 background. Intraperitoneal injection of pristane induces apoptosis of mesothelial cells, followed by granulomatous peritonitis with the formation of ectopic lymphoid tissue [29]. In this model, the persistent abundance of apoptotic peritoneal cells in the context of chronic inflammation triggers TLR7 signalling, type I interferon expression and the subsequent evolution of antinuclear antibodies, immune complex disease and lupus nephritis [30,31]. We hypothesized a role for Tir8/Sigirr in limiting pristane-induced SLE by suppressing intraperitoneal inflammation and/or autoantibody generation.

Methods

Animal studies

Sigirr-deficient mice on a F6 C57BL/6 genetic background were generated as previously described [19]. The genotype was assured by PCR in each mouse at 5 weeks of age before mice of both genotypes were intraperitoneally injected with 0.5 ml pristane (Sigma-Aldrich, Steinheim, Germany). Blood samples were taken at monthly intervals after pristane injection (at age 6 weeks) until sacrifice at 6 months after pristane injection. In a subgroup of mice, peritoneal lavage fluid was obtained at 2 and 28 days after pristane injection. All experiments were performed in accordance with the German animal care and ethics legislation and had been approved by the local government authorities.

Phenotype analysis

Flow cytometry, real-time quantitative (TaqMan) RT–PCR, and autoantibody analysis were performed as previously described [22,32]. PCR primers are listed in Table 1. Formalin-fixed tissue sections (2 μm) for periodic acid–Schiff (PAS) stains were prepared following routine protocols. The severity of kidney disease was graded by an observer blinded to the genotype of the mice, using a glomerulonephritis activity score (0–24) normally used for the assessment of human lupus nephritis [31]. Immunostaining was performed on either paraffin-embedded or frozen sections as described [26], using the following primary antibodies: anti-mouse C3c (complement, GAM/C3c/FITC, 1 : 200; Nordic Immunological Laboratories, Tilburg, The Netherlands) or

anti-mouse B220 (BD Pharmingen, Heidelberg, Germany). Negative controls included incubation with a respective isotype antibody. Semi-quantitative scoring of glomerular C3c deposits from 0 to 3+ was performed on 15 cortical glomerular sections, as described [33].

Structure and interaction model predictions

Amino acid sequences of human TLR7, MyD88 and SIGIRR (targets) were extracted from the NCBI protein database [34]. TIR domains of TLR7, MyD88 and SIGIRR (TYR165-PRO308, without the C-terminal extension) were modelled by homology modelling. Four template structures were obtained via BLAST search against the Protein Data Bank (PDB) [35]: TLR1 (PDB code 1FYV), TLR2 (1FYW), TLR10 (2J67) and IL-1RAPL (1T3G). Multiple alignments of target-template sequences and structural coordinates of templates were submitted to MODELLER 9v3 [36] to generate the three-dimensional (3D) target structures. Since the C-terminal extension of SIGIRR has no structure-known homologue, we built its structure using protein threading (THREADER 3.5 [37]). The resulting models were then evaluated by ProQ [38] and MetaMQAP [39]. The protein docking programs GRAMM-X [40] and ZDOCK [41] were used to predict the pairwise interactions between these TIR domains. Both programs can return 10 models ranked as the most probable predictions, selected from thousands of candidates, based on geometry, hydrophobicity and electrostatics complementarity of molecule surfaces.

In vitro studies

HEK 293 cells (2×10^5), stably transfected with hTLR7, were cultured overnight in 1 ml DMEM complete medium before being transiently transfected with lipofectamine 2000 (Invitrogen, Carlsbad, CA, USA) and pUNO, full-length hSIGIRR or SIGIRR mutants, all in pUNO expressing vector (Invivogen, San Diego, CA, USA) and the NF-κB luciferase reporter construct (Clontech, Mountain View, CA, USA) with a final amount of 2 μg. After 24 h the cells were stimulated with 1 μg imiquimod (Invitrogen) and luciferase activity was determined after 6 h using Promega's Dual-Glo luciferase kit. The primers were designed to anneal to the template sequences flanking the target sites, which were sequences to be deleted (ΔBB loop-SIGIRR, forward, 5′-GACTGCCCCGACCTCTTGG TGAACCTGAG-3′, reverse, 5′-CAAGAGGTCGGGG CAGTCGCTGTAGGAG-3′; ΔTIR-SIGIRR, forward, 5′-GTGGAGATACGGAAGGTGCAGTACAGGC-3′, reverse, 5′-CACCTTCCGTATCTCCACCTCCCCAT AC-3′). The pUNO-hSIGIRR plasmid was used as the template for mutagenesis. A 25 μl PCR reaction was composed of 1 μl template (200 ng), 1 μl each primer (20 pM each), 2 μl dNTP mixture, 2.5 ml 10× buffer, 0.5 μl Pfu Turbo DNA polymerase (2.5 U)

and dH$_2$O. The reaction was started with 2 min at 95 °C to pre-denature the template. This was followed by 18 cycles of 1 min at 95 °C, 1 min at 58 °C and 1 min/kbp at 68 °C. Following the PCR reaction, 1 μl DpnI (20 U; NEB, Ipswich, MA, USA) was added and the mixture was incubated at 37 °C for 1 h to degrade the original unmodified plasmid templates. After DpnI digestion, 2 μl of the mixture was used to transfect DHα-competent cells by heat shock. After a 1 h recovery in 300 μl LB medium without antibiotics, the transformed *Escherichia coli* was spread on Blas-Agar Blasticidin plates (Invivogen, San Diego, CA, USA) and incubated at 37 °C overnight. Colonies were selected and grown overnight in 3 ml LB with blasticidin.

Statistical analysis

Statistical significance was evaluated by ANOVA or by two-tailed Student's *t*-test (two group comparisons) at $p < 0.05$. Data were expressed as mean ± SEM.

Results

Sigirr modulates peritoneal cytokine production after pristane exposure

Intraperitoneal injection of pristane induces massive apoptosis of mesothelial cells and infiltrating neutrophils [29], lipogranuloma formation and interferon signalling by peritoneal macrophages [30]. Macroscopically we did not detect any difference in the peritoneal cavities of *Sigirr*$^{+/+}$ and *Sigirr*$^{-/-}$ mice 2 and 28 days after pristane injection (Figure 1A, left). Lavage fluids from these time points revealed large numbers of dead mesothelial cells and monocyte/macrophages often ingesting apoptotic neutrophils (Figure 1A, right), but cell counts were identical in *Sigirr*$^{+/+}$ and *Sigirr*$^{-/-}$ mice (not shown). Lavage fluid flow cytometry for propidium iodine and annexin V revealed comparable levels of early apoptotic (annexin V$^+$) cells and late apoptotic (annexin V/propidium iodine$^+$) cells in *Sigirr*$^{+/+}$ and *Sigirr*$^{-/-}$ mice at all time points (not shown). Real-time RT–PCR from peritoneal lavage fluid cell mRNA showed significantly higher levels for *IL-12* and *TNFα* at 2 days and *IFNγ* and the IFNα/β-dependent gene *Mx1* 28 days after pristane injection (Figure 1B). Lavage fluid ELISA revealed significantly higher levels of TNFα but not of IL-12p40 2 days after pristane injection, while IFNα, -β and -γ were not detectable by ELISA (Figure 1C). At 28 days, TNFα and IL-12p40 levels had increased but were genotype-independent (Figure 1C).

Sigirr suppresses the activation of dendritic cells 6 months after pristane exposure

We used flow cytometry to quantify the numbers of splenic CD11c dendritic cells that stain positive for the activation marker CD40 at 6 months of age. Lack of Sigirr significantly increased the numbers of CD40$^+$ dendritic cells (Figure 2A). Lack of Sigirr was also associated with increased mRNA levels of *Mx1*, *TNFα*, *IL-4* and *IL-12* in these cells (Figure 2B). *Sigirr*-deficient spleen dendritic cells also expressed higher levels of Baff and Bcl2 (Figure 2C), which support the survival of B and/or T cells [42]. Consistent with the stronger activation of dendritic cells, *Sigirr*-deficient mice had higher IL-12p40 serum levels as compared to wild-type mice injected with pristane at 6 months of age (5.9 ± 1.6 versus 1.1 ± 0.8 ng/ml, $p < 0.0001$). Thus, Sigirr suppresses dendritic cell activation and serum IL-12p40 levels 6 months after pristane exposure.

Sigirr suppresses pristane-induced lymphoproliferation

Pristane induced mild splenomegaly at 6 months in wild-type mice. Lack of Sigirr caused a trend towards higher spleen weights, but with considerable interindividual variability (Figure 2D), but flow cytometry revealed sigificantly higher numbers of spleen cells in *Sigirr*-deficient mice treated with pristane (Figure 2E). This was due to lymph follicle hyperplasia with massive enlargement of B220$^+$ B cell areas (Figure 2F). We also observed higher numbers of CD4/CD8 double-negative 'autoreactive' T cells and CD4$^+$CD25$^+$ 'regulatory' T cells in *Sigirr*-deficient mice treated with pristane (Figure 3C, D). The latter was consistent with a significant induction of *Foxp3* mRNA levels in CD3$^+$CD4$^+$CD25$^+$ cells of *Sigirr*-deficient mice (Figure 3E). The numbers of CD3$^+$CD4$^+$ and CD3$^+$CD8$^+$ cell were not affected by the *Tir8* genotype (Figure 3A, B). However, in CD4$^+$CD25$^-$T cells, lack of Sigirr was associated with higher mRNA expression levels of the Th1 markers *T-bet* and *IFNγ* (Figure 3F) and the Th2 markers *Gata* and *IL-4* (Figure 3G). The Th17 marker *Ror-γ* was significantly down-regulated, although *IL-17* mRNA levels were markedly induced in pristane-treated *Sigirr*-deficient mice (Figure 3H). Together, Sigirr suppresses the expansion of spleen B cells as well as of autoreactive and regulatory T cells after pristane injection.

Sigirr suppresses pristane-induced autoantibodies to nuclear autoantigens

We obtained serum samples at monthly intervals from pristane-treated mice of both genotypes and antibody levels were determined by ELISA. Total serum IgG levels were comparable at all time points in *Sigirr*-deficient and wild-type mice (Figure 4). Small amounts of antibodies directed against dsDNA IgG of the IgG1 isotype and against nucleosomes were detectable by ELISA but the levels did not differ between *Sigirr*-deficient and wild-type mice (Figure 4). The specificity of dsDNA autoantibodies was confirmed by *Critidiae luciliae* assay (not shown).
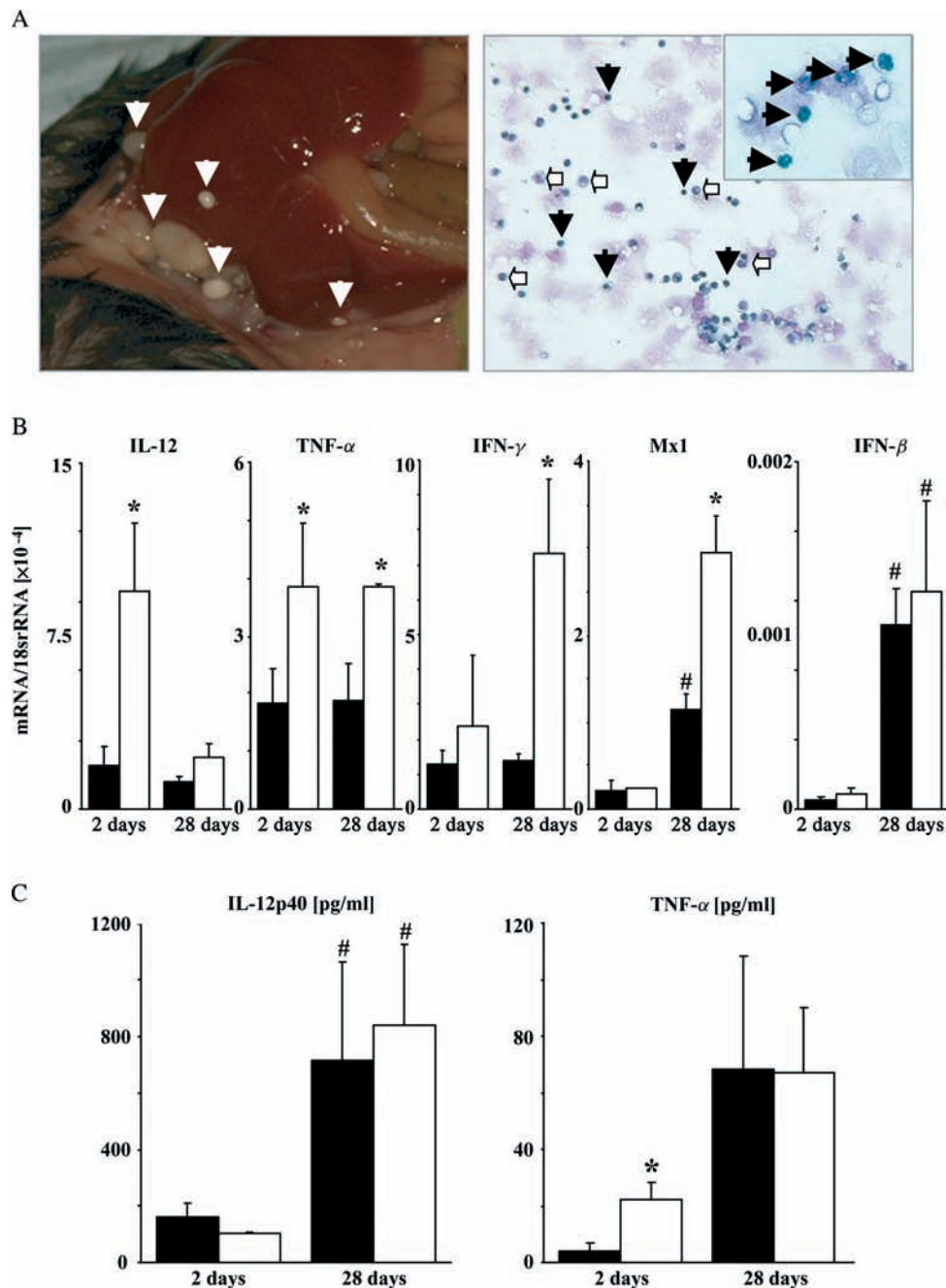
Figure 1. *Tir8/Sigirr* genotype and pristane-induced peritonitis. Pristane injection into *Sigirr*$^{+/+}$ and *Sigirr*$^{-/-}$ mice caused lipogranuloma formation in the peritoneal cavity, as indicated by white arrows in the left image of (A). The right image of (A) shows microscopic analysis of peritoneal fluids, which revealed large amounts of apoptotic cells (black arrows) inside and outside of phagocytes (white arrows and insert), independent of the *Sigirr*$^{-/-}$ genotype. (B) Real-time RT–PCR of peritoneal fluid samples taken 2 and 28 days after pristane injection was used to quantify intraperitoneal mRNA expression. Data are expressed as a ratio to respective *18s* rRNA as a reference gene. (C) Peritoneal fluid levels of TNFα and IL-12p40 were determined by ELISA. Data in (B, C) are expressed as means $\pm$ SEM of 14 mice in each group of *Sigirr*$^{+/+}$ (black bars) and *Sigirr*$^{-/-}$ mice (white bars). *$p < 0.05$ versus wild-type; $^{\#}p < 0.05$ versus 2 days

Anti-dsDNA of the IgG2a/c, IgG2b and IgG3 isotypes remained undetectable at all time points (not shown). By contrast, lack of Sigirr significantly induced the production of rheumatoid factor and anti-SnRNP IgG from 4 and 5 months after pristane exposure, respectively (Figure 4). Antibodies against the Smith antigen were produced from month 4, but the levels did not differ between the two genotypes (Figure 4). Thus, Sigirr specifically suppresses the production of rheumatoid factor and anti-SnRNP IgG but does not affect DNA autoantibody production after pristane exposure in mice.

Sigirr prevents pristane-induced lupus nephritis

Pristane does not cause major autoimmune tissue lesions in C57BL/6 mice, although mild glomerulonephritis may develop [30]. Lack of Sigirr
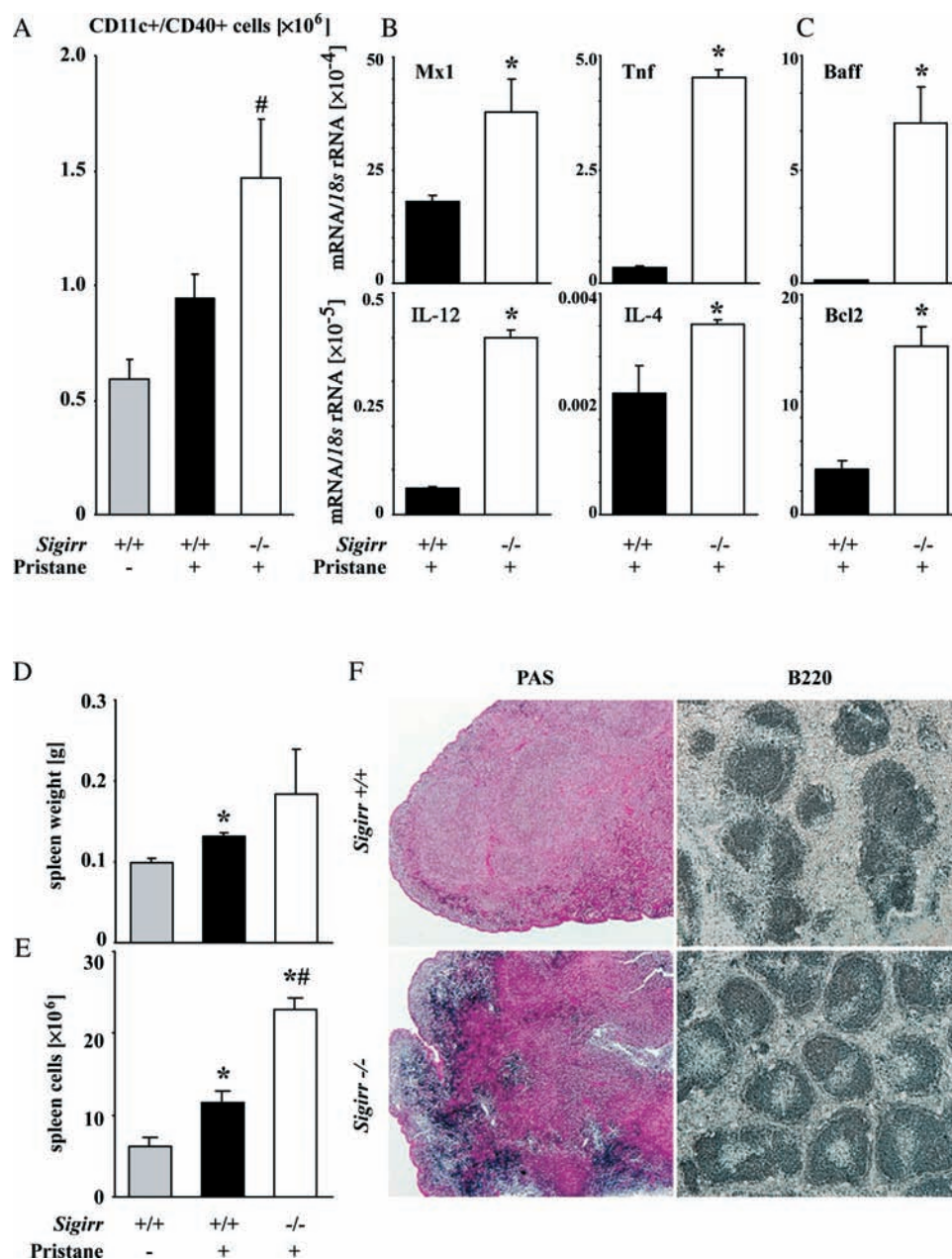
Figure 2. *Sigirr* genotype, dendritic cell activation and spleen morphology. (A) The total number of spleen CD11c^{+} dendritic cells positive for the activation marker CD40 was quantified 6 months after pristane injection by flow cytometry. Data represent means ± SEM from 14 mice in each group. [#]$p < 0.05$ versus pristane-injected wild-type mice. (B, C) RNA was isolated from spleen CD11c^{+} cells from *Sigirr*^{−/−} (white bars) and *Sigirr*^{+/+} mice (black bars) 6 months after pristane injection for real-time RT−PCR analysis. Data are expressed as means of the ratio of the specific mRNA to that of 18S rRNA ± SEM. [*]$p < 0.05$ versus wild-type mice. (D, E) Spleen weight (D) was determined 6 months after pristane injection in untouched wild-type mice (grey bar), pristane-injected wild-type mice (black bar) and *Sigirr*-deficient mice (white bar). Total spleen cell numbers (E) were determined by flow cytometry, as described in Methods. [*]$p < 0.05$ versus untouched wild-type mice; [#]$p < 0.05$ versus pristane-injected wild-type mice. (F) Representative images of spleen PAS stains and B220 immunostaining from mice at 6 months. Original magnification, ×100

was associated with diffuse mesangio-proliferative glomerulonephritis, as indicated by glomerular hypercellularity, PAS-positive matrix expansion and glomerular leukocyte infiltrates (Figure 5A). Glomerular C3c deposits were scored 1.2 ± 0.2 in *Sigirr*^{−/−} mice and 0.3 ± 0.1 in wild-type mice ($p = 0.003$; Figure 5A). The composite activity score for lupus nephritis was 6.8 ± 0.6 in *Sigirr*^{−/−} mice and 3.5 ± 0.3 in wild-type mice ($p = 0.0002$; Figure 5B). Albuminuria constantly increased in *Sigirr*-deficient mice and started to be significantly higher at 5 months as

compared to wild-type mice (Figure 5C). The difference was highest at 6 months. Together, Sigirr protects mice from diffuse proliferative lupus nephritis after pristane exposure.

In silico structure analysis predicts the BB loop of Sigirr's TIR domain as the interaction site with TLR7 and Myd88

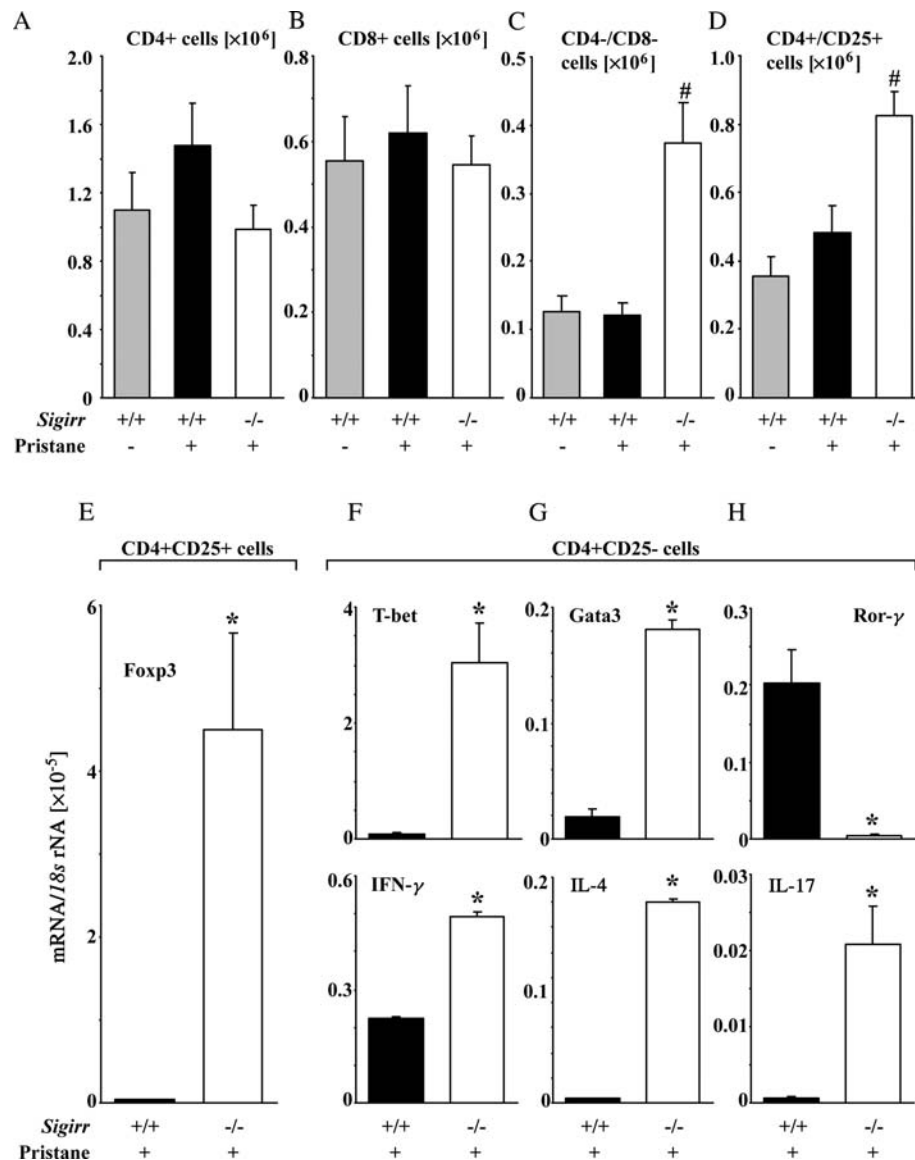Because lupus autoantigens drive SLE by ligating TLR7, we speculated that Sigirr is induced by

Figure 3. *Sigirr* genotype and T cell subsets. Six months after pristane injection, spleen T cell subsets were assessed by flow cytometry (A–D), as described in Methods. The histograms presents mean ± SEM of at least 14 mice in each group. (E–H) Real-time RT–PCR from CD4$^+$CD25$^+$ cells or CD4$^+$CD25$^-$ cells was used to quantify additional T cell markers. Data ratios to respective *18s* rRNA as a reference gene and are expressed as means ± SEM of 10 mice in each group. $^\#p < 0.05$ versus pristane-injected wild-type mice

inflammation and that it suppresses TLR7 signalling, especially in antigen-presenting cells. *Sigirr* mRNA was induced in spleen monocytes by LPS or TNFα/IFNγ, with a maximum expression level at 18 h of stimulation (Figure 6A, B). In addition, the TLR7 agonist imiquimod activated bone marrow dendritic cells to produce IL-12, a response that was five-fold higher in *Sigirr*-deficient dendritic cells (Figure 6C), perhaps also because the basal *TLR7* mRNA expression was significantly higher in *Sigirr*-deficient dendritic cells (Figure 6D). But can Sigirr directly interfere with TLR7 signalling at the structural level?

Because crystallographic structures of human TLR7, MyD88 and SIGIRR TIR domains are not available, we developed 3D structural models based on homology modelling and protein threading. The predicted structures of TLR7, MyD88 and SIGIRR TIR

domains were evaluated as *extremely good* or *ideal* by several model quality assessment programs (data not shown). The BB loop (face) and the α-helix E region (neck) appeared to be conserved among all the different TIR domains (Figure 7A) and are localized on opposite regions of the SIGIRR TIR domain (Figure 7B). Then, the protein-docking softwares GRAMM-X and ZDOCK were used to predict pairwise molecular interaction sites of complexes formed by TLR7–TLR7, MyD88–MyD88, TLR7–SIGIRR and MyD88–SIGIRR. The top-ranked dimer model was selected for each complex (Figure 7C). According to these predictions, receptor activation would trigger the formation of TLR7 TIR dimers in a face-to-neck orientation, recruiting MyD88 TIR face-to-face dimers and forming a T-shaped signalling tetramer (complex B in Figure 7C). The
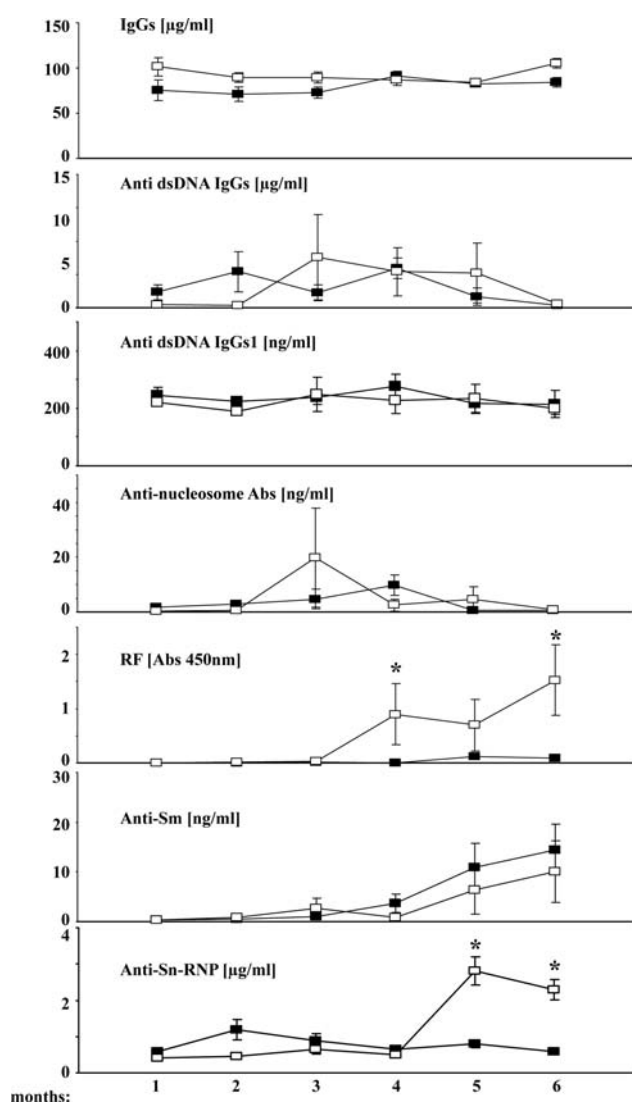
Figure 4. *Sigirr* genotype and serum immunoglobulin and lupus autoantibody levels. Wild-type mice (open squares) and *Sigirr*-deficient mice (black squares) were bled at monthly intervals after pristane injection to determine serum levels of IgG and a number of different autoantibodies, as indicated by ELISA. Data represent means ± SEM from at least 14 mice in each group. $^*p < 0.05$ versus wild-type mice at the same time point

Table 1. Primers used for RT–PCR

Gene name		Primer sequence
Baff	Forward	5′-CCTCCAAGGCATTTCCTCTT-3′
	Reverse	5′-GACTGTCTGCAGCTGATTGC-3′
Bcl2	Forward	5′-GATCCAGGATAACGGAGGCT-3′
	Reverse	5′-GGTCTTCAGAGACAGCCAGG-3′
FoxP3	Forward	5′-TTCATGCATCAGCTCTCCAC-3′
	Reverse	5′-CTGGACACCCATTCCAGACT-3′
Gata3	Forward	5′-GCCTGCGGACTCTACCATAA-3′
	Reverse	5′-AGGATGTCCCTGCTCTCCTT-3′
Ifn-γ	Forward	5′-ACAGCAAGGCGAAAAAGGAT-3′
	Reverse	5′-TGAGCTCATTGAATGCTTGG-3′
Il-4	Forward	5′-TGAACGAGGTCACAGGAGAA-3′
	Reverse	5′-CGAGCTCACTCTCTGTGGTG-3′
Il-12	Forward	5′-CTAGACAAGGGCATGCTGGT-3′
	Reverse	5′-GCTTCTCCCACAGGAGGTTT-3′
Il-17	Forward	5′-TCCAGAAGGCCCTCAGACTA-3′
	Reverse	5′-TGAGCTTCCCAGATCACAGA-3′
Mx1	Forward	5′-TCTGAGGAGAGCCAGACGAT-3′
	Reverse	5′-CTCAGGGTGTCGATGAGGTC-3′
Ror-γ	Forward	5′-ACAGAGACACCACCGGACAT-3′
	Reverse	5′-GGTGATAACCCCGTAGTGGA-3′
Tbet	Forward	5′-TCAACCAGCACCAGACAGAG-3′
	Reverse	5′-ATCCTGTAATGGCTTGTGGG-3′
Tnf-α	Forward	5′-CCACCACGCTCTTCTGTCTAC-3′
	Reverse	5′-AGGGTCTGGGCCATAGAACT-3′
18s RNA	Forward	5′-GCAATTATTCCCCATGAACG-3′
	Reverse	5′-AGGGCCTCACTAAACCATCC-3′

A Sigirr TIR mutant lacking the BB loop can no longer block TLR7 signalling

To verify the functional role of the BB loop for TLR7 signalling, we over-expressed full-length TLR7 in HEK293 cells, together with full-length Sigirr or various Sigirr mutants. Full-length Sigirr potently suppressed NF-κB reporter gene expression 6 h after stimulation with the TLR7 agonist imiquimod (Figure 7D). By contrast, lack of the TIR domain or the BB loop only completely abrogated this inhibitory effect on TLR7 signalling. Together, Sigirr TIR's BB loop mediates the inhibitory effect of Sigirr on TLR7 signalling.

Discussion

Lack of Sigirr clearly aggravated pristane-induced autoimmune tissue injury. In the kidney, *Sigirr*-deficiency was associated with diffuse proliferative lupus nephritis and significant albuminuria as compared to wild-type C57BL/6 mice, which revealed only minor glomerular abnormalities. The role of Sigirr in inhibiting pristane-induced autoimmunity was clearly documented by increased dendritic cell activation, increased numbers of CD4/CD8 double-negative T cells and B cells in spleen as well as increased serum

stimulus-induced dimerization of TIR domains creates a molecular pocket for the binding of α-helix E of the MyD88 adaptor. Model predictions, including SIGIRR's TIR, revealed that SIGIRR interacts with TLR7 by occupying TLR7 TIR's α-helix E region with its BB loop, which should interrupt TLR7 homodimer formation (complex A in Figure 7C). In addition, SIGIRR's BB loop was predicted to interact with the BB loop of MyD88, which should interrupt MyD88 homodimer formation (complex C in Figure 7C). According to our model, SIGIRR TIR's unique C-terminal extension (ca. 100 amino acids; Figure 7B) is located distant from the BB loop, consistent with the observation that this extension is not required for SIGIRR's inhibitory effect on TLR signalling (16).
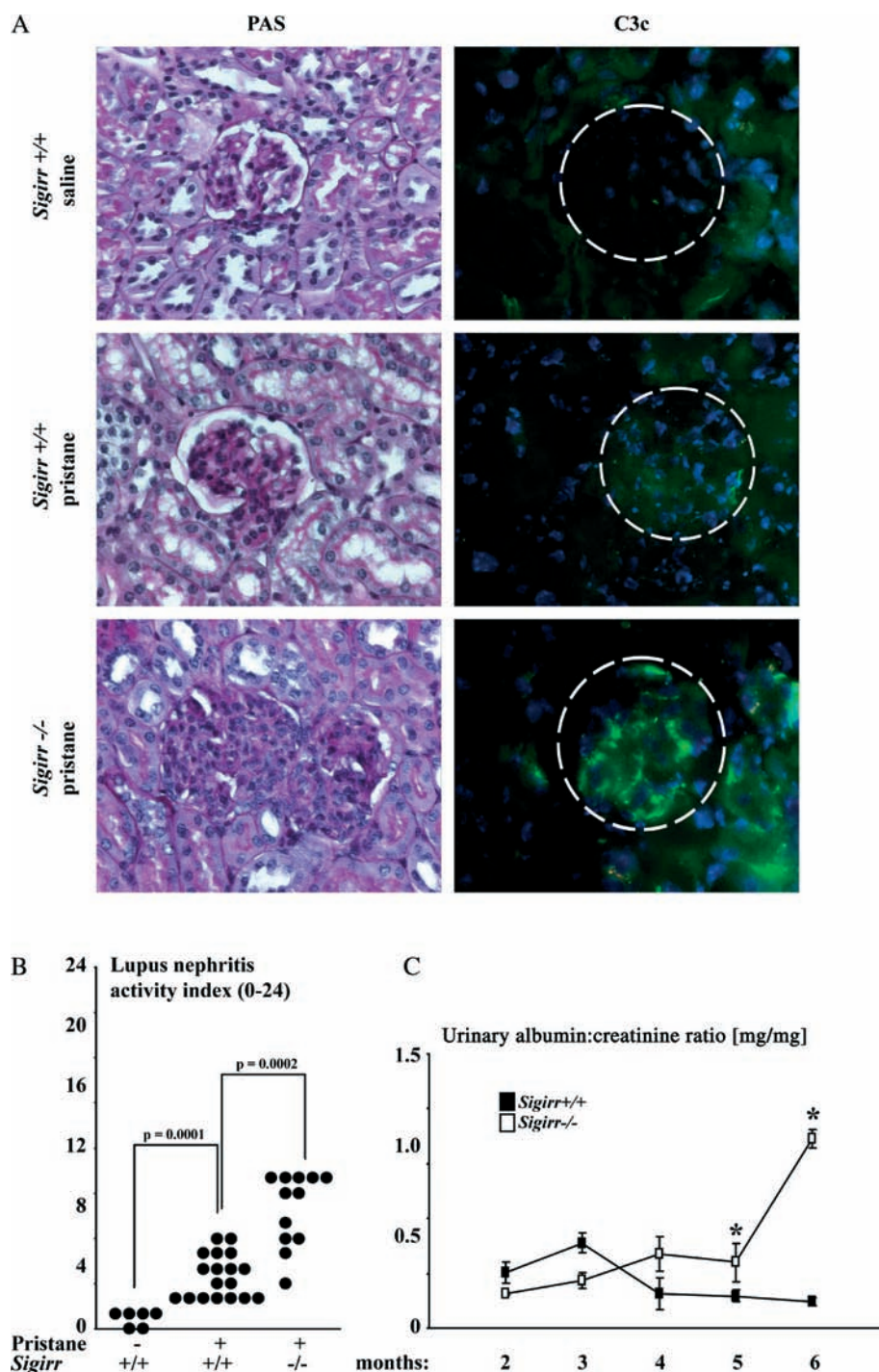
Figure 5. *Sigirr* genotype and lupus nephritis 6 months after pristane injection. (A) Renal sections were stained with PAS and immunostaining was performed for complement factor C3c (DAPI stains cell nuclei blue), as indicated. Original magnification, ×200. Images are representative for 10 mice in each group. (B) The lupus nephritis activity index (range 0–24) was assessed on renal PAS-stained sections at 6 months after pristane injection, as described in Methods. (C) Urinary albumin : creatinine ratio was determined from urine samples taken from at least 14 wild-type mice (open squares) and *Sigirr*-deficient mice (black squares) at monthly intervals after pristane injection. #$p < 0.05$ versus pristane-injected wild-type mice

levels of IL-12 and selected autoantibodies in *Sigirr*-deficient mice. In this regard, the data from pristane-induced lupus matches our previous data obtained from *Sigirr*-deficient C57BL/6[lpr/lpr] mice with spontaneous autoimmunity [22]. However, in C57BL/6[lpr/lpr] mice Sigirr had a global suppressive effect on the evolution of hypergammaglobulinaemia and autoantibodies of multiple specificities as early as at 2 months of age [22]. By contrast, in pristane-induced lupus, lack of Sigirr massively increased the production of rheumatic factor and RNA autoantibodies, but not before 4–5 months after pristane exposure. This was most obvious for anti-Sm IgG and anti-U1snRNP, because the Sm (Smith) antigen is the protein component and U1snRNP the RNA component of the U1snRNP ribonucleoprotein complex [43,44].
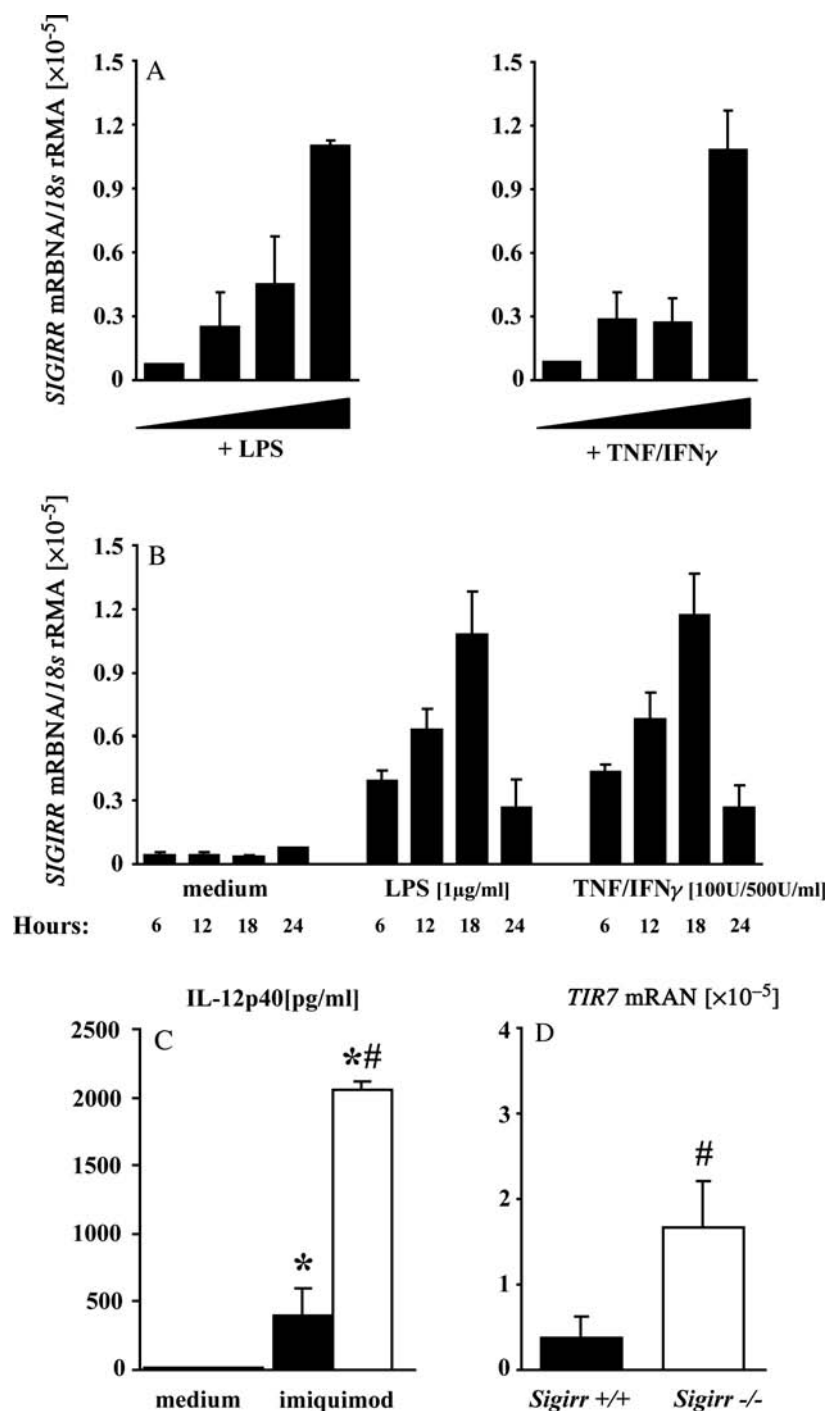
Figure 6. Sigirr suppresses TLR7 signalling in dendritic cells. (A) *Sigirr* mRNA expression was determined by real-time RT–PCR on RNA samples from spleen monocytes 12 h after stimulation with various doses of LPS or TNFα/IFNγ. (B) Sigirr induction was quantified in spleen monocytes at various time intervals after stimulation with a given dose of LPS or TNFα/IFNγ. Data represent mean ratios of Sigirr/*18s* rRNA ± SEM from three independent experiments. (C) Bone marrow dendritic cells from wild-type mice (black bars) and *Sigirr*-deficient mice (white bars) were stimulated with imiquimod, as described in Methods. IL-12p40 was determined after 24 h in cell culture supernatants. (D) Basal *TLR7* mRNA expression was determined in the same cells by real-time RT–PCR and is illustrated as a ratio to the respective *18s* rRNA expression. Data represent means ± SEM from three independent experiments. $^*p < 0.05$ versus medium; $^\#p < 0.05$ versus wild-type mice

Because *Sigirr*-deficient mice did not display a broader spectrum of autoantibodies than wild-type mice, Sigirr does not seem to directly promote loss-of-tolerance or epitope spreading. Obviously, Sigirr rather specifically fosters the expansion of IgG and RNA autoreactive lymphocyte clones that produce the necessary components for pathogenic RNA immune complexes. In turn, such RNA immune complexes are known trigger TLR7 activation and type I interferon signalling, a positive amplification loop [24,45–46]. In fact, pristane-induced lupus is driven by TLR7 signalling [30,31] and, most interestingly, lack of *TLR7* selectively impaired the production of pristane-induced snRNP antibodies [30,31]. We therefore
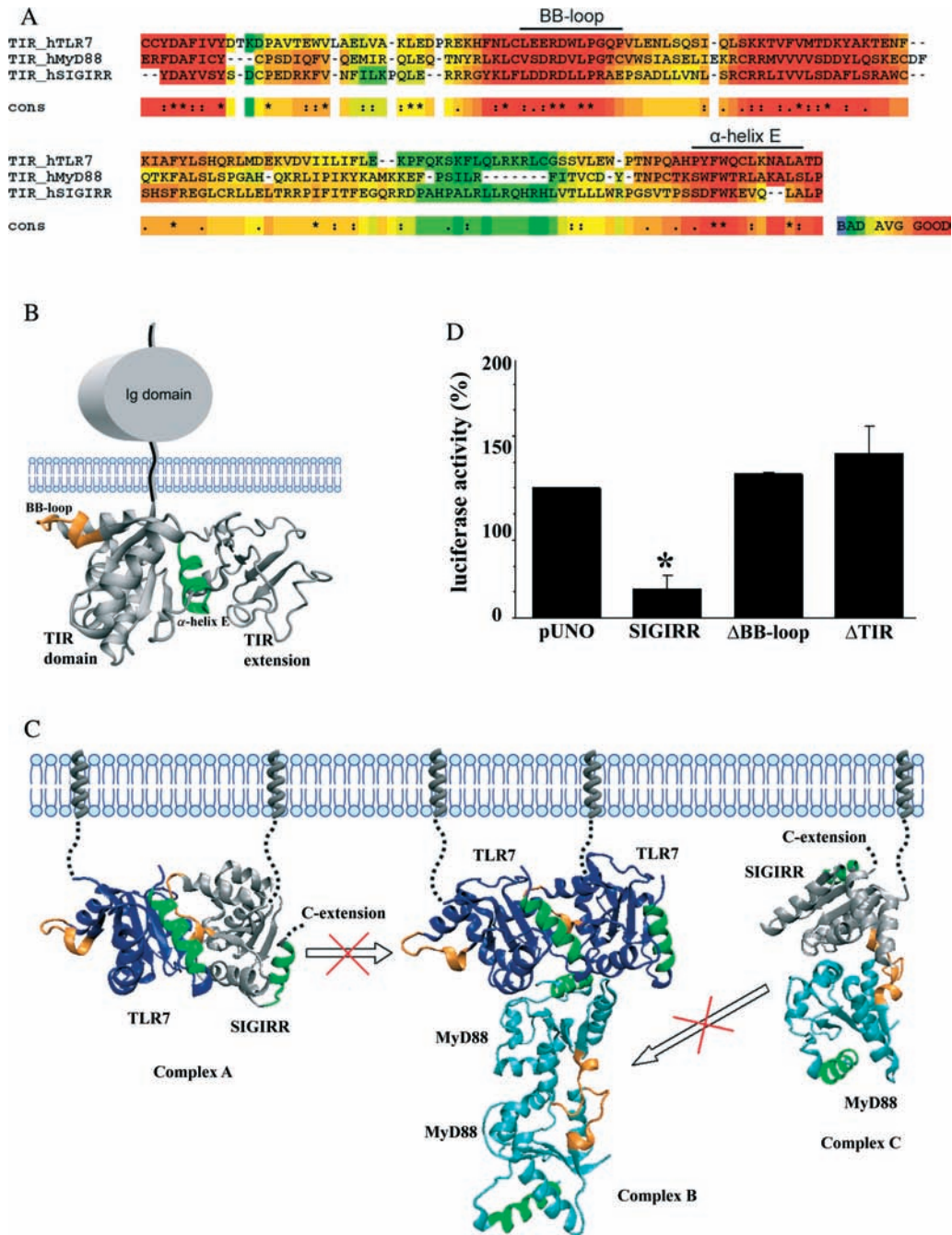
Figure 7. Models of SIGIRR inhibiting the TLR7 signalling pathway. (A) Amino acid sequence homologies of the intracellular TIR domains of human TLR7, MyD88 and SIGIRR. (B) The 3D structural model of SIGIRR's intracellular TIR domain was predicted as described in Methods. The BB loop is indicated in orange; the α-helix E region is indicated in green. Note that the SIGIRR-specific C-terminal extension links at the α-helix E. (C) Complex B, TLR7 homodimers (dark blue), linked by BB loop (orange)−α-helix E (green) interaction, bind MyD88 homodimers (light blue), forming a T-shaped conformation. MyD88 homodimers are formed by BB loop interactions (orange). The TLR7−MyD88 complex may not form when SIGIRR recruits to this complex as follows: the predicted TLR7−SIGIRR interaction (complex A) should affect TLR7 homodimer formation, and SIGIRR−MyD88 interaction (complex C) may affect MyD88 homodimer formation (SIGIRR interfering sites indicated by open arrows). (D) HEK293 cells, constitutively expressing TLR7, were seeded at a concentration of 2×10^5 cells/well in a 12-well plate, and cultured overnight in 1 ml DMEM complete medium. The next day the cells were transfected with *TIR8* or *TIR8* mutants or pUNO control vector and the NF-κB luciferase reporter construct, as described in Methods. Cells were stimulated with 1 μg imiquimod and luciferase activity was determined after 6 h. The values are percentages of the imiquimod-stimulated cells expressing empty pUNO vector. Data represent means ± SEM of at least two independent experiments. *$p < 0.05$ versus pUNO control

hypothesized that Sigirr may directly inhibit TLR7 signalling.

Previous studies suggested that Sigirr can inhibit TLR4 (but not TLR3 or TLR5) signalling via interaction at the level of their respective intracellular TIR domains, which inhibits the necessary recruitment of its adaptor Myd88 [17]. Our structure-based prediction model of putative TIR−TIR interaction sites identified the BB loop of SIGIRR's intracellular TIR domain as the most likely interaction site with TLR7, as well

as with MyD88. Deletion of the BB loop completely abrogated SIGIRR's inhibitory effect on TLR7 signalling, as did the deletion of the entire TIR domain. These data are in line with the report of Qin *et al* [17] and further prove that SIGIRR also inhibits TLR7 via this mechanism. In addition, Sigirr suppresses *TLR7* mRNA expression, which adds to its suppressive effect on TLR7 signalling.

In pristane-induced lupus, the immunoregulatory function of Sigirr clearly localizes to the central lymphoid organs, as indicated by the impact of *Sigirr* deficiency on lymphocyte numbers and activation states and autoantibody production.

We conclude that genes that regulate autoantigen-driven dendritic cell activation determine environmentally triggered autoimmunity, and that *Tir8/Sigirr* loss-of-function mutations represent a novel genetic risk factor for hydrocarbon oil-induced autoimmunity in mice.

Acknowledgements

References

1. Goodnow CC. Multistep pathogenesis of autoimmune disease. *Cell* 2007;**130**:25–35.
2. Rahman A, Isenberg DA. Systemic lupus erythematosus. *N Engl J Med* 2008;**358**:929–939.
3. Harley JB, Alarcon-Riquelme ME, Criswell LA, Jacob CO, Kimberly RP, Moser KL, *et al*. Genome-wide association scan in women with systemic lupus erythematosus identifies susceptibility variants in ITGAM, PXK, KIAA1542 and other loci. *Nat Genet* 2008;**40**:204–210.
4. Tsokos GC, Nambiar MP, Tenbrock K, Juang YT. Rewiring the T-cell: signaling defects and novel prospects for the treatment of SLE. *Trends Immunol* 2003;**24**:259–263.
5. Cohen PL, Eisenberg RA. Lpr and gld: single gene models of systemic autoimmunity and lymphoproliferative disease. *Annu Rev Immunol* 1991;**9**:243–269.
6. Botto M, Dell'Agnola C, Bygrave AE, Thompson EM, Cook HT, Petry F, *et al*. Homozygous C1q deficiency causes glomerulonephritis associated with multiple apoptotic bodies. *Nat Genet* 1998;**19**:56–59.
7. Hibbs ML, Tarlinton DM, Armes J, Grail D, Hodgson G, Maglitto R, *et al*. Multiple defects in the immune system of Lyn-deficient mice, culminating in autoimmune disease. *Cell* 1995;**83**:301–311.
8. Napirei M, Karsunky H, Zevnik B, Stephan H, Mannherz HGMoroy T. Features of systemic lupus erythematosus in Dnase1-deficient mice. *Nat Genet* 2000;**25**:177–181.
9. Shull MM, Ormsby I, Kier AB, Pawlowski S, Diebold RJ, Yin M, *et al*. Targeted disruption of the mouse transforming growth factor-β1 gene results in multifocal inflammatory disease. *Nature* 1992;**359**:693–699.
10. Lartigue A, Courville P, Auquit I, Francois A, Arnoult C, Tron F, *et al*. Role of TLR9 in anti-nucleosome and anti-DNA antibody production in lpr mutation-induced murine lupus. *J Immunol* 2006;**177**:1349–1354.
11. Mohan C, Alas E, Morel L, Yang P, Wakeland EK. Genetic dissection of SLE pathogenesis. Sle1 on murine chromosome 1 leads to a selective loss of tolerance to H2A/H2B/DNA subnucleosomes. *J Clin Invest* 1998;**101**:1362–1372.
12. Shimizu S, Sugiyama N, Masutani K, Sadanaga A, Miyazaki Y, Inoue Y, *et al*. Membranous glomerulonephritis development with Th2-type immune deviations in MRL/lpr mice deficient for IL-27 receptor (WSX-1). *J Immunol* 2005;**175**:7185–7192.
13. Yin Z, Bahtiyar G, Zhang N, Liu L, Zhu P, Robert ME, *et al*. IL-10 regulates murine lupus. *J Immunol* 2002;**169**:2148–2155.
14. Polentarutti N, Rol GP, Muzio M, Bosisio D, Camnasio M, Riva F, *et al*. Unique pattern of expression and inhibition of IL-1 signalling by the IL-1 receptor family member TIR8/SIGIRR. *Eur Cytokine Netw* 2003;**14**:211–218.
15. Thomassen E, Renshaw BR, Sims JE. Identification and characterization of SIGIRR, a molecule representing a novel subtype of the IL-1R superfamily. *Cytokine* 1999;**11**:389–399.
16. Wald D, Qin J, Zhao Z, Qian Y, Naramura M, Tian L, *et al*. SIGIRR, a negative regulator of Toll-like receptor-interleukin 1 receptor signaling. *Nat Immunol* 2003;**4**:920–927.
17. Qin J, Qian Y, Yao J, Grace C, Li X. SIGIRR inhibits interleukin-1 receptor- and toll-like receptor 4-mediated signaling through different mechanisms. *J Biol Chem* 2005;**280**:25233–25241.
18. Garlanda C, Di Liberto D, Vecchi A, La Manna MP, Buracchi C, Caccamo N, *et al*. Damping excessive inflammation and tissue damage in *Mycobacterium tuberculosis* infection by Toll IL-1 receptor 8/single Ig IL-1-related receptor, a negative regulator of IL-1/TLR signaling. *J Immunol* 2007;**179**:3119–3125.
19. Garlanda C, Riva F, Polentarutti N, Buracchi C, Sironi M, De Bortoli M, *et al*. Intestinal inflammation in mice deficient in Tir8, an inhibitory member of the IL-1 receptor family. *Proc Natl Acad Sci USA* 2004;**101**:3522–3526.
20. Huang X, Hazlett LD, Du W, Barrett RP. SIGIRR promotes resistance against *Pseudomonas aeruginosa* keratitis by down-regulating type-1 immunity and IL-1R1 and TLR4 signaling. *J Immunol* 2006;**177**:548–556.
21. Xiao H, Gulen MF, Qin J, Yao J, Bulek K, Kish D, *et al*. The Toll-interleukin-1 receptor member SIGIRR regulates colonic epithelial homeostasis, inflammation, and tumorigenesis. *Immunity* 2007;**26**:461–475.
22. Lech M, Kulkarni OP, Pfeiffer S, Savarese E, Krug A, Garlanda C, *et al*. Tir8/Sigirr prevents murine lupus by suppressing the immunostimulatory effects of lupus autoantigens. *J Exp Med* 2008;**205**:1879–1888.
23. Reap EA, Leslie D, Abrahams M, Eisenberg RA, Cohen PL. Apoptosis abnormalities of splenic lymphocytes in autoimmune lpr and gld mice. *J Immunol* 1995;**154**:936–943.
24. Lau CM, Broughton C, Tabor AS, Akira S, Flavell RA, Mamula MJ, *et al*. RNA-associated autoantigens activate B cells by combined B cell antigen receptor/Toll-like receptor 7 engagement. *J Exp Med* 2005;**202**:1171–1177.
25. Savarese E, Chae OW, Trowitzsch S, Weber G, Kastner B, Akira S, *et al*. U1 small nuclear ribonucleoprotein immune complexes induce type I interferon in plasmacytoid dendritic cells through TLR7. *Blood* 2006;**107**:3229–3234.
26. Pawar RD, Ramanjaneyulu A, Kulkarni OP, Lech M, Segerer S, Anders HJ. Inhibition of Toll-like receptor-7 (TLR-7) or TLR-7 plus TLR-9 attenuates glomerulonephritis and lung injury in experimental lupus. *J Am Soc Nephrol* 2007;**18**:1721–1731.
27. Christensen SR, Shupe J, Nickerson K, Kashgarian M, Flavell RA, Shlomchik MJ. Toll-like receptor 7 and TLR9 dictate autoantibody specificity and have opposing inflammatory and regulatory roles in a murine model of lupus. *Immunity* 2006;**25**:417–428.
28. Kumagai Y, Kumar H, Koyama S, Kawai T, Takeuchi O, Akira S. Cutting edge: TLR-dependent viral recognition along with type I IFN positive feedback signaling masks the requirement of viral replication for IFN-α production in plasmacytoid dendritic cells. *J Immunol* 2009;**182**:3960–3964.
29. Calvani N, Caricchio R, Tucci M, Sobel ES, Silvestris F, Tartaglia P, *et al*. Induction of apoptosis by the hydrocarbon

oil pristane: implications for pristane-induced lupus. *J Immunol* 2005;**175:**4777–4782.

30. Lee PY, Kumagai Y, Li Y, Takeuchi O, Yoshida H, Weinstein J, *et al*. TLR7-dependent and Fcγ R-independent production of type I interferon in experimental mouse lupus. *J Exp Med* 2008;**205:**2995–3006.

31. Savarese E, Steinberg C, Pawar RD, Reindl W, Akira S, Anders HJ, *et al*. Requirement of Toll-like receptor 7 for pristane-induced production of autoantibodies and development of murine lupus nephritis. *Arthritis Rheum* 2008;**58:**1107–1115.

32. Patole PS, Schubert S, Hildinger K, Khandoga S, Khandoga A, Segerer S, *et al*. Toll-like receptor-4: renal cells and bone marrow cells signal for neutrophil recruitment during pyelonephritis. *Kidney Int* 2005;**68:**2582–2587.

33. Allam R, Pawar RD, Kulkarni OP, Hornung V, Hartmann G, Segerer S, *et al*. Viral 5′-triphosphate RNA and non-CpG DNA aggravate autoimmunity and lupus nephritis via distinct TLR-independent immune responses. *Eur J Immunol* 2008;**38:**3487–3498.

34. Wheeler DL, Barrett T, Benson DA, Bryant SH, Canese K, Chetvernin V, *et al*. Database resources of the National Center for Biotechnology Information. *Nucleic Acids Res* 2008;**36:**D13–21.

35. Berman HM, Bhat TN, Bourne PE, Feng Z, Gilliland G, Weissig H, *et al*. The Protein Data Bank and the challenge of structural genomics. *Nat Struct Biol* 2000;**7:**(suppl): 957–959.

36. Fiser A, Do RK, Sali A. Modeling of loops in protein structures. *Protein Sci* 2000;**9:**1753–1773.

37. Jones DT, Taylor WR, Thornton JM. A new approach to protein fold recognition. *Nature* 1992;**358:**86–89.

38. Wallner B, Elofsson A. Identification of correct regions in protein models using structural, alignment, and consensus information. *Protein Sci* 2006;**15:**900–913.

39. Pawlowski M, Gajda MJ, Matlak R, Bujnicki JM. MetaMQAP: a meta-server for the quality assessment of protein models. *BMC Bioinformat* 2008;**9:**403.

40. Tovchigrechko A, Vakser IA. GRAMM-X public web server for protein–protein docking. *Nucleic Acids Res* 2006;**34:**W310–314.

41. Chen R, Li L, Weng Z. ZDOCK: an initial-stage protein-docking algorithm. *Proteins* 2003;**52:**80–87.

42. Mackay F, Silveira PA, Brink R. B cells and the BAFF/APRIL axis: fast-forward on autoimmunity and signaling. *Curr Opin Immunol* 2007;**19:**327–336.

43. Marshak-Rothstein A, Rifkin IR. Immunologically active autoantigens: the role of toll-like receptors in the development of chronic inflammatory disease. *Annu Rev Immunol* 2007;**25:**419–441.

44. Pomeranz Krummel DA, Oubridge C, Leung AK, Li J, Nagai K. Crystal structure of human spliceosomal U1 snRNP at 5.5 Å resolution. *Nature* 2009;**458:**475–480.

45. Barrat FJ, Meeker T, Gregorio J, Chan JH, Uematsu S, Akira S, *et al*. Nucleic acids of mammalian origin can act as endogenous ligands for Toll-like receptors and may promote systemic lupus erythematosus. *J Exp Med* 2005;**202:**1131–1139.

46. Lech M, Garlanda C, Mantovani A, Kirschning CJ, Schlondorff D, Anders HJ. Different roles of TiR8/Sigirr on toll-like receptor signaling in intrarenal antigen-presenting cells and tubular epithelial cells. *Kidney Int* 2007;**72:**182–192.

CV

Personal

Name: Tiandi Wei
Sex: Male
Born: 1978 in Shandong, China
Nationality: Chinese

Education

since 02/2007	PhD candidate Ludwig-Maximilians-Universität München Dissertation: Homology modeling of Toll-like receptor ligand-binding domains: a leucine-rich repeat assembly approach
10/2002-01/2007	Diplom (BS+MS), Bioinformatics Munich Technical University & Ludwig-Maximilians-Universität München Thesis: Analysis of correlation between the subcellular localization and structure of proteins
11/2001-08/2002	DSH German Certificate Ludwig-Maximilians-Universität München
09/1997-07/2001	BS, Biological Technology Ocean University of China Research project: Effect of N/P ratio on the growth of a red tide diatom *Skeletonema costatum*
09/1985-07/1997	Primary, middle and high schools Final grade: A

Journal Publications

1. **Tiandi Wei**, Jing Gong, Ferdinand Jamitzky, Wolfgang M. Heckl, Shaila C. Rössle, Robert W. Stark: A leucine-rich repeat assembly approach for homology modeling of human TLR5-10 and mouse TLR11-13 ectodomains. J. Mol. Model., in press.

2. Johannes Aßfalg, Jing Gong, Hans-Peter Kriegel, Alexey Pryakhin, **Tiandi Wei**, Arthur Zimek: Investigating a correlation between subcellular localization and fold of proteins. J. Univ. Comput. Sci., 2010, 16(5):604-621.

3. Jing Gong, **Tiandi Wei**, Ferdinand Jamitzky, Wolfgang M. Heckl, Shaila C. Rössle, Robert W. Stark: TollML: a Database of Toll-like Receptor Structural Motifs. J. Mol. Model., 2010, 16(7):1283-1289.

4. Maciej Lech, Veronika Skuginna, Onkar P. Kulkarni, Jing Gong, **Tiandi Wei**, Robert W. Stark, Cecilia Garlanda, Alberto Mantovani, Hans-Joachim Anders: Lack of SIGIRR/TIR8 aggravates hydrocarbon oil-induced systemic lupus. J. Pathol., 2010, 220(5):596-607.

5. Jing Gong, **Tiandi Wei**, Robert W. Stark, Ferdinand Jamitzky, Wolfgang M. Heckl, Hans J. Anders, Maciej Lech, Shaila C. Rössle: Inhibition of the Toll-like receptors TLR4 and 7 signaling pathways by SIGIRR: a computational approach. J. Struct. Biol., 2010, 169(3):323-330.

6. **Tiandi Wei**, Jing Gong, Ferdinand Jamitzky, Wolfgang M. Heckl, Robert W. Stark, Shaila C. Rössle: Homology modeling of human Toll-like receptors TLR7, 8 and 9 ligand-binding domains. Protein Sci., 2009, 18(8):1684-1691.

7. Johannes Aßfalg, Jing Gong, Hans-Peter Kriegel, Alexey Pryakhin, **Tiandi Wei**, Arthur Zimek: Supervised ensembles of prediction methods for subcellular localization. J. Bioinform. Comput. Biol., 2009, 7(2):269-85.

8. **Tiandi Wei**, Jing Gong, Ferdinand Jamitzky, Wolfgang M. Heckl, Robert W. Stark, Shaila C. Rössle: LRRML: a conformational database and an XML description of leucine-rich repeats (LRRs). BMC Struct. Biol., 2008, 8:47.

9. Dongyan Liu, Jun Sun, Zongtao Chen, **Tiandi Wei**: Growth of Platymonas helgolandica var. tsingtaoensis, Cylindrotheca closterium and Karenia mikimotoi and their survival strategies under different N/P ratios. Chin. J. Appl. Ecol., 2004, 15(11):2122-2126.

10. Dongyan Liu, Jun Sun, Zongtao Chen, **Tiandi Wei**: Effect of N/P ratio on the growth of a red tide diatom Skeletonema costatum. Trans. Oceanol. Limnol., 2002, 2:39-43.

Conference Proceedings

1. Jing Gong, **Tiandi Wei**, Ferdinand Jamitzky, Wolfgang M. Heckl, Robert W Stark, Shaila C. Rössle: Moldels of SIGIRR inhibiting the Toll-like receptor TLR4 signaling pathway. In Proc. International Workshop on Computational and Integrative Biology, 2009, Hangzhou China, page:1-13.

2. Johannes Aßfalg, Jing Gong, Hans-Peter Kriegel, Alexey Pryakhin, **Tiandi Wei**, Arthur Zimek: Supervised Ensembles of Prediction Methods for Subcellular Localization. In Proc. 6th Asia Pacific Bioinformatics Conference, 2008, Kyoto, Japan, page: 29-38.

3. Jing Gong, **Tiandi Wei**, Ferdinand Jamitzky, Wolfgang M. Heckl, Shaila C. Rössle: TollML – a User Editable Database for Toll-like Receptors and Ligands. In Proc. 2nd IAPR International Workshop on Pattern Recognition in Bioinformatics, 2007, Singapore, paper ID: 231.

Presentations and Posters

1. Invited speaker, International Workshop on Computational and Integrative Biology, Hangzhou, China, "Models of SIGIRR inhibiting the Toll-like receptor TLR 4 signaling pathway", September, 2009

2. Poster, International Workshop on Computational and Integrative Biology, Hangzhou, China, "Homology modeling of human Toll-like receptors 7, 8 and 9 ligand-binding domains", September, 2009

3. Invited speaker, 3rd Annual Workshop on Oligonucleotides in Cell Biology and Therapy, Graduated School 1202 of the DFG, Frauenchiemsee, Germay, "Homology Modeling of Toll-like receptors", September, 2008

4. Poster, European Conferences on Computational Biology, Sardinia, Italy, "LRRML – a conformational database of leucine-rich repeats (LRRs)", September, 2008

5. Poster, 2nd IAPR International Workshop on Pattern Recognition in Bioinformatics, Singapore, "TollML – a user editable database of Toll-like receptors and ligands", October, 2007

Awards and Honors

2007-2010   Ph.D. Scholarship, German Research Foundation (DFG)

2007-2010   Travel Award, German Research Foundation (DFG)

1998-2001   Bronze Medal Student Scholarship, Ocean University of China